Rolf Alexander Skar

Chemical and Electrochemical Characterisation of Oxide/Hydroxide Impurities in the Electrolyte for Magnesium Production

INSTITUTT FOR KJEMI

NORGES TEKNISK-
NATURVITENSKAPELIGE UNIVERSITET
NTNU

AVHANDLING NR. 104 – SEPTEMBER 2001

This thesis has been submitted to

Institutt for Kjemi

Norges Teknisk-Naturvitenskapelige Universitet

in partial fulfilment of the requirements for

the Norwegian academic degree

DOKTOR INGENIØR

July 2001

URN:NBN:no-2317

Acknowledgement

First of all, I would like to thank my main supervisor, Prof. Dr. Techn. Terje Østvold, for helping and guiding me through the work on this thesis. His knowledge and experience in working with molten salts has been of great value to me. I would also like to thank my co-supervisor, Geir Martin Haarberg, for always being available to discuss electrochemical problems.

Secondly, I have to give a big thanks to Heidi Mediaas. Our co-operation during the experimental work was very valuable to me, she taught me a lot of what I know of experimental work. She has also been of great comfort when I have thought my progress to be slow.

I also want to thank all the people and technical staff at the Department of Chemistry, and especially everybody at "Inorganic Chemistry". Furthermore I want to thank Norsk Hydro's Magnesium division for their financial support, helpful guidance and patience, and also Norwegian Research Council for their financial support.

Finally, I want to thank my "samboer" Heidi and my family for their encouragement and support, and also to all my friends in Trondheim and the rest of the world for being able to make me think of other things than just this thesis.

Abstract

This work is part of a research program where the aim is to develop an electroanalytical technique to determine the amount of dissolved oxide and hydroxide in industrial Mg electrolytes. The systems studied were mixtures of $MgCl_2$ and NaCl, ranging from pure $MgCl_2$ to melts containing 10 mole % $MgCl_2$ / 90 mole % NaCl. To these melts, additions of MgO and MgOHCl were done at temperatures ranging from 475 to 850°C. Voltammetric measurements were performed before and after addition of MgO or MgOHCl and melt samples were taken for analysis. The quenched melt samples were analysed by carbothermal reduction analysis and the acid consumption method to obtain the O^{2-} and OH^- contents in the samples. Linear sweep voltammetry was performed with a sweep rate of 200 mV/sec in two potential regions to detect the concentration of dissolved MgOHCl and MgO. The experiments were performed inside a glove box having water and oxygen contents of, respectively, <1 ppm and <2 ppm. The results indicate that the rate of decomposition of MgOHCl increases with increasing temperature, as expected. In melts with high content of NaCl the underpotential deposition of sodium has a large influence on the uncertainty in the reading of the current density of MgOHCl reduction. Linear relations between MgO and MgOHCl concentrations and the peak current densities for the electrochemical reactions of the dissolved MgO and MgOHCl species in the melt, respectively, were observed. The diffusion coefficients of MgO and MgOHCl in the different melts were calculated. The diffusion coefficients decrease with increasing content of $MgCl_2$. For MgOHCl the diffusion coefficient decreases from $5.6*10^{-5}$ cm^2/sec in 20 mole % $MgCl_2$ / 80 mole % NaCl to $2.1*10^{-5}$ cm^2/sec in pure $MgCl_2$, both measurements done at 800°C. For MgO the diffusion coefficient decreases from $6*10^{-5}$ cm^2/sec in 41.5 mole % $MgCl_2$ / 58.5 mole % NaCl to $0.8*10^{-5}$ cm^2/sec in pure $MgCl_2$, both measurements done at 730°C. The results show that it is possible to use cyclic voltammetry for quantitative analysis of MgOHCl in $MgCl_2$ based melts.

Contents

1. Introduction

1.1. General considerations

1.1.1. Introduction to magnesium electrolysis

In 1990 more than 70% of the total magnesium production was produced by electrolysis of magnesium chloride dissolved in a mixture of molten salts[1,2]. This value is now (2000) closer to 50% due to increase in metallothermic production[3]. The exact composition of the melt used for electrolysis differs from producer to producer and is kept a secret, but most melts consist of NaCl, KCl, $CaCl_2$ and $MgCl_2$. LiCl and $BaCl_2$ may also be present. The content of $MgCl_2$ varies from 5-15 wt%[4a], but up to 25 wt% has been suggested[1,5]. Too low content of $MgCl_2$ will result in reduction of other metals, while too high content leads to enhanced melt hydrolysis[4a].

There have traditionally been two different designs of electrolysis cells, depending on the quality of the feed used. One design was used for hydrous feed containing approximately 1.5 mole H_2O per mole of magnesium chloride[6]. In this design the anodes were continuously consumed, and they had to be adjusted at regular intervals to keep the right anode-cathode distance. This process was in use by Dow Chemicals, but has currently ceased operation. Norsk Hydro has developed an anhydrous process. This is a process where ideally no water is introduced to the electrolyte with the feed. The cell is fed with pure liquid $MgCl_2$ or dry anhydrous solid $MgCl_2$.

The electrolysis reactions produce magnesium metal and chlorine gas. The temperature of the cell is kept above the melting point of magnesium. The reaction can be divided into a cathodic reaction and an anodic reaction, according to the following scheme:

Cathode: $$Mg^{2+} + 2e^- = Mg(l) \quad (1.1)$$

Anode: $$2Cl^- = Cl_2(g) + 2e^- \quad (1.2)$$

Total: $$MgCl_2(l) = Mg(l) + Cl_2(g) \quad (1.3)$$

The metal is produced at the cathode and in the anhydrous process of Norsk Hydro it is transported with the electrolyte flow and in this way separated from the chlorine gas. This process leads the metal to the separation chamber where the magnesium droplets rise to the surface. The rest of the electrolyte is circulated back to the electrodes, Fig. 1.1. The chlorine gas is produced at the anode and the gas bubbles rising to the surface are responsible for the liquid flow. The chlorine gas is collected above the melt and is recycled to the chlorination process.

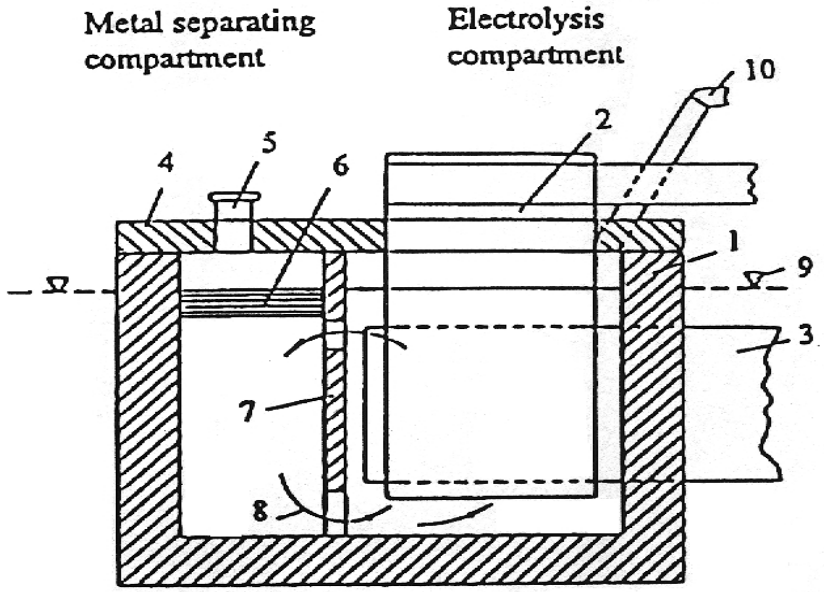

Figure 1.1 Schematic drawing of the Norsk Hydro diaphragmless electrolyser. 1) refractory material, 2) graphite anodes, 3) steel cathode, 4) refractory cover, 5) metal outlet, 6) metal, 7) partition wall, 8) electrolyte flow, 9) electrolyte level, 10) chlorine outlet[7].

1.1.2. Water impurities in $MgCl_2$ electrolyte

Water in the electrolyte is known to have a detrimental effect on the electrolysis of magnesium. According to Strelets[4b] the main source of MgO in the electrolyte is the reaction between Mg and/or $MgCl_2$ with moisture in the atmosphere above the electrolyte. This is no longer correct, since new technology has reduced the importance of these reactions. Currently most of the MgO found in the electrolyte is introduced with the feed[3].

Water dissolved in the electrolyte may be electrolysed to form carbon monoxide at the anode and hydrogen at the cathode, resulting in increased anode consumption and reduced current efficiency. This has been verified by analysis of the anodic gases during electrolysis and by following the current yield on the anode at different stages of the electrolysis[4b]. Dissolved water will also react with Mg and/or $MgCl_2$ in the electrolyte to form MgO or MgOHCl according to the reactions[8]:

$$Mg(l) + H_2O(g) = MgO(s) + H_2(g) \quad (1.4)$$

$$MgCl_2(l) + H_2O(g) = MgO(s) + 2HCl(g) \quad (1.5)$$

$$MgCl_2(l) + H_2O(g) = MgOHCl(l) + HCl(g) \quad (1.6)$$

MgO introduced to the melt through reaction 1.4 will influence the electrolysis in two different ways. Firstly, the reaction results in a loss of produced Mg. The amount of moisture in the electrolyte is usually less than 0.1%, so this loss in current efficiency is not a serious problem[4b]. Secondly, the MgO produced by this reaction forms a MgO-film on the metal surface. This MgO-film changes the wetting conditions of the metal and reduces coalescence of droplets at the cathode. The droplets become too small and will not rise to the surface in the separation chamber. These small droplets will follow the electrolyte flow and eventually react with Cl_2 (g) in the melt to give $MgCl_2$ [9,10,11], a major source for current loss in the electrolysis cell.

According to Strelets[4b] another source for loss of produced magnesium is that small droplets of Mg are coated with MgO. The specific weight of the coated Mg droplets increases and they will deposit as sludge at the bottom of the electrolysis cell.

MgO produced from reaction 1.5 is less detrimental, since this reaction occurs in the bulk electrolyte. At least some of the MgO formed will sink to the bottom of the electrolysis cell and deposit as sludge.

Reaction 1.6 produces magnesium hydroxychloride, which may be present in the electrolyte as positive ions. $MgOH^+$ and $Mg_2(OH)_2^{2+}$ has been suggested[4c,12] in the literature. Then these ions will migrate towards the cathode and can there be reduced to H_2(g) and MgO(s). The MgO(s) forms a layer on the cathode and may cause passivation[8].

Some of the MgO introduced with the cell feed will also deposit as sludge. Still, since there is some solubility of MgO in the electrolyte, dissolved MgO will react with the graphite anodes and form carbon monoxide. This process of anode consumption can be described by the electrochemical reaction:

$$MgO + C = CO(g) + Mg^{2+} + 2e^{-} \quad (1.7)$$

In addition to the consumption of the anode, reaction 1.7 gives some loss in current yield since some of the current is used for production of CO (g). In addition the produced chlorine becomes contaminated with carbon monoxide.

MgOHCl is unstable at high temperature and will decompose to form MgO and HCl according to reaction 1.8. The MgO formed will precipitate and increase the amount of sludge in the cell.

$$MgOHCl(l) = MgO(s \ or \ l) + HCl(g) \quad (1.8)$$

1.1.3. Aim of the work

The aim of the present work is to develop an electroanalytical technique to determine the amount of dissolved oxide and hydroxide in both liquid $MgCl_2$ and industrial electrolytes used in Mg production. Experiments with additions of MgO and MgOHCl to NaCl-$MgCl_2$ melts have been performed, and concentration measurements from analyses of melt samples have been compared with current densities obtained by cyclic voltammetry. The dissolution and decomposition rates of MgOHCl have been studied by analytical methods. Both iodometric titration and carbothermal analysis have been performed, and a combination of these methods will distinguish between MgO and MgOHCl. The effect of temperature and melt composition on dissolution and decomposition has also been investigated.

Current methods for measuring oxide and hydroxide are based on chemical analysis of samples taken from the electrolyte or the liquid $MgCl_2$ feed. Real time values cannot be obtained. One major problem is the unstability of hydrogen and oxygen containing species, especially the decomposition of MgOHCl. An *in situ* technique should therefore be of great value. The goal is therefore to establish such a technique, using cyclic voltammetry. This method is fast and easy to perform, if a suitable probe can be designed. Research to develop such a probe has already been started at Norsk Hydro Research Center and NTNU.

1.2. Review of literature

1.2.1. Solubility of MgO and MgOHCl in $MgCl_2$-containing melts

Boghosian et al.[13] investigated the solubility of MgO in $MgCl_2$-NaCl melts. They found that the solubility of MgO increases with increasing content of $MgCl_2$, up to 0.36 mole % MgO in pure $MgCl_2$ at 730 °C. They observed no temperature effect on the oxide solubility from 730 to 830 °C for $0.5 < x_{MgCl_2} > 0.75$. The following dissolution mechanism for MgO was suggested:

$$MgO(s) + MgCl_2 = Mg_2OCl_2(l) \tag{1.9}$$

The existence of this complex has also been suggested earlier by Combes et al[14]. Mediaas et al.[15] found that the solubility of MgO was temperature dependent in pure $MgCl_2$ and they found an almost twofold increase going from 730 to 840 °C. This change in behaviour is due to the fact that $MgCl_2$ changes from a partly ionic, partly network-like melt in the pure state to a typically ionic molten salt when alkali chlorides are introduced[16]. Mediaas et al.[15] suggested that MgO dissolves in pure $MgCl_2$ by breaking up the polynuclear complexes of $MgCl_2$ as indicated by the reaction:

$$MgO(s) + [MgCl_2]_n = Mg_{n-m+1}OCl_{2(n-m)} + [MgCl_2]_m \tag{1.10}$$

Vinstad et al.[17] pointed out the similarities between MgOHCl and MgO, suggesting that a complex equilibrium involving MgOHCl and $MgCl_2$ is established in the melt. They argued that the $MgOH^+$ ion is likely to be bent. In pure $MgCl_2$ interactions between the positive Mg^{2+} ions and the negative end of the $MgOH^+$ dipoles are likely to occur. The interaction is given by the reaction:

$$MgCl_2(l) + MgOHCl(l) = Mg_2OHCl_3(l) \tag{1.11}$$

Schenin-King and Picard[12] claimed that MgOHCl would dissolve as a dimer according to the reaction:

$$2MgOHCl(s) = (MgOHCl)_2(l) \tag{1.12}$$

Their electrochemical investigation was performed in a LiCl-KCl-$MgCl_2$ melt[12]. They claimed that the nature of the melt cations strongly influenced the nature and the solubility of the OH^- species in the melts. According to Schenin-King and Picard, the $(MgOHCl)_2$-dimer exists in LiCl-KCl-$MgCl_2$ melt, while the ZnOHCl-monomer exists in LiCl-KCl-$ZnCl_2$ melt. The solvated species were identified by means of potentiometric measurements with an yttria-stabilised zirconia membrane electrode. This electrode measures the ion activity in molten salts. The difference in nature of the OH^- species in the two melts was postulated to be due to the difference in the electronic structure of the two cations, Mg^{2+} and Zn^{2+}. This postulate was not verified in any way.

Vilnyansky and Savinkova[18,19] studied the formation of MgOHCl in solid $MgCl_2$ by equilibrating a mixture of MgO and anhydrous $MgCl_2$ with a gas of known partial pressure of HCl and H_2O. They found that the solubility of MgOHCl in $MgCl_2$ increased with increasing temperature. They also found that MgOHCl was formed in solid solution with $MgCl_2$ and claimed that HCl (g) formed from the decomposition of MgOHCl could react and give a saturated solid solution, according to the reaction:

$$MgOHCl(s) + HCl(g) = MgCl_2(ss) + H_2O(g) \qquad (1.13)$$

Vilnyansky and Bakina[20] investigated the solubility of water and magnesium oxide in fused carnallite, which consists of 47% $MgCl_2$, 45% KCl and 8% NaCl. By visual study of the settlement of particles suspended in the liquid and by analysing for oxide and hydrogen content in the top layer of the liquid after settlement, they concluded that all oxygen present was in the form of hydroxide and that MgO was practically insoluble in molten carnallite.

Savinkova et al.[21] investigated the kinetics of the decomposition reaction of MgOHCl. The melt used was a mixture of NaCl, KCl and $MgCl_2$ and the temperature of investigation ranged from 450 to 750°C. They reported that the dissociation kinetic of MgOHCl is described by a first order equation and that the dissociation rate increases with increasing temperature. The dissociation product was reported to be MgO(s).

Muzhzhavlev and Ivanov[22] measured the influence of the humidity in argon on the rate of hydrolysis of magnesium chloride in electrolytes consisting of $BaCl_2$, $CaCl_2$, LiCl, KCl and NaCl, all with a $MgCl_2$ concentration between 5 and 20 wt.%. The argon gas was bubbled through the melt, and the rate of

magnesium oxide formation was measured. The conclusion was that the rate of formation of magnesium oxide increased proportional to the square root of the increase in moisture content of the argon gas.

Ivanov and Zuev[23] investigated the saturation mole fraction of MgOHCl in carnallite melts based on previously published results. Saturation of the melt with MgOHCl and MgO gave rise to a third phase, solid magnesium oxide, and with this three-phase equilibrium the hydrolysis reaction is given by reaction 1.5:

$$MgCl_2(l) + H_2O(g) = MgO(s) + 2HCl(g) \qquad (1.5)$$

Ivanov and Zuev argued that the only hydrogen containing specie that needed to be considered in such melts was $MgOH^+$. The argument was based upon the observation that pure alkali chlorides do not undergo hydrolysis, i.e. free OH^- ions are not likely to exist. Furthermore they claimed that mixed complexes like $[MgOHCl_2]^-$ and $[MgOHCl_3]^{2-}$ must be very unstable due to the counterpolarization of chlorine by protons and the sharp difference in nature of the chlorine-magnesium and oxygen-magnesium bonds.

Savinkova and Lelekova[24] studied the NaCl-KCl-$MgCl_2$-MgOHCl system. Their goal was to investigate the hydrolysis of the melt by equilibrating with a gas consisting of HCl, H_2O and CO_2 of known partial pressures. The $MgCl_2$ concentration was determined by complexometric titration and the MgOHCl concentration was determined by measuring the different rates of interaction of MgO and MgOHCl with acid. The activities of $MgCl_2$ and MgOHCl were calculated from data for reactions 1.5 and 1.6.

$$MgCl_2(l) + H_2O(g) = MgO(s) + 2HCl(g) \qquad (1.5)$$

$$K_{1.5} = \frac{P_{HCl}^2}{P_{H_2O} \cdot a_{MgCl_2}} \qquad (1.14)$$

$$MgCl_2(l) + H_2O(g) = MgOHCl(l) + HCl(g) \qquad (1.6)$$

$$K_{1.6} = \frac{P_{HCl} \cdot a_{MgOHCl}}{P_{H_2O} \cdot a_{MgCl_2}} \qquad (1.15)$$

They found that the activity of $MgCl_2$ increased with increasing temperature and $MgCl_2$ content, while at constant $MgCl_2$ content the activity increased with increasing NaCl content. Furthermore they found a very low activity up to 30-35 mole % $MgCl_2$, but it was rising sharply upon further increase in the $MgCl_2$ concentration. This dependence on the activity of $MgCl_2$ is due to complex formation in the system, i.e. $MgCl_4^{2-}$. They also found that the activity of $MgCl_2$ in hydrolysed melts was substantially higher than in anhydrous melts. The MgOHCl content was also investigated with respect to temperature and composition of the melt, and it was found that an increase in $MgCl_2$ concentration and a decrease in temperature lead to an increase of the MgOHCl content. Keeping the $MgCl_2$ concentration constant, an increase in MgOHCl content with an increase in NaCl concentration was observed.

1.2.2. Size of MgO-particles

Savinkova et al.[21] investigated how the size of MgO-particles changed during thermal dissociation of MgOHCl in a NaCl-KCl-$MgCl_2$ melt. They found that the size was dependent on the supersaturation of MgOHCl. The supersaturation ratio given as C^{super}/C^{eq} was the important parameter. At higher supersaturation ratios more MgO-particles formed and the radius decreased, while at lower ratio existing particles of MgO continued to grow on the expense of new nuclei. They also found that the supersaturation of MgOHCl in the melt increased with increasing $MgCl_2$ content and increasing temperature, but since the equilibrium concentration also increases with increasing $MgCl_2$ content and increasing temperature, the ratio C^{super}/C^{eq} was nearly constant and close to 2.5.

1.2.3. Some thermodynamic properties of relevant compounds for Mg-electrolysis

Molar weights and thermodynamic properties for pure substances relevant to the present work are given in Tab. 1.1.

Table 1.1 Thermodynamic properties of relevant pure substances, from JANAF Thermochemical Tables.

Compound	**M_r** [g/mole]	**T_{fus}** [°C]	**ΔH_{fus}** [kJ/mole]	**S°** [J/K mole]	**ΔH_f °** [kJ/mole]
$MgCl_2$	95.2	714	43.10	228.66	-596.73
MgO	40.3	2832	78	82.26	-608.46
MgOHCl	76.8	-	-	169.42	-703.09
NaCl	58.5	801	28.16	139.30	-407.46
HCl	36.5	-	-	222.90	-94.39
H_2O	18	-	-	232.74	-247.86

1.2.4. The binary system NaCl-$MgCl_2$.

The binary phase diagram NaCl-$MgCl_2$ has been investigated extensively. The works of Klemm and Weiss[25] and Grjotheim et al.[26] are in good agreement with each other, the main difference being the solidus temperatures. Grjotheim et al. used thermal analysis, differential thermal analysis and X-ray diffraction studies at room temperature as investigation methods. Two incongruently melting binary compounds were observed, corresponding to $NaMgCl_3$ and Na_2MgCl_4 with melting points 468 and 475 °C, respectively. The eutectic point was found to be at 41.5 mole % $MgCl_2$ at 445 °C.

Enthalpies of mixing of $MgCl_2$ with all the alkali chlorides have been measured by Kleppa and McCarty[27]. Negative deviations from ideality were observed and the absolute values of the enthalpies of mixing increases in the sequence Li<Na<K<Rb<Cs. Sharp minima in the interaction parameter, $\Delta H^m_{mix}/(x_{alk.Cl}\, x_{MgCl_2})$, were found for all the alkali chlorides except for LiCl in mixtures with $MgCl_2$. These minima were found at $x_{MgCl_2} = 0.33$, and were attributed to the special stability of the ionic configuration $MgCl_4^{2-}$.

Chemical potentials of NaCl and $MgCl_2$ in mixtures have been obtained using e.m.f.-measurements by several authors, including Østvold[28]. Kosnyrev et al.[29] used a different approach for determination of a_{MgCl_2} in molten salt mixtures containing NaCl, KCl, $MgCl_2$ and $CaCl_2$. The method involves the use of the equilibrium constant, $K_{1.16}$, for the following reaction:

$$MgCl_2(l) + \frac{1}{2}O_2(g) = MgO(s) + Cl_2(g) \qquad (1.16)$$

$$K_{1.16} = \frac{P_{Cl_2}}{a_{MgCl_2}\sqrt{P_{O_2}}} \tag{1.17}$$

At a given temperature and x_{MgCl_2}, the ratio $P_{Cl_2}/\sqrt{(P_{O_2})}$ was determined, and a_{MgCl_2} was calculated from $K_{1.16}$. The activity data for $MgCl_2$ have been fitted to obtain Eq. 1.18, while Karakaya and Thompson[30] made a fit to obtain Eq. 1.19:

$$\ln \gamma_{MgCl_2} = -3.864(1 - x_{MgCl_2}) \tag{1.18}$$

$$\begin{aligned} RT \ln \gamma_{MgCl_2} = {} & (-16.78x_{NaCl}^2 - 5.680x_{NaCl}^3 - 23.19x_{NaCl}^4) \cdot 10^3 \\ & - T \cdot (-2.405x_{NaCl}^2 - 2.65x_{NaCl}^3) \end{aligned} \tag{1.19}$$

The Raoultian standard state have been used for $MgCl_2$ and large, negative deviations from ideality due to complex formations in the melt were observed[16, 31].

1.2.5. A brief review of the structure of $MgCl_2$-alkali chloride melts.

Flood and Urnes[31] first suggested the existence of complex ions in $MgCl_2$-alkali chloride melts. Assuming that all magnesium in the melt was complexed as $MgCl_4^{2-}$, they predicted the alkali chloride liquidus lines in the $MgCl_2$-MCl (M=Na, K and Rb) systems with good agreement. Raman measurements performed by Maroni et al.[32,33] confirmed the existence of $MgCl_4^{2-}$, although they initially had some problems identifying correctly the different Raman spectra. Capwell[34] performed measurements on $MgCl_2$ just above and below its melting point and found residual lattice bands in the melt indicating structural similarities to the solid $MgCl_2$. Brooker and Huang[16,35] presented further confirmations of $MgCl_4^{2-}$, and suggest $Mg_2Cl_7^{3-}$ as the second complex species in the melt. They based this suggestion on the similarities between Raman spectra recorded in CsCl-$MgCl_2$ and in CsCl-$AlCl_3$ melts. At the same time they rejected the existence of the species $MgCl_3^-$ and Mg_2Cl_4 and found that the scattering from the polynuclear species gradually disappeared as NaCl was added to pure $MgCl_2$. For $x_{MgCl_2} \leq 0.33$ only the $MgCl_4^{2-}$ complex was assumed to be present.

1.2.6. Electrochemical considerations

Haarberg et al.[36] performed visual observations during electrolysis in molten eutectic NaCl-KCl mixture with 5-10 wt% $MgCl_2$. Addition of $Mg(OH)_2$ (0.05 wt%) to this melt caused gas evolution, probably H_2, on the cathode before Mg droplets were formed, and the droplets became smaller and more spherical due to deterioration of the wetting between the magnesium liquid and the iron cathode. Børresen et al.[37] studied the nucleation of Mg from various halide melts ($MgCl_2$, $MgCl_2$-MgF_2 and mixed alkali chloride melts with small amount of $MgCl_2$) by classical electrochemical techniques. They found that the nucleation kinetics varied with the substrate and the potential. The stability of the Mg nuclei formed seemed to depend on the substrate and on the oxide level in the melt. Increasing content of oxide seemed to stabilise the nuclei, probably by changing their surface energy. They used a platinum rod as reference electrode in their investigations, and since platinum is not a proper reference in this melt, instability of the electrode system could be the reason for the observed variations in nucleation kinetics reported. Underpotential deposition of magnesium on glassy carbon was also reported. The charge of the prepeak corresponded to deposition of 1-3 monolayers of magnesium. Some further studies by using electrochemical impedance spectroscopy and relaxation method with galvanostatic perturbation were performed by Kisza et al.[38] to investigate the kinetics and mechanism of the magnesium electrode reaction in pure molten $MgCl_2$. A three-step electrode process was found, a preceding chemical reaction followed by two one-electron transfer reactions. The same investigation procedures were performed in $MgCl_2$-NaCl binary mixtures[39], and a three-step electrode process was also found in these melts. The melt structure, i.e. change in composition, showed a pronounced influence on the kinetic and transport parameters in the binary melts. This could be due to the release of more magnesium ions in the process of changing the melt structure from polynuclear complexes in pure molten $MgCl_2$, to a more ionic structure as NaCl is added to the melt.

The electrochemical behaviour of dissolved oxides in molten $CaCl_2$-CaO and $MgCl_2$-MgO has been studied by linear sweep voltammetry and potential step measurements[40,41]. Several different materials were employed as working electrode, but only high purity glassy carbon was found to give reproducible results. The anodic reaction due to oxidation of dissolved oxide was found to be irreversible. A linear relationship between the anodic peak current density from linear sweep voltammetry and the concentration of dissolved CaO was

obtained in dilute solutions with less than 0.2 wt% CaO. Voltammetry and potential step measurements of MgO in $MgCl_2$ (less than 0.1 wt% MgO) indicated a diffusion-controlled reaction. They also found an n-value of 1, where n is the number of electrons transferred, indicating that dissolved MgO is present as an $(MgOCl)_x$ species. This is, however, not reasonable in view of the stability of divalent oxygen in these melts, found by Boghosian et al[13].

The anodic behaviour of carbon electrodes in CaO-$CaCl_2$ melts was studied by Mohamedi et al.[42] by cyclic voltammetry and convolution voltammetry. They found two current peaks corresponding to oxidation of CaO, both peaks being irreversible 2-electron transfer reactions. The reaction scheme is quite complicated, the first step involving electrochemical adsorption:

$$O^{2-}(diss) + xC \rightarrow C_xO(ads) + 2e^- \tag{1.20}$$

This is followed by electrochemical desorption:

$$O^{2-}(diss) + C_xO(ads) \rightarrow CO_2(g) + (x-1)C + 2e^- \tag{1.21}$$

The current peaks were plotted vs. the square root of sweep rate. The conclusion was that at high sweep rate the reaction was diffusion controlled, but at slower sweep rate the process was not totally governed by diffusion and charge transfer was preceded by a chemical reaction.

Bjørgum et al.[43] studied electrochemically, using voltammetry, the hydrolysis products in liquid $MgCl_2$–NaCl containing $Mg(OH)_2$, NaOH and HCl. Working electrodes studied were glassy carbon and platinum. The anodic limit for the glassy carbon electrode was Cl_2-evolution, while dissolution of the electrode was the limit for the platinum electrode. Practical cathodic limits were magnesium deposition/underpotential deposition and alloying potential for the glassy carbon and platinum electrodes respectively. Two reduction peaks, or waves/shoulders, more positive than the Mg deposition potential were observed, one at about 1.2-1.3V positive of Mg-deposition and one at about 0.9-1.1V. These peaks were suggested to correspond to a metastable hydrogen containing species e.g. MgOHCl and a hydrogen containing species with short lifetime in the melt, suggested specie were H_2O and HCl, respectively. Addition of HCl to the melt was also investigated, and two cathodic current increases were found. The first reduction wave at about 1.7V was believed to be reduction of dissolved HCl in the melt while the second wave at about 1.2V was believed to be reduction of MgOHCl.

Eie et al.[39] did a preliminary investigation of the electrochemical behaviour of hydroxy-ion by adding NaOH to a NaCl-KCl melt. The materials for the different working electrodes tested were glassy carbon and platinum, and the reference electrode was made of a Mg/Ni-alloy. Their conclusion was that the hydroxy-ion was very stable in the melt, the reduction occurred at potentials close to the corresponding potential for Mg deposition. They also suggested that on carbon electrodes it was possible to produce methane. After further investigations in the same system, Haarberg and Tunold[44] found that the reduction of the hydroxy-ion was irreversible and at least partly diffusion controlled. Two cathodic peaks were observed, and the second cathodic peak was suggested to correspond to reduction of H_2O or some C-H specie. This second peak was found to be diffusion controlled. Addition of HCl to the melt was also investigated and a cathodic peak corresponding to reduction of HCl was found. The peak was reversible and diffusion controlled, and appeared at a potential about 1.4-1.5V positive of OH^- reduction. Electrochemical investigations of NaOH in pure $MgCl_2$ revealed that H_2 evolution from MgOHCl took place at a less positive potential (referred to Mg deposition) than in melts containing alkali chlorides. The reduction reaction was diffusion controlled. Addition of HCl gave rise to two cathodic waves at about 1.5V and 1.2V corresponding to H_2 evolution from HCl and MgOHCl respectively. Passivation of the electrode due to formation of MgO at the electrode was reported to be a problem.

1.2.7. Hydrogen reduction in chloride melts.

Ito et al[45] investigated the electrode behaviour of hydrogen reduction in a LiCl-KCl melt. They used metal electrodes made of Fe, Ni, Co and Cu, and investigations were made using linear and cyclic sweep voltammetry. Hydrogen gas was cathodically reduced at about 0.58V (*vs* Li+/Li) and hydride ions were generated according the following reaction:

$$H_2 + 2e^- = 2H^- \tag{1.22}$$

An anodic peak was observed on the reverse anode sweep, corresponding to oxidation of the hydride ion. The oxidation reaction is given below:

$$2H^- = H_2(g) + 2e^- \tag{1.23}$$

Adsorbed hydrogen was also considered, and by using metal electrodes with different solubility and diffusivity of hydrogen, two different hydrogen

reduction reactions were identified. One was a two-electron transfer reaction, (reaction 1.22), and the other was a one-electron transfer reaction, corresponding to reduction of hydrogen adsorbed in the metal according to:

$$H_{ads} + e^- = H^- \tag{1.24}$$

The thermodynamics of the system Mg-H was reviewed by Zeng et al.[46], and the general agreement is that three condensed phases exists, the liquid phase, the terminal solid solution α-(Mg) and a hydride β-MgH_2. Based on the experiments of several authors, a model for the Mg-H-system was made. A set of thermodynamic functions was chosen and the parameters optimised using the least squares method. The phase diagram was calculated together with the influence of pressure, and compared with experimental results. The solubility of H in molten Mg is temperature dependent with a maximum at about 927°C. The calculated eutectic composition and temperature are 0.093 mole % H and 694.7°C respectively.

1.3. Concluding remarks

At the start of the current research, measurements of oxide in industrial systems with analytical methods were well advanced. At the same time, some electrochemical investigations to examine oxide- and hydroxide-species in melts of interest had also been performed, although none of them were conclusive. No papers were published in which current densities and concentrations of oxide- and hydroxide-species were investigated.

To develop a working *in situ* method using cyclic voltammetry, some work was needed to correlate the current densities and concentrations of oxide- and hydroxide-species. This work was divided in two parts, one to investigate industrial melts, and one to study pure melts with known additions of oxide and hydroxide. It was also necessary to develop an electrochemical measuring probe which could be used.

This work might also give a better understanding of how the oxide and hydroxide species are formed and decompose in the melt. Furthermore, by having a faster way of detecting these species, a better understanding of how these species influence the electrolysis could be obtained.

2. Theory

2.1. Cyclic voltammetry

This part is taken from "Instrumental methods in electrochemistry"[47]. Cyclic voltammetry involves sweeping of the electrode potential between two limits E_1 and E_2. This is done at a known and constant sweep rate, ν. The cell current is recorded as a function of the applied potential. The sweep rates range from a few mVs^{-1} to several thousands Vs^{-1}, but too high sweep rates cause the double layer charging and iR_u drop effects to be very large. A typical current response of a reversible reaction, with soluble reactant and product, is given in Fig. 2.1. The potential is swept from E_1 to E_2 and then back to E_1.

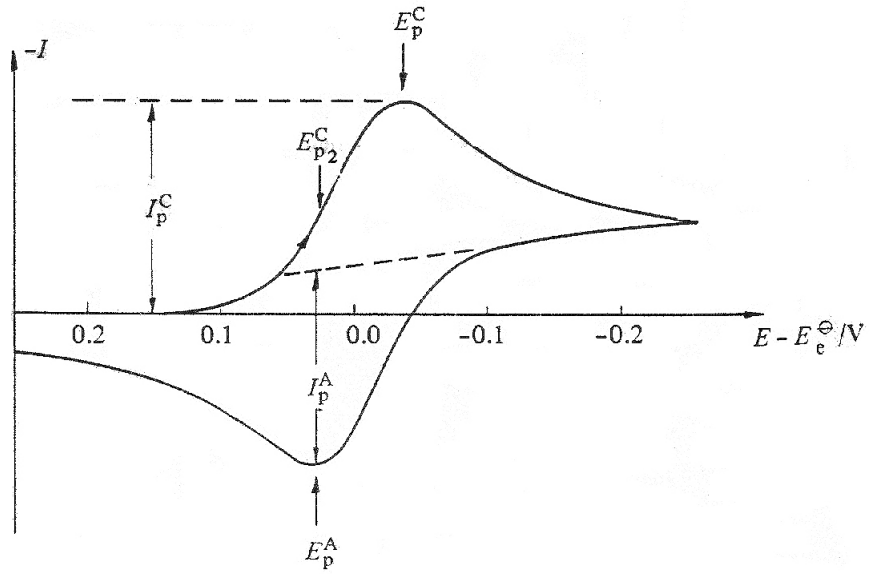

Figure 2.1. Cyclic voltammogram of a reversible electrochemical reaction[47].

If the reactant and product is soluble, and the process is reversible, the peak current, i_p, is given by Eq. 2.1:

$$i_p = 0.4463 \frac{(nF)^{3/2}}{(RT)^{1/2}} c^{\infty} D^{1/2} \nu^{1/2} \qquad (2.1)$$

where i_p is the peak current density in A/m^2, n is the number of electrons transferred in the reaction, F is Faraday's constant in C/mole, R is the universal gas constant in J/K•mole, T is the temperature in K, c^{∞} is the bulk concentration of the reacting species in mole/m^3, D is the diffusion coefficient in m^2/s and ν is the potential sweep rate in V/s.

The reversibility of the system may be checked by plotting i_p as a function of $\nu^{1/2}$. This plot should be linear and pass through the origin. Several other diagnostic tests should also be satisfied by a reversible system, namely:

1) Separation of anodic and cathodic peak potentials, $E_p^A - E_p^C$, at 25°C is 59/n mV.
2) The ratio between anodic and cathodic peak current densities, i_p^A / i_p^C, is equal to 1.
3) The peak potential, E_p, is independent of sweep rate, ν.
4) At potentials beyond E_p, the current is proportional to $t^{-1/2}$ at 25°C, where t is time.

In a reversible system the electron transfer rate is significantly greater than the mass transport rate, and Nernstian equilibrium is maintained at the electrode surface. When the rate of electron transfer is insufficient to maintain this equilibrium, the process is said to be irreversible, and the shape of the voltammogram changes. The most noticeable effect is an increase in the peak separation and a reduced height of the reverse peak. For a totally irreversible system, there is no reverse peak at all. Another change is that the peak potential is no longer independent of sweep rate.

2.1.1. Monolayer formation.

Monolayer formation has frequently been observed during deposition processes. The reason for this is that thermodynamically stable nuclei must be formed at the surface for a deposition process to occur. The formation of such nuclei requires a potential more negative than that required to reduce the cations, and lead to what is known as a nucleation overpotential. This

overpotential may depend on the substrate material. This implies that monolayer formation may occur if the overpotential needed for deposition is higher for the metal itself than for the original material of the working electrode.

2.1.2. Double layer charging effects.

In addition to faradic current we have double layer charging current.

$$I_{dl} = C_{dl} * v \tag{2.2}$$

$$I_{tot} = I_{far} + I_{dl} \tag{2.3}$$

Since I_{far} is proportional to $v^{1/2}$ and I_{dl} is proportional to v, Eq. 2.2, I_{dl} becomes more important as scan rate is increased. Typical values of C_{dl} are between 20 and 40 μF cm^{-2} and this gives values for I_{dl} between 2 and 4 μA cm^{-2} at scan rates of 100 mVs^{-1}. These values are much smaller than I_{far}. At scan rates like 100 Vs^{-1} the I_{dl} ranges between 2 and 4 mA cm^{-2} and is no longer negligible. Thus the double layer charging current distorts the shape of cyclic voltammograms recorded at high sweep rates.

2.1.3. Potential drop between electrodes

If there exists an IR drop between the working and reference electrodes, the applied voltage changes from E to E - iR_u. The sweep will then no longer be linear since the current changes during a sweep. As a result one will have decreasing peak heights and increasing peak separations.

2.2. Analytical techniques

2.2.1. Acid consumption method – iodometric tritration

Iodometric titration is an oxidation-reduction titration technique that can determine the amount of basic oxide in a sample. The sample is dissolved in a known amount of HCl. The dissolution reaction is:

$$O^{2-} + 2HCl = 2Cl^{-} + H_2O \tag{2.4}$$

The excess HCl reacts with KIO_3 and KI to form I_3^- ions:

$$IO_3^- + 8I^- + 6H^+ = 3I_3^- + 3H_2O \tag{2.5}$$

and the I_3^- ions are titrated with thiosulphate:

$$2S_2O_3^{2-} + I_3^- = S_4O_6^{2-} + 3I^- \tag{2.6}$$

The same procedure is followed for a sample without oxide to have a blank sample used in the calculations. The amount of oxide per gram melt sample can then be found according to the equation:

$$n_0^{bas}\left[ppmO^{2-}\right] = 10^3 * \frac{16V_{HCl}c_{HCl}(1-\frac{V_s}{V_b})}{2m_{sample}} \tag{2.7}$$

where V_s is the titration volume of $Na_2S_2O_3$; V_b the titration volume of $Na_2S_2O_3$ used in the blind test; m grams of sample dissolved; V_{HCl} the volume HCl used and c_{HCl} the HCl concentration.

If OH^- is dissolved and not O^{2-}, the dissolution reaction will be:

$$OH^- + HCl = Cl^- + H_2O \tag{2.8}$$

and:

$$n_0^{bas}\left[ppmO^{2-}\right] = 10^3 * \frac{16V_{HCl}c_{HCl}(1-\frac{V_s}{V_b})}{m_{sample}} \tag{2.9}$$

This can be used to measure both O^{2-} and OH^- in a sample if we in addition can determine the total oxygen concentration in the sample. This will be explained below.

2.2.2. Carbothermal reduction analysis

Carbothermal reduction analysis is used to determine the total oxygen content in a sample. The sample is stored in a tin capsule, which is heated in graphite powder to a chosen temperature. The oxygen in the sample reacts with the graphite to form CO, which is further oxidised to CO_2 in a CuO tower. The CO_2 formed is detected by infrared absorption at a frequency characteristic of CO_2. All oxygen in the sample will have to react to give the total amount of oxygen.

The analysis can be done using the commercial equipment, LECO TC-436 Oxygen and Nitrogen Determinator. At the start of analysis the sample to be analysed is kept in a loader mechanism while the graphite crucible and graphite powder is preheated to a temperature above the analysis temperature for 60 seconds or more. The temperature is then lowered to a starting temperature, the sample is dropped into the crucible and the analysis starts. It is possible to choose 3 different analysis methods, and they differ in the way of heating the sample. The methods are scan, automatic and step analysis.

The automatic analysis is simple and fast. Only one high temperature is used during the whole analysis, and all oxides are detected simultaneously. Some oxides may evaporate without reacting with the graphite crucible at this high temperature, and are therefore not detected during automatic analysis. For such samples, the scan analysis method is better. Then the temperature is increased at a constant rate from the starting temperature to a given temperature. The start and stop temperatures, and the rate of temperature increase are preset by the operator. By this method it is possible to determine different oxides in the sample, if each individual oxide species reacts with carbon at different temperatures.

During step analysis, the temperature is raised in steps. Up to 9 different temperature steps can be programmed by the operator. This method is well suited to distinguish between contributions from different oxides with different carbothermal decomposition temperatures.

2.2.3. Combination of the above analytical techniques

Taking as an example the oxide containing species MgO and MgOHCl dissolved in $MgCl_2$–NaCl melts the total amount of oxygen in the melt sample, n_O^{tot}, is found using the carbothermal reduction analysis, and is given by:

$$n_O^{tot} = n_{MgO} + n_{MgOHCl} \quad (2.10)$$

Basic oxygen equivalents, n_O^{bas}, as found by iodometric titration analysis is given by:

$$n_O^{bas} = 2n_{MgO} + n_{MgOHCl} \quad (2.11)$$

Solving for n_{MgO} and n_{MgOHCl} we get:

$$n_{MgO} = n_O^{bas} - n_O^{tot} \quad (2.12)$$

$$n_{MgOHCl} = 2n_O^{tot} - n_O^{bas} \quad (2.13)$$

Since Eqs. 2.12 and 2.13 give a small difference between to large numbers, they will give relatively uncertain values of n_{MgO} and n_{MgOHCl}. If possible, other solutions should be used. At some compositions the solubility of MgO in a $MgCl_2$-NaCl melt is very low. When adding MgOHCl to such a melt already saturated with MgO, the change in MgO concentration is negligible. The saturation concentrations of MgO in such melts are well known. The MgOHCl concentration can then be calculated by subtracting the MgO saturation concentration from the total oxygen concentration of the melt, as given by Eqs. 2.14 and 2.15. Both the carbothermal reduction and the acid consumption analysis, n_O^{tot} and n_O^{bas}, respectively, can be used for this purpose.

$$n_{MgOHCl} = n_O^{tot} - n_{MgO}^{sat} \quad (2.14)$$

$$n_{MgOHCl} = n_O^{bas} - 2n_{MgO}^{sat} \quad (2.15)$$

2.3. Area determination of the electrodes

If the peak current using linear sweep voltammetry is proportional to the area of the working electrode, this area can be found by using different depths of

immersion of the electrode. When the radius of the electrode is known, the area change when the electrode is lowered/raised can be calculated. The current density at a given electrode depth is given as:

$$i_0 = \frac{I_0}{A_0} \tag{2.16}$$

where I_0 is the current measured and A_0 is the electrode area in the melt.

By plotting *i* vs A for at least 3 different depths of immersion, the slope $\Delta I/\Delta A$ gives the current density:

$$i = \frac{\Delta I}{\Delta A} \tag{2.17}$$

The initial area can then be found using:

$$A_0 = \frac{I_0}{i} \tag{2.18}$$

3. EXPERIMENTAL

3.1. Chemicals

The electrolytes to be studied were made up from $MgCl_2$ and NaCl. The chemicals used in the different experiments are listed in Tab. 3.1. Anhydrous $MgCl_2$ was prepared by slowly heating $MgCl_2 \bullet 6H_2O$ from room temperature to 450°C under a steady HCl(g) flow. The heating rate varied from 3 to 25°C per hour, depending on the temperature range and the HCl flow rate. The dehydrated $MgCl_2$ was cooled to 100°C and flushed with N_2(g) for 24 hours to remove remaining HCl. It was then distilled under vacuum ($\approx 10^{-7}$ bar) at 1000°C and stored in sealed quartz ampoules.

NaCl was dried under vacuum at 400°C for 3-4 hours, and recrystallised twice from the molten state in a platinum crucible under N_2 atmosphere. MgO was heated to 600°C under vacuum for 48 hours to convert impurities of $MgCO_3$ to MgO.

MgOHCl was prepared by Aa. Aasheim, Norsk Hydro. $MgCl_2 \bullet 6H_2O$ was heated in three steps at 120, 180 and 260°C respectively, while flushing with a stream of synthetic air. At the final temperature of 260°C, water (5 vol. %) and HCl (2 vol. %) were added to the air. The MgOHCl was analysed by XRD and chemical analysis to check its purity.

Table 3.1. Chemicals used in electrolytes

Chemical	Quality	Supplier
$MgCl_2 \bullet 6H_2O$	p.a., >99%	E. Merck A. G. Germany
NaCl	p.a., >99.5%	E. Merck A. G. Germany
MgO	>97%	Fluka A.G., Switzerland
N_2	99.998%	Hydrogas, Norway
HCl	99.8%	Messer Griesheim, Germany
Ar	99.998%	Hydrogas, Norway
He	>99,998%	Hydrogas, Norway
$Na_2S_2O_3$	Titrisol (0.001M)	E. Merck A. G. Germany
HCl (aq)	Titrisol (0.001M)	E. Merck A. G. Germany
KI	p.a., >99.5%	E. Merck A. G. Germany
KIO_3	p.a., >99.5%	E. Merck A. G. Germany
Soluble starch	p.a.	E. Merck A. G. Germany

3.2. Electrodes

Glassy carbon was used as the working electrode. A rod (ϕ=3mm) of glassy carbon was screwed into a rod (ϕ=6mm) of graphite. The counter electrode was made of graphite (ϕ=6mm). Suppliers and quality of the electrode materials are given in Tab. 3.2. Cleaning of the electrodes were done by first boiling them in dilute HCl solution and then in distilled water, and subsequently treated with ultrasound in ethanol. The last traces of impurities were removed by heating the electrodes to 900°C under vacuum for 12 hours. The electrodes were both connected to nickel rods and the nickel rods were placed inside sintered alumina tubes for electric insulation and protection against corrosion.

A platinum rod (ϕ=1.5mm) was used as reference electrode. All the alumina and platinum were cleaned by boiling the material first in a dilute HCl solution and distilled water and then finally rinsed in ethanol. It was then placed in a furnace and slowly heated to 1150°C to remove last traces of impurities and to remove stress. The platinum reference electrode was also placed inside an alumina tube for electric insulation. A tip of length 3 cm of the platinum rod was left outside the tube, so that the alumina protection tube did not come in contact with the melt.

The potential of this platinum reference electrode is not stable in the melt. This means that the measured potentials may change due to changes in the reference. This can be omitted if all potentials are referred to either magnesium deposition or chlorine evolution. In this work all potentials will be referred to the magnesium deposition potential and denoted with (Mg). The use of the Pt reference also resulted in that the potential varied somewhat with time. This is a big problem when doing potential step or similar measurements where a small, stable change in potential is needed. For cyclic voltammetry, the reference electrode is “stable enough”, i.e. it doesn’t change many mV during one cyclic scan, but can change several tenth’s of mV between scans done 2-3 minutes apart.

Table 3.2. Materials used for the electrodes.

Material	Quality	Supplier
Glassy carbon	GC-20S	Tokai, Japan
Graphite	Spectrotec 99.99%	Johnson Matthey
Platinum	99.99%	K. A. Rassmussen, Norway

3.3. Apparatus

The experimental set-up is shown schematically in Fig. 3.1. A platinum crucible was used as melt container. It was placed in the bottom of a quartz tube 350 mm deep. Radiation shields made of alumina was placed at regular intervals above the Pt crucible inside the quartz tube, and had holes to accommodate the stirring rod, salt charger or sample extraction tube, three electrodes and a thermocouple. To reduce effect of IR-drop in the melt during sweep voltammetry the working and reference electrodes were placed as close together as possible. The radiation shields were mounted on alumina rods, and separated by alumina tubes about 2 cm long. The stirring rod was made of alumina, with Pt covering the part immersed in the melt. The thermocouple was contained in an alumina tube for protection, and the immersed part was covered with Pt.

The entire cell assembly was placed inside a Kanthal tube tightly connected to the glove box. This tube was inserted into a cylindrical core of a Fibrothal RAC 100/500 wirewound, water-cooled furnace whose temperature was controlled by a proportional controller. The cell assembly was open to the glove box argon atmosphere.

Two different types of sample extraction tubes were used. One type was made of quartz and had a quartz sinter of porosity 3 (15-40 μm pore size) or 4 (4-15 μm pore size) at the end. The other type of tube was made of graphite and is shown in Fig. 3.2. It had a graphite filter with pore size 4-15 μm at one end and the other end was screwed onto an iron tube. The other end of the iron tube was connected to a syringe or a membrane pump used to suck melt into the sampling tube.

The working electrode was connected to a micrometer screw at the top of the lid. In this way it was possible to make small changes of the depth of immersion with high accuracy (± 0.1 mm). The electrochemical measurements were carried out using a PAR Model 273 Potentiostat/Galvanostat connected to a Toshiba (T3100e) computer using Par Model 270 Received Electrochemistry software 4.11.

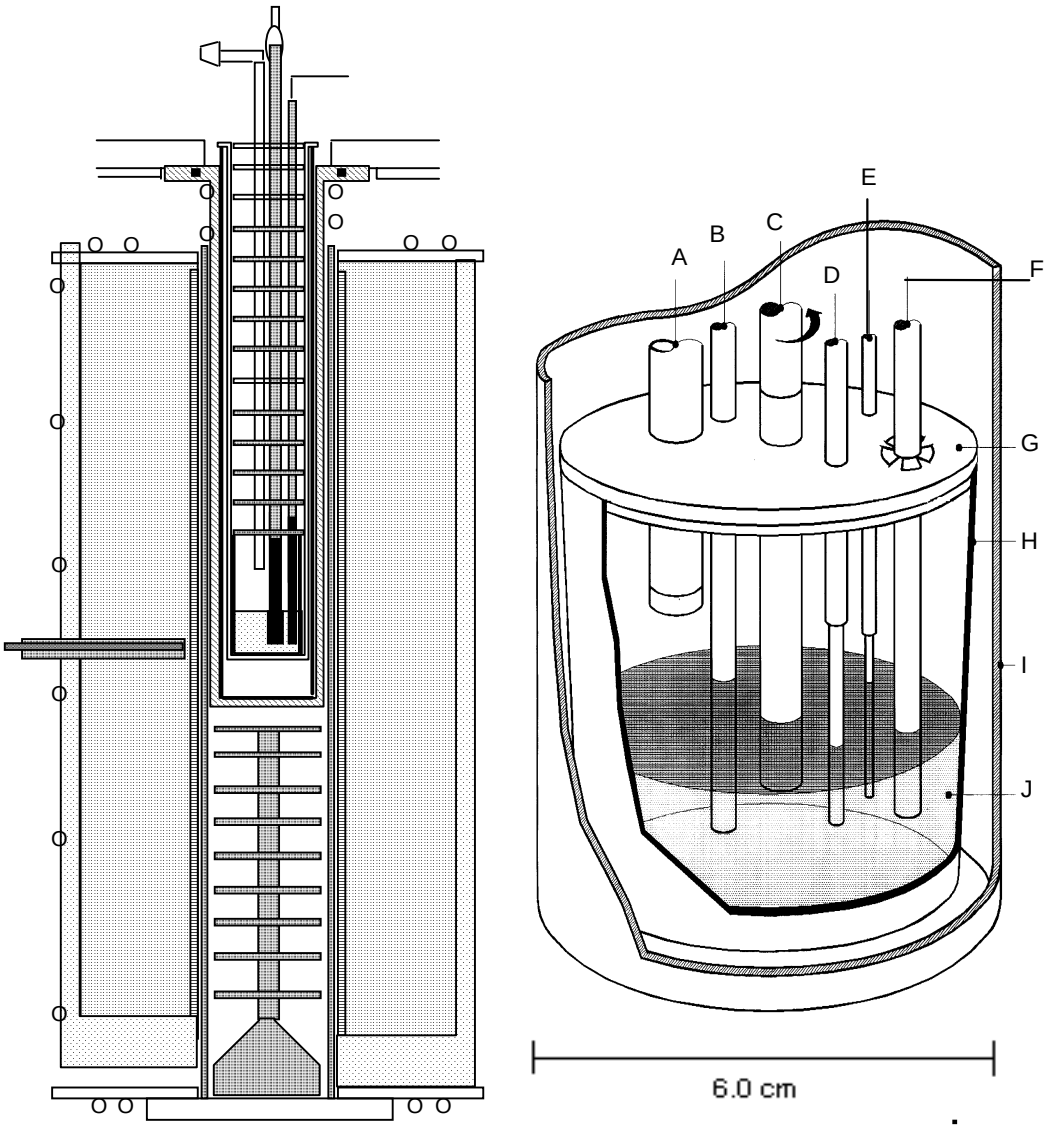

Figure 3.1. Experimental set-up: (A) quartz sampling tube; (B) graphite counter electrode; (C) stirrer; (D) glassy carbon indicator electrode; (E) platinum reference electrode; (F) thermocouple; (G) radiation shield; (H) platinum crucible; (I) quartz container; (J) melt.

a) b)

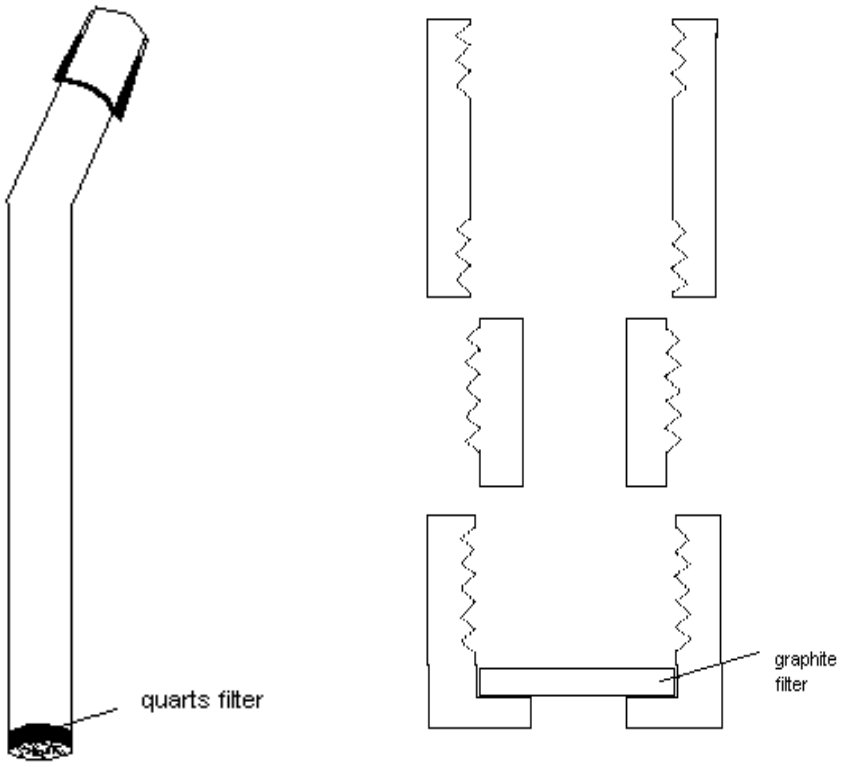

Figure 3.2. a) shows the quartz sampling tube. At the bottom the quartz filter can be seen and at the top the tube was connected to the syringe or membrane pump. b) shows the graphite sampling tube. At the bottom the graphite filter can be seen, and all parts were screwed tightly together and the upper part was screwed on to an iron tube connected to the membrane pump.

3.4. Procedure

All experiments were performed inside a argon filled glove box with water and oxygen content < 1 ppm and < 2 ppm, respectively. The entire cell assembly was heated to 870°C inside the glove box and left overnight. The temperature was reduced to 400°C before addition of the salts. For each experiment, between 100 and 120 g of salt was added to the Pt-crucible. The salt was melted and kept at the chosen experimental temperature for 24 hours

before the experiment was started. The different compositions of $MgCl_2$ and NaCl used are given in Tab. 3.3, and each composition was investigated at three different temperatures. The temperatures ranged from 475°C to 850°C.

Table 3.3. Compositions for the $MgCl_2$-NaCl binary melt.

Mole % $MgCl_2$
100
90
80
41.5
30
20
10

Tablets of MgOHCl were added to the liquid melt, and the content of hydroxide and oxide in the melt was measured as a function of time after addition. In some experiments the starting melt was free from oxygen, while for other experiments MgO(s) was added in excess of saturation. In this way some experiments were performed with a MgO saturated melt during decomposition of MgOHCl. The equilibration time for MgO saturation was determined by Boghosian et al.[13] to be around 20 hrs, depending on the composition of the $MgCl_2$ / NaCl melt.

Melt samples were withdrawn from the melt using the sampling device described in 3.3. The sampling device was kept just above the melt for a little while just prior to sample extraction to preheat the device to melt temperature. Then the tube end was dipped into the melt and the melt was sucked into the tube through the filter. Using the quartz sampling device, the sampling procedure was done as fast as possible (20 seconds) to keep SiO_2 from reacting with the melt. Using the graphite sampling device, the graphite filters had smaller pores and it took about 1 minute to get sufficient melt into the sampling tube. The samples were quenched by quickly raising the sampling tube into the cold part of the furnace or directly into the glove box.

The hydroxide and oxide contents in the solidified melt samples were determined by the carbothermal reduction analysis (Leco TC-436) and the acid consumption method (Iodometric titration). Samples for carbothermal reduction analysis were prepared immediately after sampling to avoid absorption of small amounts of water on the sample surface. When heated, water absorbed on a $MgCl_2$ containing melt will react with $MgCl_2$ and form

MgO and MgOHCl. It is thus not possible to distinguish between oxygen present in the melt and oxygen from water absorbed on the sample. A proper procedure for handling the hygroscopic sample is therefore very important[15]. The sampling tube was cut in as few parts as possible, and the remaining quartz or graphite was carefully brushed off the melt sample. The sample was split into small bits using an agate mortar. The samples being 0.1-0.2 g each were transferred into pre-weighted tin-capsules using a pair of tweezers. The tin-capsules were closed tight, the weight determined and put into numbered glass containers with plastic caps. 3 or 4 samples were prepared for each melt sample. The samples for analysis were transferred to the LECO instrument, and analysis performed immediately to avoid exposure of the salt in the tin-capsules to air.

The rest of the melt sample was used for iodometric titration. The sample was crushed to a fine powder in an agate mortar and samples of 0.5-1.5 g were put into marked glass containers and stored in the glove box until the next day. From 2 to 4 samples were made for each melt. The salt to be analysed was transferred to Pyrex bottles containing 10-30 ml of 0.005M HCl solution. The walls were flushed with distilled water, a magnet added and the bottles were covered with plastic film. The bottles were left overnight under magnetic stirring. In this way the samples dissolved. Blank samples were prepared in the exact same way. After dissolution 20 ml KI (18 g/l) and 20 ml KIO_3 (15 g/l) were added to the solutions and a dark orange colour appeared. The solutions were then titrated with 0.005M $Na_2S_2O_3$ until the colour was bright yellow. 2 ml soluble starch (2 g/l) was then added and a dark blue colour appeared. The solutions were then titrated further with sodium thiosulphate until the solutions became clear, and the amount of sodium thiosulphate used was registered. The blank solutions were titrated using the same procedure. The amount of basic oxygen in the melt, ppm O, measured as if all were in the form of OH^-, was then calculated using Eq. 2.9:

$$n_0^{bas}\left[ppmO^{2-}\right] = 10^3 * \frac{16 V_{HCl} c_{HCl} (1 - \frac{V_s}{V_b})}{m_{sample}} \qquad (2.9)$$

Voltammetric measurements were performed during each experimental run. Linear sweep voltammetry was run with a sweep rate of 200 mV/sec. This sweep rate had previously proven to give reproducible results in this type of melt[43]. Linear sweeps were done at regular intervals after addition of MgOHCl and just after a sample had been removed from the melt. Linear sweeps were also performed before addition of MgOHCl. For experiments starting with MgO-saturated melts, sweeps were done before and after

addition of MgO. Several linear sweeps in short order using different sweep rates can give information about diffusion control. This was done before addition of MgOHCl to the melt and at the end of the experiment. This was also tried during the experiment, but due to the rapid change in the concentration of MgOHCl dissolved in the melt these measurements did not give reliable data.

The area of the working electrode was determined by measuring the voltammetric current responses at different depths of immersion, as described in chapter 2.3. This determination was done both before and after the experiment. The area of the electrode changed after each melt sampling due to the reduction in the melt level after sampling. The area was therefore recalculated after each sampling. If the radii of the crucible and the electrode, the amount of melt withdrawn, and the melt density, are also known, the area change of the electrode can be found using Eq. 3.1:

$$\Delta A = \frac{m}{\rho \pi r_c} \bullet \pi r_e \tag{3.1}$$

where ρ is the density of the melt, m is the mass of melt withdrawn, r_c is the radius of the crucible and r_e is the radius of the electrode.

4. RESULTS AND DISCUSSION

4.1. Introduction

The dissolution and decomposition of MgOHCl in $MgCl_2$ - NaCl melts were studied as described in chapter 3. The purpose of this study was to find a relation between current density and concentration of MgOHCl dissolved in the melt. Different complexes of dissolved MgOHCl have been suggested in the literature: MgOHCl [4], $(MgOHCl)_2$ [12] and Mg_2OHCl_3 [8]. The dissolved MgOHCl complex is unstable at the temperatures of investigation and decomposes to MgO(s) or MgO(diss.) and HCl(g). HCl has a low solubility in chloride melts. Gas bubbles will form and the gas will leave the melt.

The melts studied varied over a wide range of compositions, from pure $MgCl_2$ to 10 mole % $MgCl_2$ / 90 mole % NaCl. Results will be given in separate subchapters. As discussed in 1.2.6 some preliminary investigations have been performed in similar systems, and it was found two current peaks when performing cyclic voltammetry in the cathodic region. It was suggested that the peak at about 0.4 V(Mg), i.e. 0.4 V positive of magnesium deposition, corresponds to the electrochemical reduction of MgOHCl while the peak at about 1.0 V(Mg) corresponds to the electrochemical reduction of a hydrogen containing species like HCl, H_2O or some C-H species. The electrochemical reactions are given by:

Reaction B: $$MgOH^+ + e^- = \tfrac{1}{2} H_2 \qquad (4.1)$$

Reaction C: $$H^+ + e^- = \tfrac{1}{2} H_2 \qquad (4.2)$$

This view has been adopted in this work too, and the data analysis is done on the basis that reaction B corresponds to the reduction of MgOHCl. A thorough discussion of this is done in 4.7 together with an outline of an alternative data treatment. In this alternative data treatment the possibility that both reaction B and C correspond to a two-step electrochemical reduction of a dimer, $(MgOHCl)_2$ is considered.

4.2. 100 mole % $MgCl_2$

4.2.1. Electrochemical measurements in cathodic range

A typical voltammogram obtained on a glassy carbon electrode in the cathodic range in pure molten $MgCl_2$ is given in Fig. 4.1. The magnesium deposition is observed as reaction A_1. By reversing the potential scan at the potential of magnesium deposition, a cyclic voltammogram is obtained and reaction A'_1, being typical for stripping of a deposit, is recorded. The prepeak A_2 corresponds to formation of a monolayer of magnesium on the electrode, and the reaction A'_2 is the stripping of this monolayer. The total current for the prepeak A_2 has been calculated to give the total number of coulombs transferred. The calculations show that approximately 1.5 monolayers of Mg were deposited. The electrochemical reactions observed are given by:

Reaction A_1 and A_2: $$Mg^{2+} + 2e^- = Mg \quad (4.3)$$

Reaction A_1' and A_2': $$Mg = Mg^{2+} + 2e^- \quad (4.4)$$

Addition of MgOHCl(s) to the pure $MgCl_2$-melt gives rise to two additional reactions in the cyclic voltammogram. These reactions are shown in Fig. 4.2 marked as B and C. Reaction C starts at about 1.2 V(Mg) with the current peak at about 1.0 V(Mg). B starts at about 0.7 V(Mg) and reaches maximum current at about 0.4 V(Mg). The cyclic voltammograms were recorded every few minutes, and it was observed that the highest current density values occurred within a few minutes after addition. The current densities then declined and disappeared after 3-5 hours, depending on temperature and the added amount of MgOHCl.

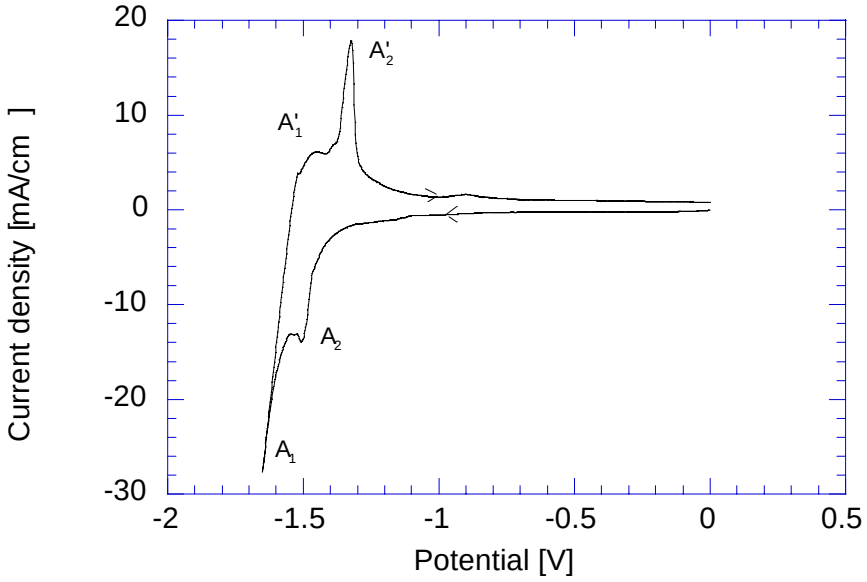

Figure 4.1. Cyclic voltammogram in the cathodic potential range obtained on a glassy carbon electrode in pure molten $MgCl_2$ at 728°C. Sweep rate: 200 mV/sec. Pt reference.

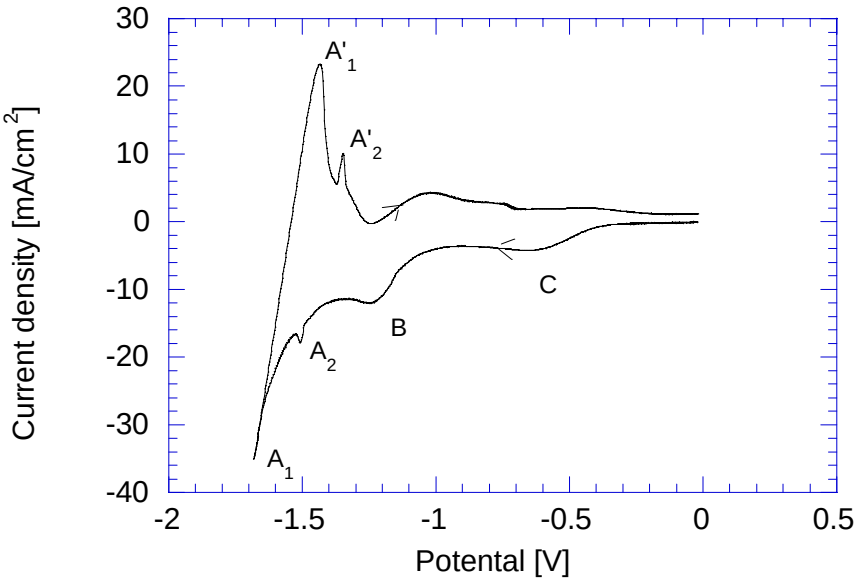

Figure 4.2. Cyclic voltammogram in the cathodic potential range obtained on a glassy carbon electrode in molten $MgCl_2$ after addition of MgOHCl at 728°C. Sweep rate: 200 mV/sec. Pt reference.

The current density for the electrochemical reaction is determined as the peak height of the wave, I_p, divided by the measured area of the working electrode. This value is corrected for the background current by subtracting the current density at the same potential before addition of MgOHCl to the melt. This is rather straight forward in the case of reaction C. In pure $MgCl_2$ the background current will be very close to zero, since there are no reactions going on at this potential, although some impurities in the melt may result in some background current. This procedure will give a accurate value for the current density of reaction C. It is not so easy to calculate the current density of reaction B. Due to the nature of cyclic voltammetry, the first of two peaks following each other will contribute to the current of the second peak. One has to know how the second peak, peak B, would appear without the interference of the first peak, peak C. This means that the shape of peak C and the potential difference between the two peaks must be known. If reaction C is a 1-electron reversible Nernstian wave the shape of peak C may be calculated according to Bard and Faulkner[48]. At constant temperature the shape of the current peak is only dependent on the number of electrons transferred in the electrochemical reaction, if the IR drop in the melt is negligible. The calculations of Bard and Faulkner were done at room temperature, while our measurements are done at high temperatures. A computer program for simulation of cyclic voltammetry, DigiSim[49], has therefore been used to simulate the shape of peak C at different temperatures. At constant temperature the contribution to peak B from reaction C is a fixed percentage of the current density of reaction C, if the potential difference between peak C and B is constant. To summarise: The true i_p from reaction B, i_p(B), is equal to the current density measured for peak B minus i_p(C)*x, where x, between 0 and 1, is dependent on temperature and the potential difference between peak C and B. In addition the background current must be subtracted and this current can be found from cyclic sweeps done prior to the addition of MgOHCl.

The current density of reaction B, i_p(B), has been measured in pure $MgCl_2$ at 728, 798 and 848°C as a function of time after addition of MgOHCl tablets to a melt free of MgO. The results are given in Fig. 4.3. In Fig 4.4 i_p(B) is plotted versus time after addition of MgOHCl to a melt initially saturated with MgO, at temperatures 728, 798 and 848°C. In order to compare i_p(B) for runs at different temperatures and for different amounts of MgOHCl added, the time scale is relative. For the run at 848°C the real time is plotted at the ordinate. For each of the runs at 728 and 798°C, respectively, the i_p(B) value measured after the addition is adjusted along the ordinate to a time where the i_p(B) values for both the run in question and the run at 848°C are of the same value. That is, the timescale is the same for all runs, but the starting position

is just shifted to more positive values for some runs. In this way the change in decomposition rate of the dissolved MgOHCl may be observed more easily. It can be observed that the decomposition rate is decreasing with decreasing temperature. The data are quite unambiguous as it can be observed both in melts initially free of MgO, as seen in Fig. 4.3, and in melts saturated with MgO, as seen in Fig. 4.4. Such behaviour is expected, since it is common that decomposition occurs faster at higher temperature.

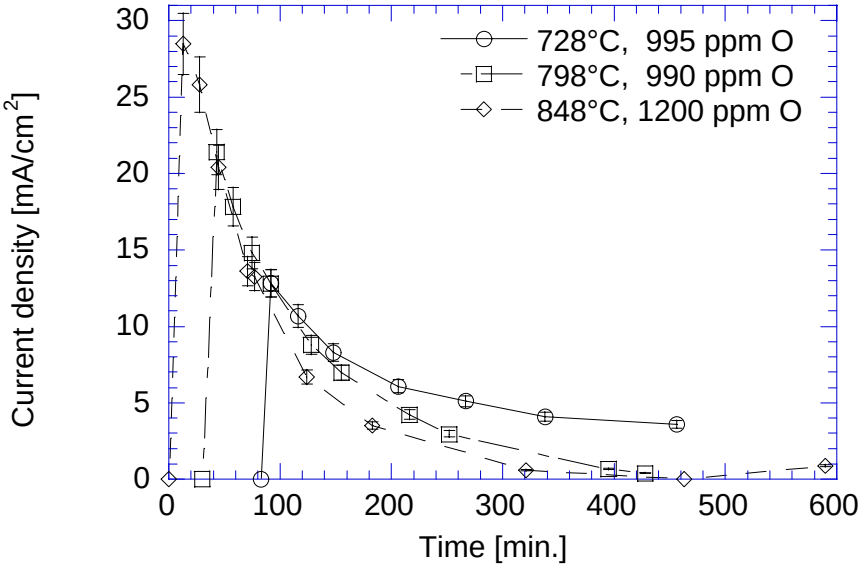

Figure 4.3. The cathodic current density of reaction B in pure $MgCl_2$ versus time after addition of MgOHCl(s). Added MgOHCl is measured as ppm O.

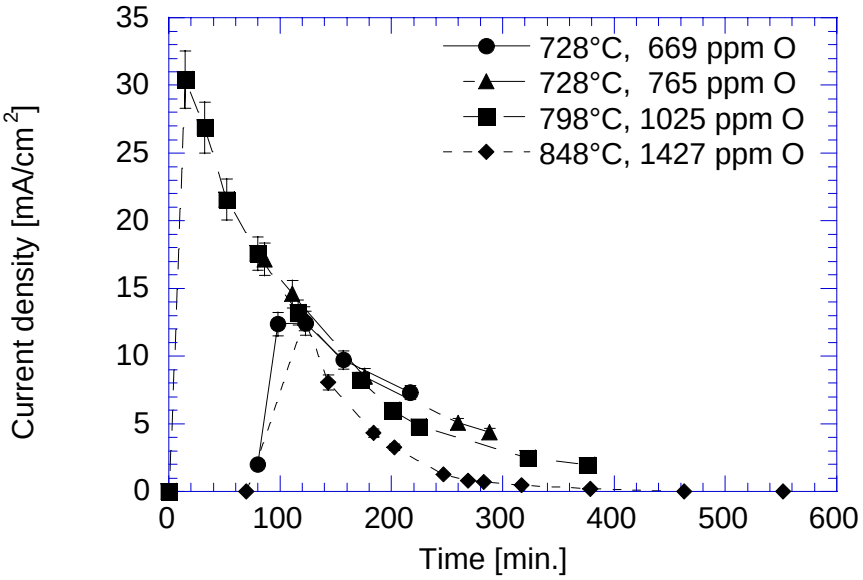

Figure 4.4. The cathodic current density of reaction B in $MgCl_2$ saturated with MgO versus time after addition of MgOHCl(s). Added MgOHCl is measured as ppm O. Batch 2 (▲) was added to batch 1 (●) after 139 minutes.

4.2.2. Analytical measurements

The concentrations of oxide and hydroxide in the $MgCl_2$ melt have been measured using the carbothermal reduction analysis and the acid consumption method. The carbothermal reduction analysis measures the total amount of oxygen in the melt, while the acid consumption analysis gives the basic oxygen. Using these two analysis methods in combination, as described in 2.2.3, one can obtain the concentration of MgOHCl. Samples for analyses were withdrawn from the melt before and at regular intervals after addition of MgOHCl. Using these data, diagrams showing concentration versus time after addition were made for the three different temperatures of investigation. These data are given in Fig. 4.5 for pure $MgCl_2$ melts, while data for $MgCl_2$ melts saturated with MgO are plotted in Fig. 4.6. It was difficult to obtain consistent analytical data. This is due to the experimental difficulties experienced with these highly hygroscopic samples. This is discussed in more detail in 4.6.2.

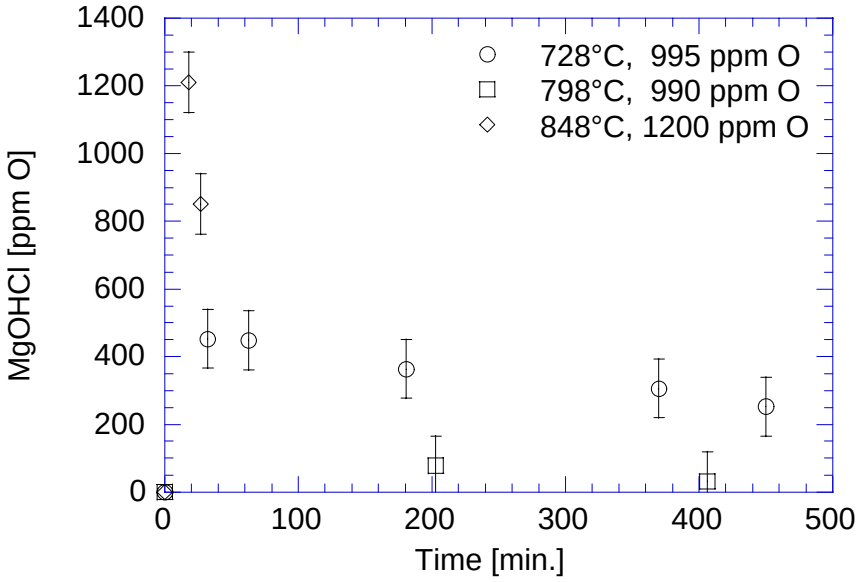

Figure 4.5. The concentration of MgOHCl(diss.) in pure $MgCl_2$ versus time after addition of MgOHCl(s). Added MgOHCl is measured as ppm O.

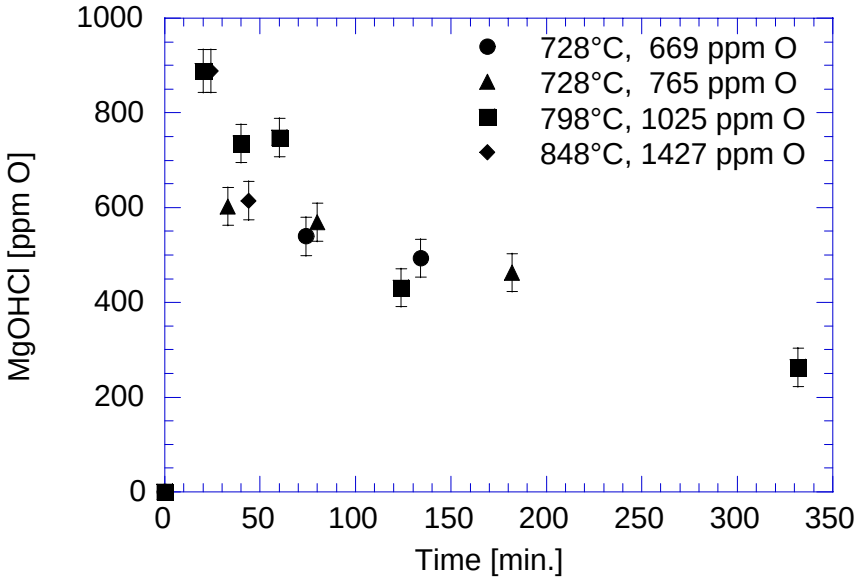

Figure 4.6. The concentration of MgOHCl(diss.) in $MgCl_2$ saturated with MgO versus time after addition of MgOHCl(s). Added MgOHCl is measured as ppm O. Batch 2 (▲) was added to batch 1 (●) after 139 minutes.

In Fig. 4.5 a rapid dissolution and decomposition of MgOHCl at 798 and 848°C can be observed, while the same reactions are much slower at 728°C. Too few measurements are available to give decomposition rates. This is due to difficulties in analysing the samples.

As in the MgO free melts, Fig. 4.6 indicates a rapid dissolution and decomposition at 798 and 848°C. At 728°C these reactions are much slower. These findings are in agreement with the electrochemical data obtained in the same melts, and in agreement with what one would expect.

It was mentioned in 2.2.3 that the two analytical methods in combination not only can give the amount of MgOHCl in the melt, but also the amount of MgO. It is therefore possible to observe that the dissolution of the added MgOHCl(s) and the decomposition of MgOHCl(diss.) occur simultaneously. This is shown in Fig. 4.7. Both the MgOHCl and MgO concentrations increase initially. After less than one hour the MgOHCl concentration starts to decrease while the MgO concentration continues to increase until the solubility limit is reached. Observe that the sum of the concentrations of MgOHCl and MgO gives about 800 ppm O, which is slightly less than represented by the amount of MgOHCl added. This may indicate that some MgO also precipitates initially when MgOHCl(s) decompose before it has time to dissolve.

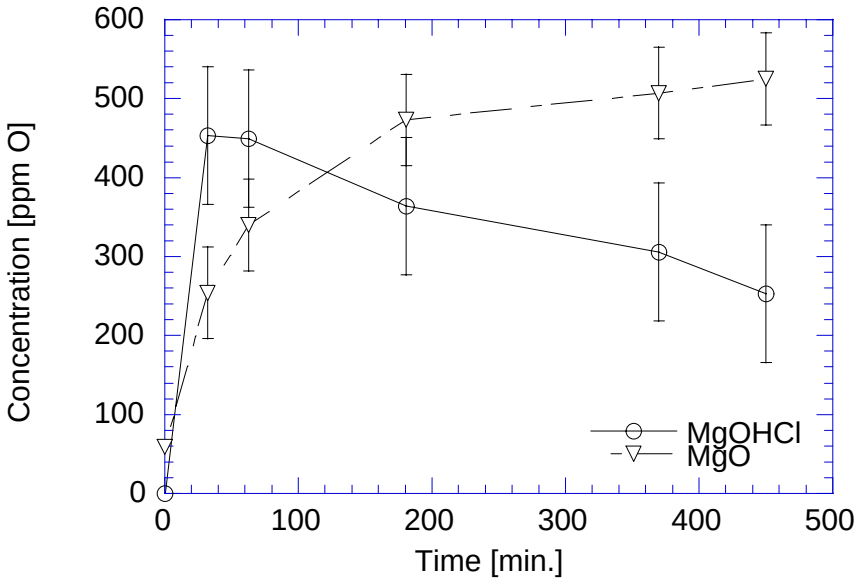

Figure 4.7. The concentration of MgOHCl (o) and MgO (∇) versus time after addition of MgOHCl(s) to a pure $MgCl_2$ melt at 728°C. Added MgOHCl: 995 ppm O.

4.2.3. Combination of results from cyclic voltammetry and analytical measurements

One of the aims of the present work is to establish the fundamental basis for cyclic voltammetry as an analytical tool during Mg production. Using this technique, concentrations of MgOHCl in the liquid $MgCl_2$ feed and in the electrolytic bath may be determined. In order to have a useful method current densities obtained by cyclic voltammetry need to be correlated with measured concentrations. This can be achieved using Eq. 2.1:

$$i_p = 0.4463\frac{(nF)^{3/2}}{(RT)^{1/2}}c^{\infty}D^{1/2}v^{1/2} \qquad (2.1)$$

According to this equation the current density should be proportional to the concentration. This means that a plot of current density versus concentration should be a straight line and it should pass through the origin. Results for all measurements (for both pure $MgCl_2$ melts and $MgCl_2$ melts saturated with MgO) are given in Fig. 4.8.

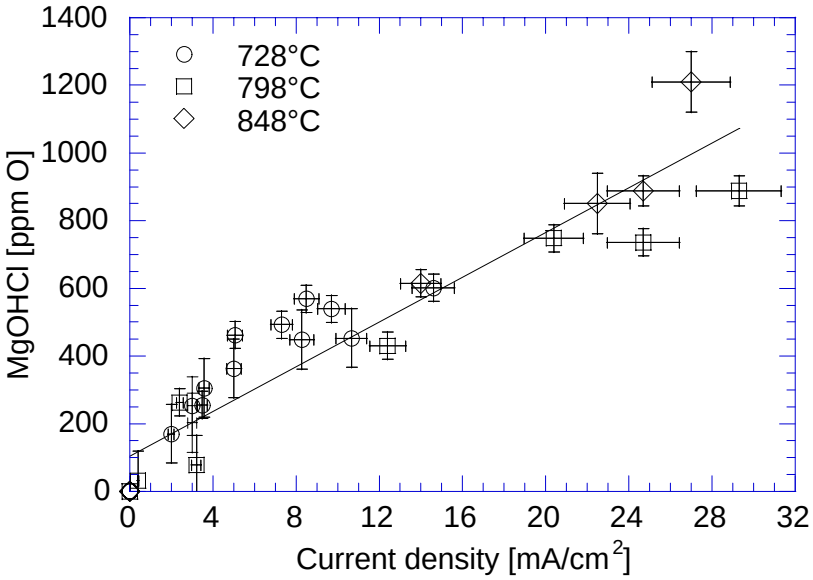

Figure 4.8. MgOHCl concentrations versus cathodic current density of reaction B in $MgCl_2$ melts at different temperatures. Solid line is the linear regression.

At first glance, it looks like there is a temperature effect for the data presented in Fig. 4.8. The data at 728°C indicate a steeper line than for those at higher temperatures. A closer inspection, however, shows that the line at 848°C falls between the lines for 728 and 798°C. This indicates that the data are not accurate enough to draw any conclusions related to the effect of temperature in the above correlation between concentration and current density. Accordingly one regression line is drawn through all data points for all temperatures. It should be noted that this line does not go through the origin.

4.2.4. Investigations in the anodic range and MgO analysis

Cyclic voltammetry was also performed in the anodic range in $MgCl_2$ melts. Typical voltammograms obtained on glassy carbon electrodes in pure molten $MgCl_2$ and in molten $MgCl_2$ with addition of MgOHCl(s) are given in Fig. 4.9 and 4.10, respectively. Chlorine evolution is observed as wave E, approximately 2.5V positive of Mg-deposition. At a potential slightly less positive than the chlorine evolution a wave D due to formation of CO or CO_2 from dissolved oxide is observed[40,41]. This wave is due to the electrochemical oxidation of MgO(diss.), and same peak is observed for both MgOHCl(s) and MgO(s) additions. This show that MgOHCl(diss.) decomposes to MgO(diss.)

and HCl(g). The peak current density is constant when the solubility limit of MgO is reached.

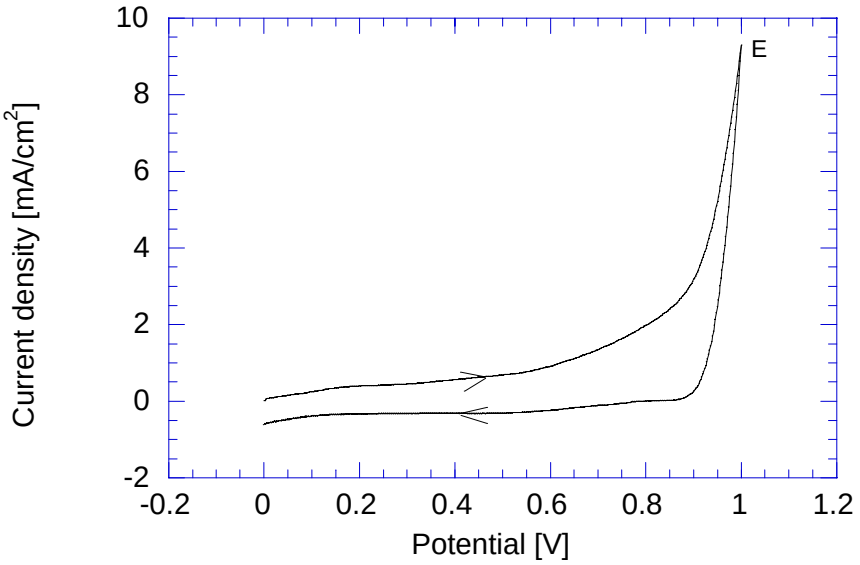

Figure 4.9. A typical cyclic voltammogram in the anodic range obtained on a glassy carbon electrode in molten $MgCl_2$ at 728°C, before addition of MgOHCl. Sweep rate: 200 mV/sec. Pt reference.

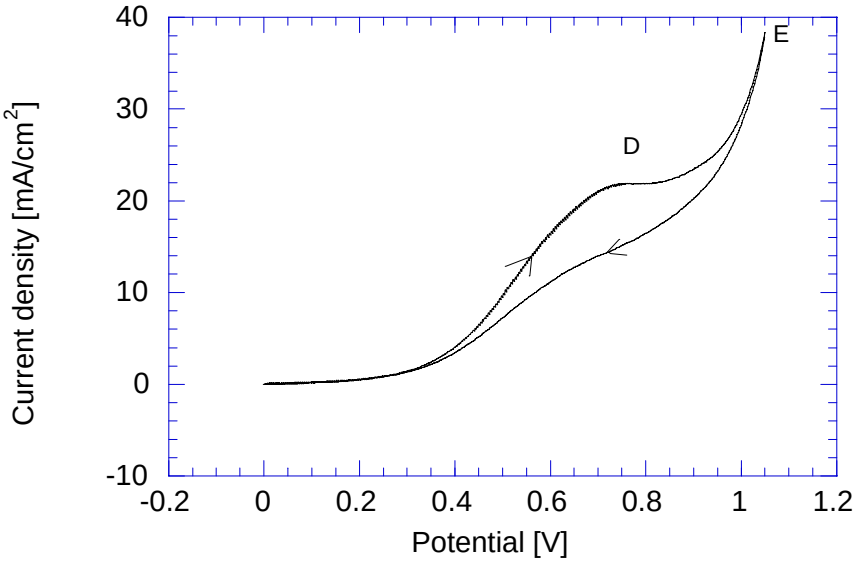

Figure 4.10. A typical cyclic voltammogram in the anodic range obtained on a glassy carbon electrode in molten $MgCl_2$ at 728°C, after addition of MgOHCl. Sweep rate: 200 mV/sec. Pt reference.

The electrochemical reactions observed are given by:

Reaction D: $$MgO + C = Mg^{2+} + CO + 2e^{-} \quad (4.5)$$

Reaction E: $$Cl^{-} = \tfrac{1}{2} Cl_2(g) + e^{-} \quad (4.6)$$

The current density for the oxidation of dissolved MgO-complex, i_p(D), is determined as the peak height of the wave, I_p, divided by the measured area of the working electrode. No correction for the Cl_2 current was made for the oxide peak since the Cl_2 background current is small at the potential of interest.

The average saturation concentrations measured using the acid consumption method were 615, 914 and 1018 ppm O at 728, 798 and 845°C, respectively. The MgO solubility has been reported by Boghosian et al[13] with similar results.

The concentration of MgO in the melt has been plotted versus the current densities for the anodic peak in Fig. 4.11. The data are obtained in two different ways, both giving the same result. In the first experiment MgOHCl(s) was added to the melt and the MgO concentration and current density were measured after equilibrium was reached. In the second experiment a known amount of MgO(s) was added to the melt and the MgO concentration and current density were measured after equilibrium was reached. For some experiments the anodic current density was also measured before equilibrium was reached. This was done to observe the increase in MgO concentration as MgOHCl(diss.) decomposed to MgO(s or diss.) and HCl(g). Unfortunately there seemed to be a shift in the potential at which MgO was reduced during the early stages of decomposition. This moved the reaction D closer to the Cl_2-evolution, making the peak height of reaction D difficult to measure. For these data a correction for the background current from the Cl_2 evolution peak was performed. Fig. 4.11 shows a linear correlation between anodic current density and the analysed amount of oxygen in the melt coming from MgO(s) additions or from decomposition of MgOHCl(diss).

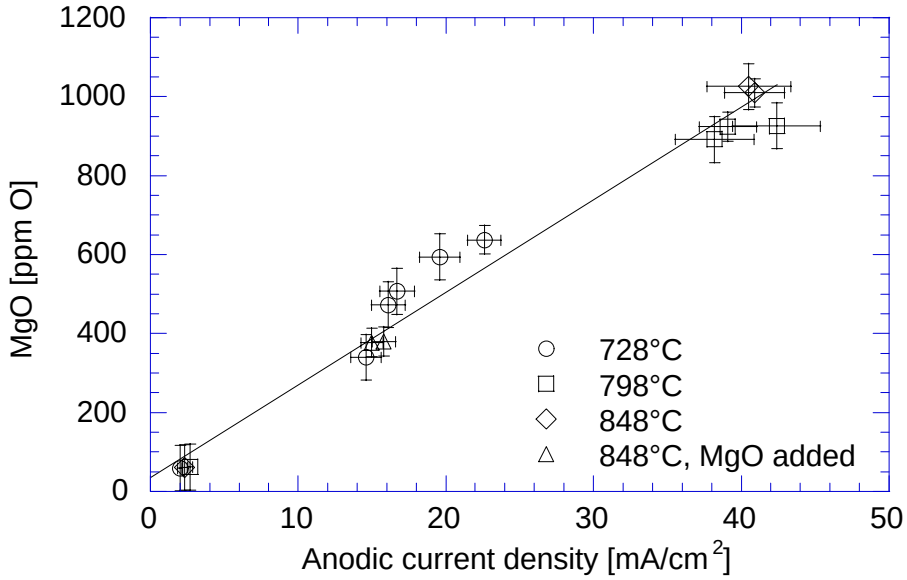

Figure 4.11. The concentration of MgO versus the anodic current density for $MgCl_2$ melts at different temperatures. For (o), (□) and (◊) MgOHCl(s) was added. For (Δ) a known amount of MgO(s) added. The solid line is the linear regression.

4.2.5. Diffusion coefficients

The current density of reaction B versus square root of sweep rate has been plotted to perform a diagnostic test of the electrochemical reaction. Such plots are not straightforward to make in this system since the concentration of MgOHCl is changing rapidly. The concentration is approximately constant during a single cyclic sweep, but not on the time span of several sweeps. Therefore the concentrations and current densities have to be recalculated to a common basis. Another problem observed was that the peak potential changed slightly with change in sweep rate. This resulted in a different background current at the peak potential and an increased uncertainty in the current density calculation. This makes such plots unreliable, and only a few plots have been made. One is shown in Fig. 4.12, and a straight line going almost through the origin can be observed. The electrochemical reaction may therefore be diffusion controlled, since such plots indicate diffusion controlled electrochemical reactions. The deviation from the origin may be due to some adsorption of either reactant or product.

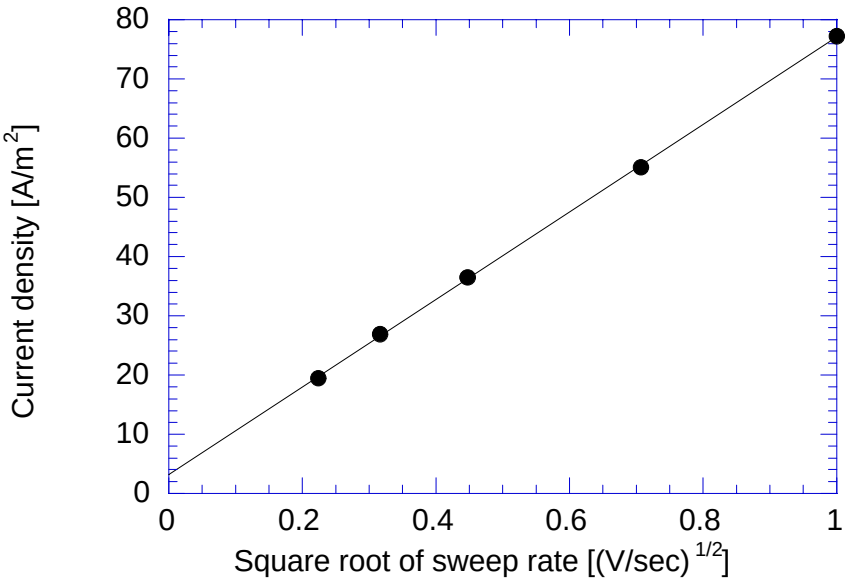

Figure 4.12. Cathodic current density of reaction B versus square root of sweep rate in a pure $MgCl_2$ melt at 728°C. The amount of oxygen from MgOHCl is 255 ppm O.

If a diffusion controlled reversible electrochemical reaction is established, the diffusion coefficient for the reacting specie can be calculated according to Eq. 2.1, if the concentration and current density of that species are known. Based on the presented data, D_{MgOHCl} has been calculated using the slope of the linear relationship between c and i_p given in Fig. 4.8. The results are presented in Tab. 4.1.

For the anodic reaction plots of current density versus square root of sweep rate are much simpler to make since the oxide-complex is stable in the melt, and the saturation concentration is at a measurable level. Two such plots are shown in Fig. 4.13. Diffusion control is observed, but the reaction is irreversible. For such reactions the coefficient, 0.4436, in Eq. 2.1 has to be changed to 0.35 [47]. This assumes a transfer coefficient, α, of 0.5, which is quite common. In the present work, diffusion coefficients have been calculated using the slope of the linear relationship between c and i_p given in Fig. 4.11, and the results are given in Tab. 4.1.

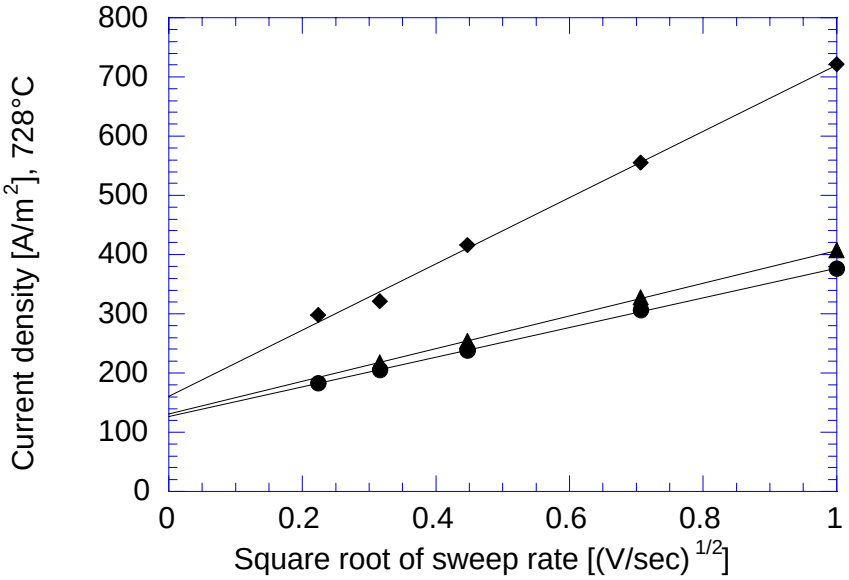

Figure 4.13. Anodic current densities versus square root of sweep rate in $MgCl_2$ melts saturated with MgO at 728 (▲, ●) and 848°C (♦).

Table 4.1. The diffusion coefficients of MgOHCl and MgO in $MgCl_2$ melts at different temperatures.

Melt composition [mole % $MgCl_2$]	**Temperature** [°C]	$\mathbf{D_{MgOHCl}}$ [$10^{-5}cm^2/sec$]	$\mathbf{D_{MgO}}$ [$10^{-5}cm^2/sec$]
100	728	1.9	0.8
	798	2.1	0.9
	848	2.3	0.9

4.3. Eutectic $MgCl_2$ - NaCl as solvent

4.3.1. Electrochemical measurements in the cathodic range

In melts containing sodium chloride, underpotential deposition of sodium occurs at the glassy carbon electrode. This gives a steady build up of current as the potential increases, since sodium starts to deposit at the electrode at potentials far more positive than the reversible deposition potential. A voltammogram recorded in an eutectic melt with no addition of MgOHCl(s) is shown in Fig. 4.14. Fig. 4.15 shows the same system after addition of

MgOHCl(s). In this plot two additional electrochemical reactions appear at potentials 0.9 (C) and 0.3V (B) positive of Mg deposition. The underpotential deposition of sodium makes it more difficult to make a correct reading of the current peaks, especially peak B. It can no longer be seen as a clear peak, as in Fig. 4.2. It shows up more like a current increase, or shoulder, on the existing current wave. Since there is no clear peak, the peak potential has been defined as the potential at which the curvature of the current plot is steepest. The potential is 0.33V positive of Mg deposition and is marked in Fig. 4.15. The same potential was used as peak potential for all voltammograms during the same experiment.

The peak height was corrected for the background current due to the underpotential deposition of sodium. This correction was done by visual correlation of voltammograms before and after addition of MgOHCl(s). The current density at the peak potential after addition of MgOHCl(s) was calculated, then the current density at the same potential before addition was subtracted from this value. The correction in the current due to reaction C was calculated by finding both the shape of peak C and the potential difference between the two peaks, as described in 4.2.1.

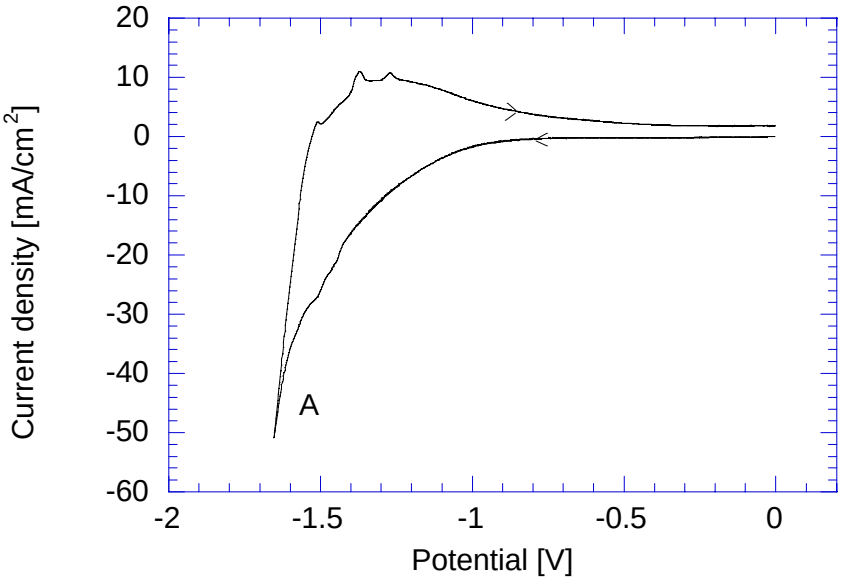

Figure 4.14. Cyclic voltammogram in the cathodic range obtained on a glassy carbon electrode in the eutectic $MgCl_2$ - NaCl melt at 730°C. Sweep rate: 200 mV/sec. Pt reference.

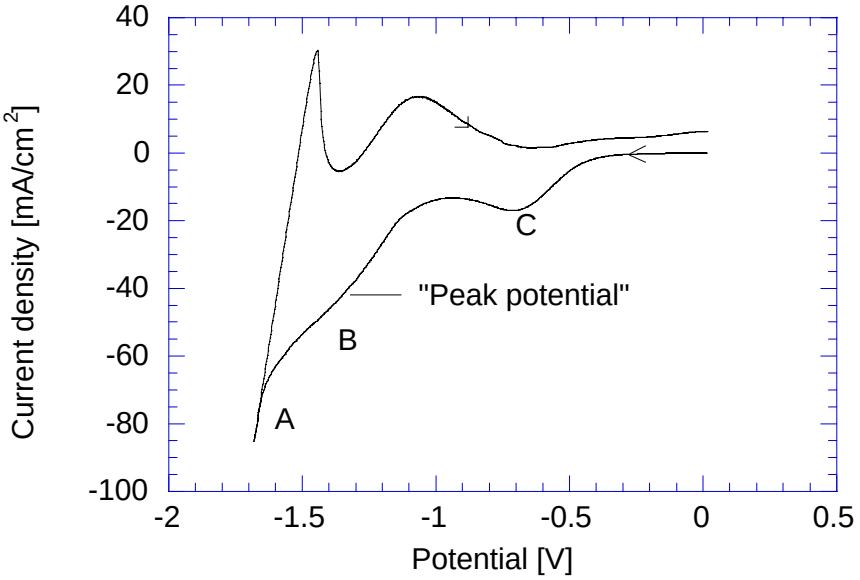

Figure 4.15. Cyclic voltammogram in the cathodic range obtained on a glassy carbon electrode in the eutectic $MgCl_2$ - NaCl melt with MgOHCl added at 730°C. Sweep rate: 200 mV/sec. Pt reference.

The current densities in the cathodic range have been measured as a function of time after addition of MgOHCl(s) to the eutectic $MgCl_2$ - NaCl melt. In Fig. 4.16 i_p(B) in the eutectic melts saturated with MgO is shown. The temperatures of investigation are 730 and 845°C. The time scale is relative as explained in 4.2.1. The run at 730°C is plotted with the real time as the ordinate, while the data set for 845°C are adjusted along the ordinate so that the measurement after addition of MgOHCl coincide with the ordinate of the 845°C run. This is done to allow for easier comparison of the decomposition rates at different temperatures. It can be seen that the decomposition rate is highest at 845°C, as expected. Another experiment was performed at 475°C, but the current density data from this experiment were disregarded due to passivation of the working electrode. It was not possible to perform experiments in melts free of MgO due to the low solubility of MgO in eutectic melts. The added $MgCl_2$ and NaCl contained enough oxygen to make the melt at least partly saturated with MgO. According to Bogoshian et al.[13] the solubility of MgO is approximately 75 ppm O at 730°C. Only melts saturated with MgO has therefore been investigated.

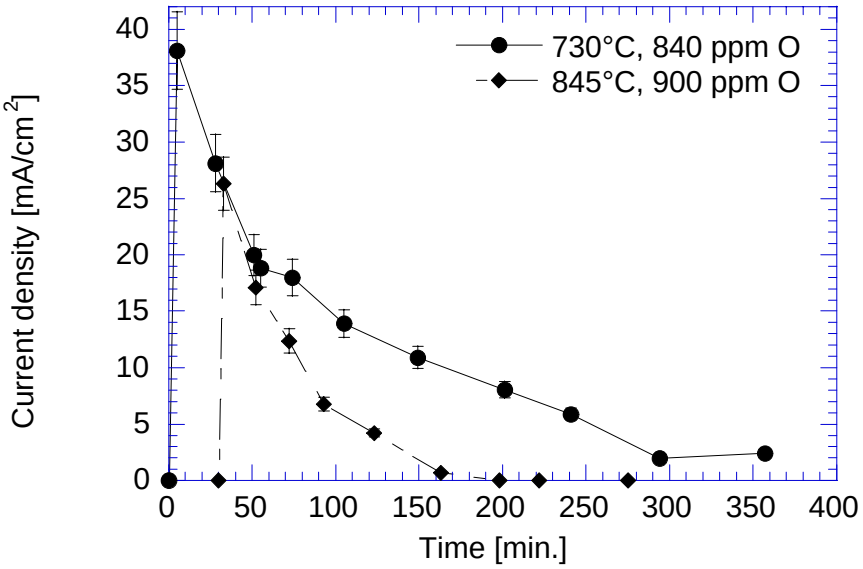

Figure 4.16. The cathodic current density of reaction B in MgO-saturated eutectic $MgCl_2$ - NaCl melts versus time after addition of MgOHCl(s). Added MgOHCl is measured as ppm O.

4.3.2. Analytical measurements

Concentration measurements of oxide and hydroxide in the eutectic $MgCl_2$ – NaCl melt have been performed using carbothermal reduction and acid consumption analysis. Samples for analysis were withdrawn from the melt at regular intervals after addition of MgOHCl(s). It was easier to obtain consistent analytical data in this study than for pure $MgCl_2$. This is believed to be due to the less hygroscopic eutectic melt. In melts saturated with MgO, the MgOHCl concentration can be found from either of the analytical methods, since the saturation concentration of MgO is well known. Using these data, diagrams showing concentration versus time after addition were made for the three different temperatures of investigation. These data are given in Fig. 4.17. The temperatures of investigation were 475, 730 and 845°C.

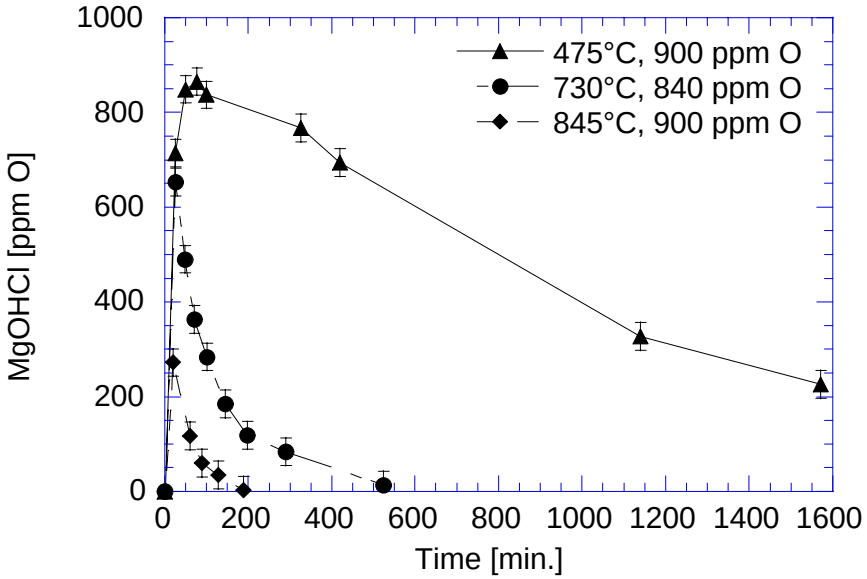

Figure 4.17. The concentration of MgOHCl(diss.) in eutectic $MgCl_2$ - NaCl melts saturated with MgO versus time after addition of MgOHCl(s). Added MgOHCl is measured as ppm O.

It can be observed that the decomposition is quite fast at high temperatures and it decreases considerably with decreasing temperature. When the eutectic melt was kept at 475°C, MgOHCl(diss.) can be observed in the melt for a long time, and it is still present in the melt 24 hours after addition.

4.3.3. Combination of results from cyclic voltammetry and analytical measurements

In Fig. 4.18 the current density of reaction B is plotted versus the concentration of MgOHCl in MgO saturated eutectic $MgCl_2$ – NaCl melts. The temperatures of investigation were 730 and 845°C. A linear regression line is drawn using data points at both temperatures. The line passes through the origin. This is in agreement with Eq. 2.1. No temperature effect can be observed in the temperature range investigated.

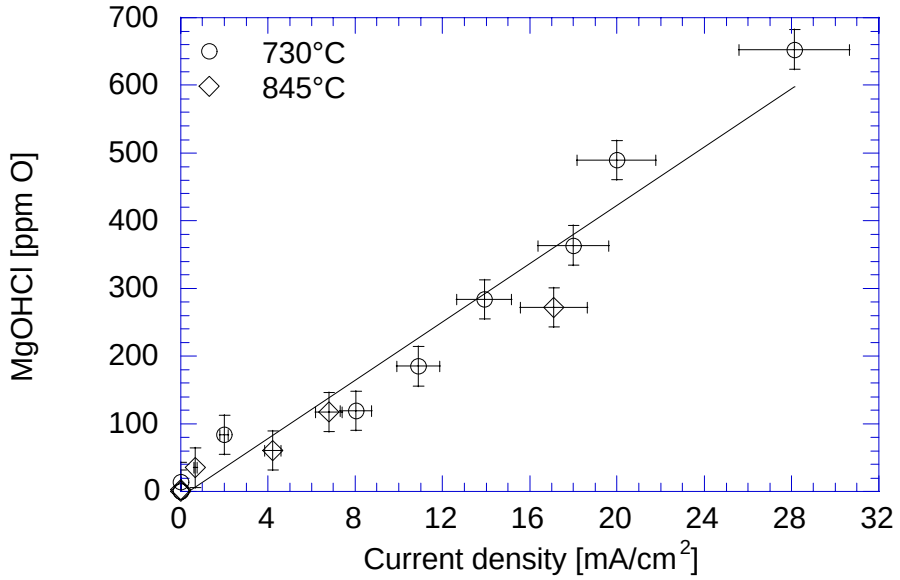

Figure 4.18. MgOHCl concentrations versus cathodic current density of reaction B in eutectic $MgCl_2$ - NaCl melts. Different symbols represent different experimental runs. The solid line is the linear regression.

4.3.4. Anodic current densities and MgO analysis

The anodic current density has also been measured in the eutectic. Due to the low solubility of MgO in the eutectic melt, only saturated melts and melts without additions of MgO(s) or MgOHCl(s) have been measured.

The average saturation concentrations measured using the acid consumption method were 88 and 72 ppm O at 730 and 845°C, respectively. These are in the same range as the value of 75 ppm O at 730°C reported by Boghosian et al[13]. The lower solubility obtained at the higher temperature may just be a reflection of experimental difficulties.

A plot of MgO concentration versus current density for equilibrated melts is given in Fig. 4.19. The slope of the regression line through these points can be used to calculate the diffusion coefficient for the MgO species in the eutectic melt.

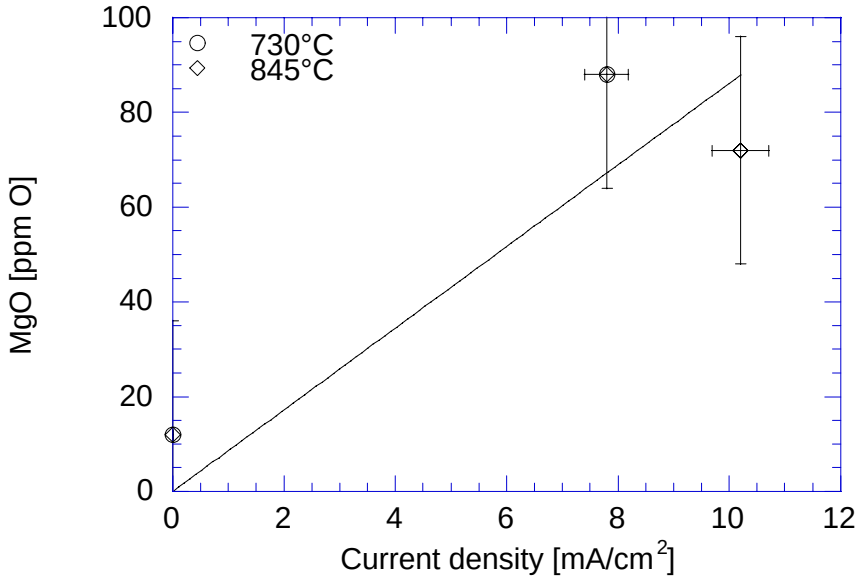

Figure 4.19. The concentration of MgO versus the anodic current density for the eutectic $MgCl_2$ – NaCl melts at different temperatures. The solid line is just an estimate of the relationship between MgO concentration and current density.

4.3.5. Diffusion coefficients

Assuming a diffusion controlled reversible electrochemical reaction as in pure $MgCl_2$, the diffusion coefficient for the reacting species can be calculated according to Eq. 2.1. The slope of the linear relationship between c and i_p in Fig. 4.18 has been used in the equation. The diffusion coefficient of MgO has also been calculated using Eq. 2.1 and the line shown in Fig. 4.19. The results are presented in Tab. 4.2.

Table 4.2. The diffusion coefficients of MgOHCl and MgO in eutectic $MgCl_2$ – NaCl melts at different temperatures.

Melt composition [mole % $MgCl_2$]	**Temperature** [°C]	**D_{MgOHCl}** [10^{-5}cm^2/sec]	**D_{MgO}** [10^{-5}cm^2/sec]
41.5	730	4.7	6
	845	5.6	7

4.4. 90 and 80 mole % $MgCl_2$ containing melts as solvents

4.4.1. Electrochemical measurements in the cathodic range

The interpretation of the current data obtained in these melts was also difficult, but less so than for the data in the eutectic. There was some underpotential deposition of sodium, but not as severe as in the eutectic melts. Both reactions, B and C, were clearly shown after addition of MgOHCl(s). An example is shown in Fig. 4.20. This figure shows a voltammogram recorded in a 80 mole % $MgCl_2$ melt after addition of MgOHCl(s). The two electrochemical reactions appear at potentials 0.95 and 0.33V positive of Mg deposition, respectively. Still, some underpotential deposition of sodium can be observed.

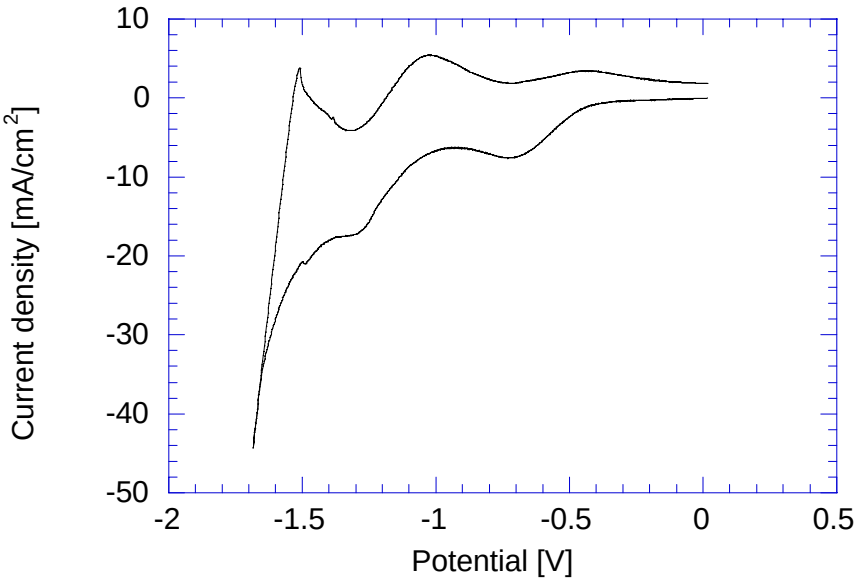

Figure 4.20. Cyclic voltammogram in the cathodic range obtained on a glassy carbon electrode in 80 mole % $MgCl_2$ after addition of MgOHCl(s) at 733°C. Sweep rate: 200 mV/sec. Pt reference.

At the same time, the uncertainties in the carbothermal reduction and acid consumption analysis are less than for pure $MgCl_2$ due to the less hygroscopic melt. As explained in 4.3.2, sodium present in the melt samples seemed to reduce the standard deviations in the analysis. Nevertheless, several of the experimental runs had to be disregarded due to difficulties obtaining consistent analytical data. For these experiments only the current density data has been used.

The current densities in the cathodic range have been measured as a function of time after addition of MgOHCl. In Figs. 4.21 and 4.22, i_p(B) in the respective binaries has been plotted versus time after addition of MgOHCl. The temperatures of investigation in the 90 mole % binary are 741, 743, 800 and 842°C and in the 80 mole % binary 730 and 847°C. The time scales are relative as explained earlier. This is done to allow for easier comparison of the decomposition rates at different temperatures.

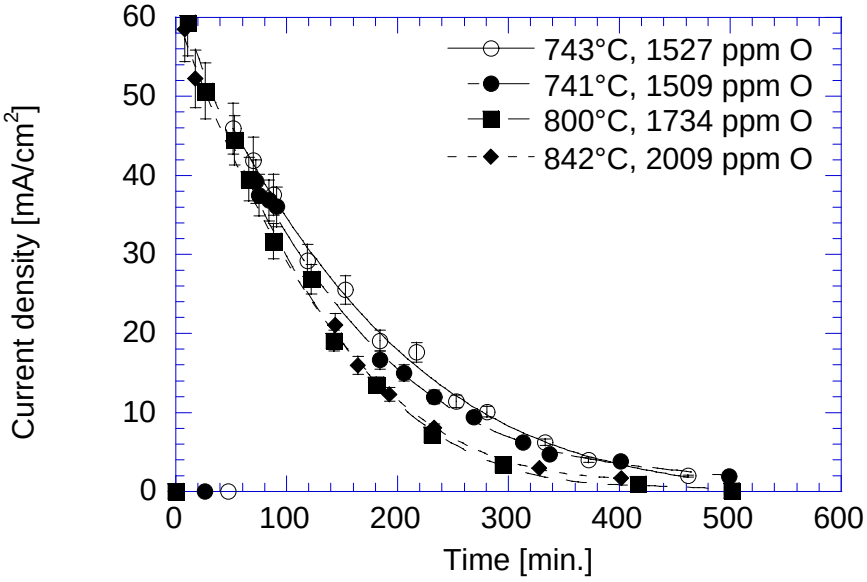

Figure 4.21. The cathodic current density of reaction B versus time after addition of MgOHCl(s) to the $MgCl_2$ - NaCl binary containing 90 mole % $MgCl_2$. Added MgOHCl is measured as ppm O. Open symbols represent melts initially free of MgO, while full symbols represent melts initially saturated with MgO. The drawn lines are regression lines.

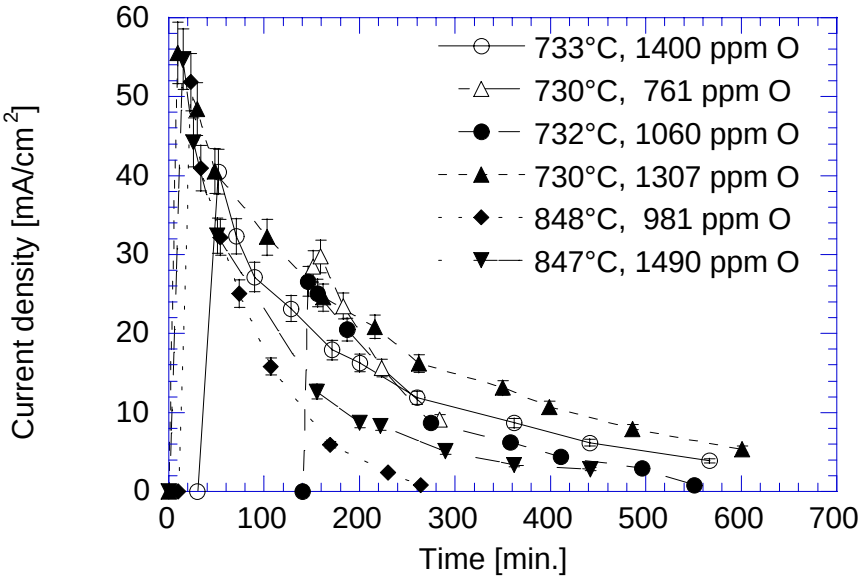

Figure 4.22. The cathodic current density of reaction B versus time after addition of MgOHCl(s) to the $MgCl_2$ - NaCl binary containing 80 mole % $MgCl_2$. Added MgOHCl is measured as ppm O. Open symbols represent melts initially free of MgO, while full symbols represent melts initially saturated with MgO.

For the 90 mole % $MgCl_2$ binary it is not possible to observe any difference in the decomposition rates between 800 and 842°C. At 742°C the decomposition rate, however, is somewhat lower. For the 80 mole % $MgCl_2$ binary there is some scatter in the data, but the general trend is that the decomposition rate is higher at higher temperature.

4.4.2. Analytical measurements

Concentrations of oxide and hydroxide have also been measured using carbothermal reduction and acid consumption analyses. Samples for analysis were withdrawn from the melt at regular intervals after addition of MgOHCl(s). Both melts have been investigated initially free of MgO and saturated with MgO. In Figs. 4.23 and 4.24 the concentration of MgOHCl is plotted versus time after addition of MgOHCl.

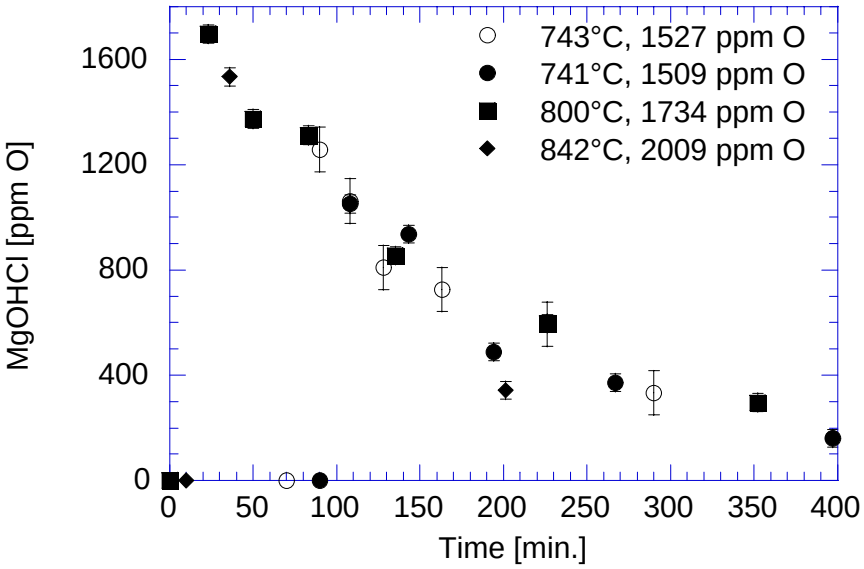

Figure 4.23. The concentration of MgOHCl versus time after addition of MgOHCl to the $MgCl_2$ – NaCl binary containing 90 mole % $MgCl_2$. Added MgOHCl is measured as ppm O. Open symbols represent melts initially free of MgO, while full symbols represent melts initially saturated with MgO.

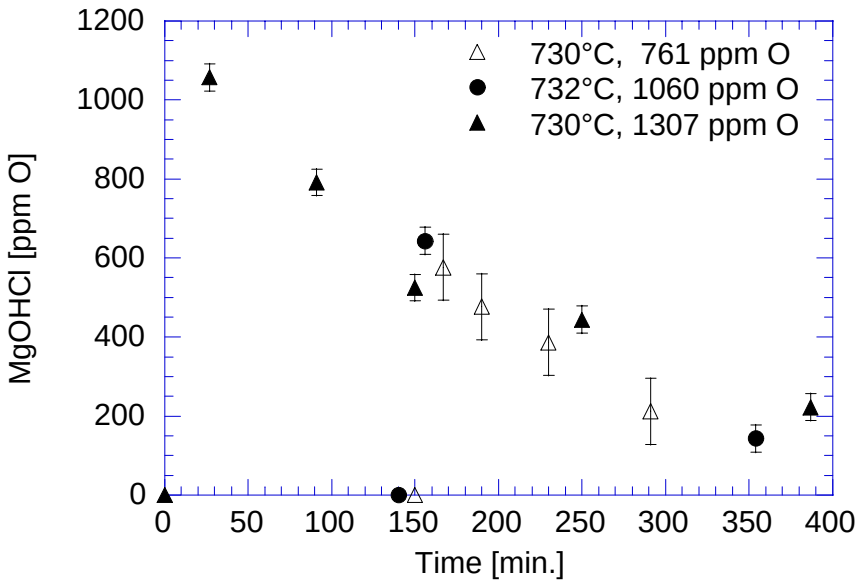

Figure 4.24. The concentration of MgOHCl versus time after addition of MgOHCl to the $MgCl_2$ – NaCl binary containing 80 mole % $MgCl_2$. Added MgOHCl is measured as ppm O. Open symbols represent melts initially free of MgO, while full symbols represent melts initially saturated with MgO.

The data in Fig. 4.23 show the same trends in the decomposition rates versus temperature as observed earlier, but the picture is less clear than observed earlier.

4.4.3. Combination of results from cyclic voltammetry and analytical measurements

In Figs. 4.25 and 4.26 the current density is plotted versus the concentration of MgOHCl. For both melt compositions a linear regression line is drawn using all data points available. The lines go through the origin. This is in agreement with Eq. 2.1. No temperature effect can be observed in the temperature range investigated as was also observed earlier.

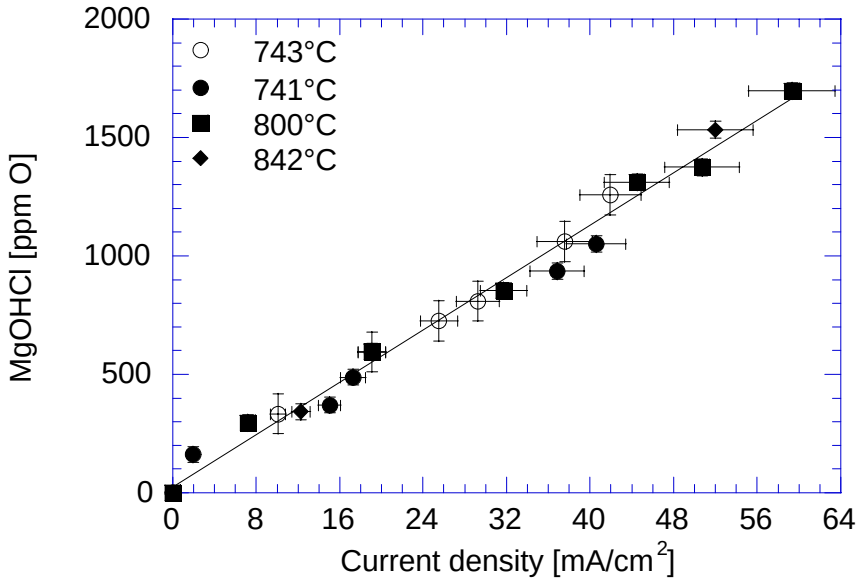

Figure 4.25. Concentration versus current density in the $MgCl_2$ – NaCl binary containing 90 mole % $MgCl_2$. Different symbols represent different experimental runs. The solid line is the linear regression.

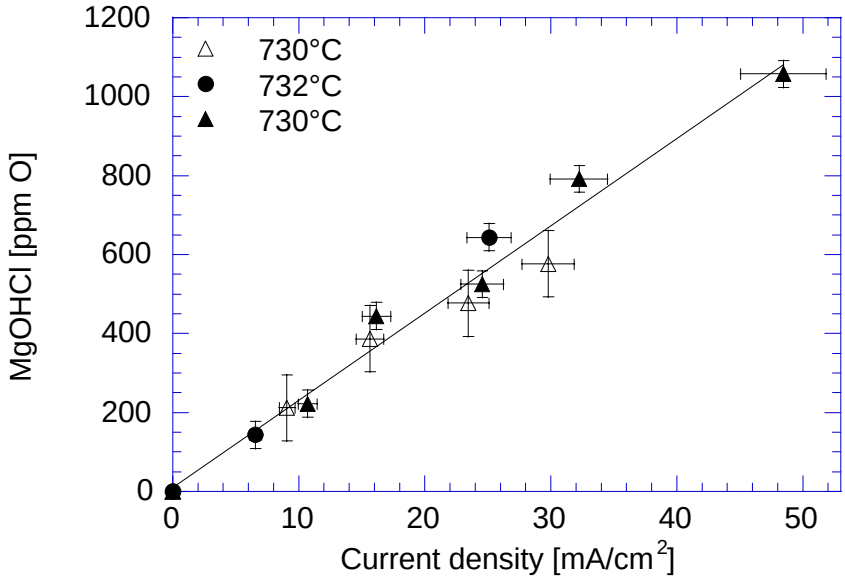

Figure 4.26. Concentration versus current density in the $MgCl_2$ – NaCl binary containing 80 mole % $MgCl_2$. Different symbols represent different experimental runs. The solid line is the linear regression.

It can be observed that the agreement between current density and concentration is much better for both binaries than for pure $MgCl_2$. A contributing factor to this is the easier analysis of melt samples, giving higher accuracy. The underpotential deposition of sodium is still small enough to allow the current density of reaction B to be easily measured.

4.4.4. Anodic current density and MgO analysis

The anodic current density has also been measured. For the 90 mole % $MgCl_2$ binary the average saturation concentrations measured using the acid consumption method were 689, 745 and 1041 ppm O at 741, 800 and 842°C, respectively. For the 80 mole % $MgCl_2$ binary the average saturation concentrations measured using the acid consumption method were 537 and 662 ppm O at 732 and 847°C, respectively. These data are in the same range as reported by Boghosian et al[13].

The plots of the MgO concentration versus current density for the two melts are given in Figs. 4.27 and 4.28. The slope of the regression lines through the data points can be used to calculate the diffusion coefficient for the MgO species.

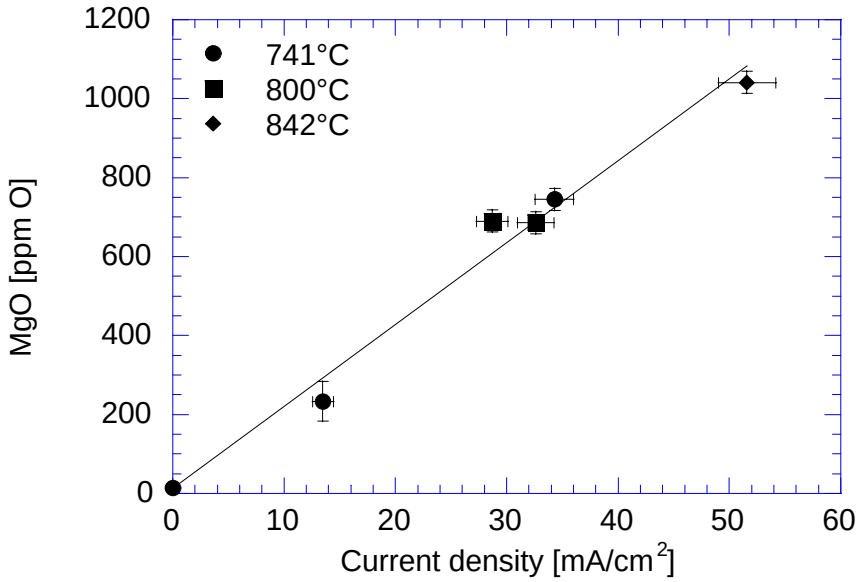

Figure 4.27. The concentration of MgO versus the anodic current density for the 90 mole % $MgCl_2$ binary at different temperatures. The solid line is the linear regression forced through the origin.

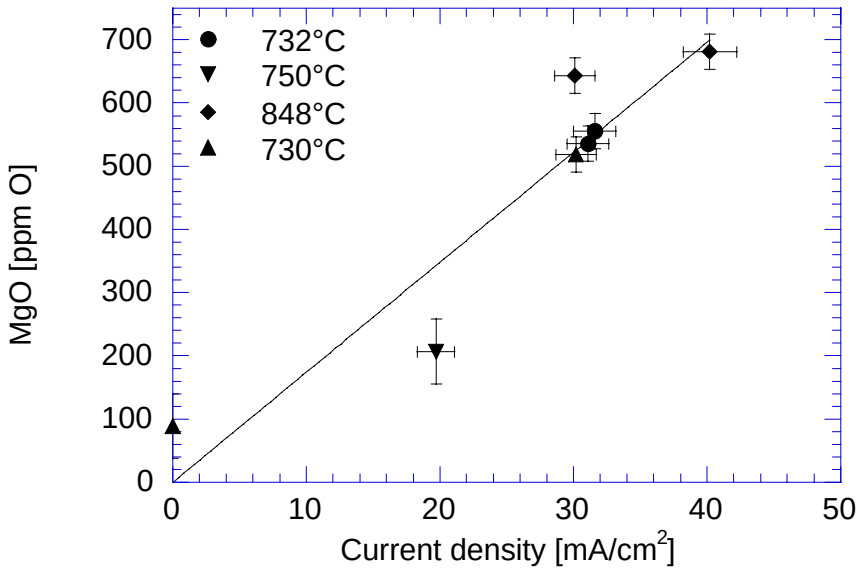

Figure 4.28. The concentration of MgO versus the anodic current density for the 80 mole % $MgCl_2$ binary at different temperatures. The solid line is the linear regression forced through the origin.

4.4.5. Diffusion coefficients

Assuming a diffusion controlled reversible electrochemical reaction as in pure $MgCl_2$, the diffusion coefficients for the reacting specie can be calculated according to Eq. 2.1. The slopes of the linear relationship between c and i_p shown in Figs. 4.25 and 4.26 have been used. The diffusion coefficients of MgO in these melts have also been calculated using Eq. 2.1 and the slopes of the linear relationship between c and i_p shown in Figs. 4.27 and 4.28. The results are presented in Tab. 4.3.

Table 4.3. The diffusion coefficients of MgOHCl and MgO in the 90 and 80 mole % $MgCl_2$ binary melts at different temperatures.

Melt composition [mole % $MgCl_2$]	**Temperature** [°C]	$\mathbf{D_{MgOHCl}}$ [$10^{-5}cm^2/sec$]	$\mathbf{D_{MgO}}$ [$10^{-5}cm^2/sec$]
90	741	2.7	0.9
	800	3.0	1.0
	842	3.2	1.1
80	730	4.2	1.4
	847	5.0	1.6

4.5. 30, 20 and 10 mole % $MgCl_2$ containing melts as solvent

4.5.1. Electrochemical measurements in the cathodic range

Current measurements done in the binary $MgCl_2$ – NaCl melts containing 30, 20 and 10 mole % $MgCl_2$ were increasingly difficult to analyse. The peak B was obscured by the high sodium underpotential deposition current, and no clear peaks could be observed. All that could be observed was a current increase in the potential range where peak B was found in melts with higher concentration of $MgCl_2$. This increased the error in i_p(B) considerably as can be observed in Fig. 4.29. This melt contains 30 mole % $MgCl_2$. Even though the results within one experiment were reproducible, the reproducibility between different experiments was not good. This was most pronounced for the 10 mole % $MgCl_2$ binary.

On the other hand the analytical data in these melts have lower standard deviations than for melts with higher content of $MgCl_2$ in agreement with earlier observations. The extremely low saturation concentration of MgO is one reason for this. According to Boghosian et al.[13] the saturation

concentration is 25 ppm O for the 30 mole % $MgCl_2$ melt, and the solubility is decreasing with decreasing $MgCl_2$ content.

The current densities in the cathodic range have been measured as a function of time after addition of MgOHCl(s). In Figs. 4.30, 4.31 and 4.32, i_p(B) in the respective binaries are shown. The temperatures of investigation in the 30 mole % binary were 730, and 850°C, in the 20 mole % binary 801°C and in the 10 mole % binary 798 and 850°C. The time scales are relative as explained in 4.2.1. This is done to allow for easier comparison of the decomposition rates at different temperatures.

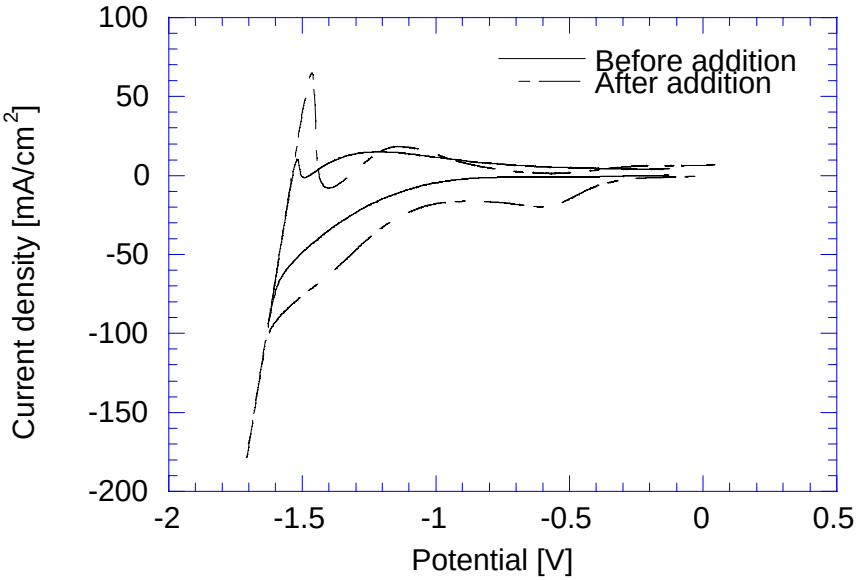

Figure 4.29. Cyclic voltammograms in the cathodic range on glassy carbon working electrodes in a 30 mole % $MgCl_2$ melt at 730°C, before and after addition of MgOHCl(s). Sweep rate: 200 mV/sec.

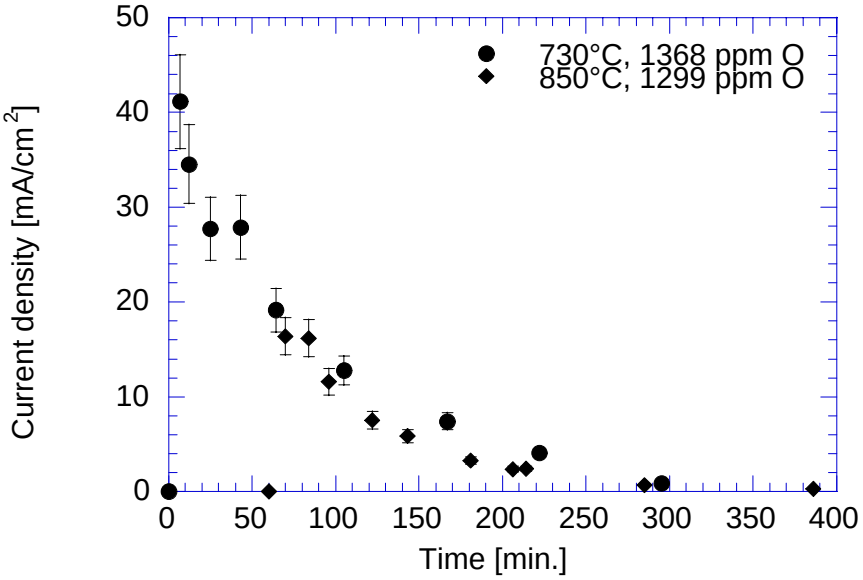

Figure 4.30. The cathodic current density of reaction B in a MgO-saturated 30 mole % $MgCl_2$ melt versus time after addition of MgOHCl(s). Added MgOHCl is measured as ppm O.

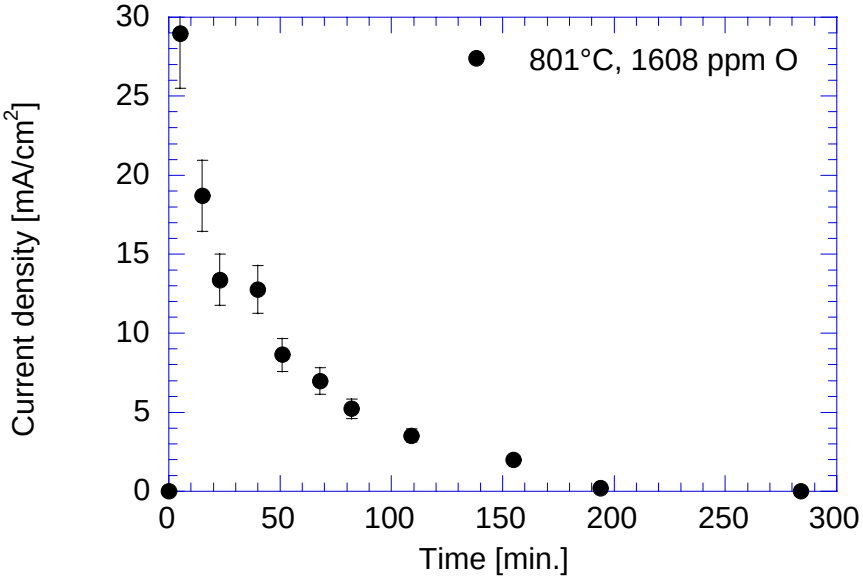

Figure 4.31. The cathodic current density of reaction B in a MgO-saturated 20 mole % $MgCl_2$ melt versus time after addition of MgOHCl(s). Added MgOHCl is measured as ppm O.

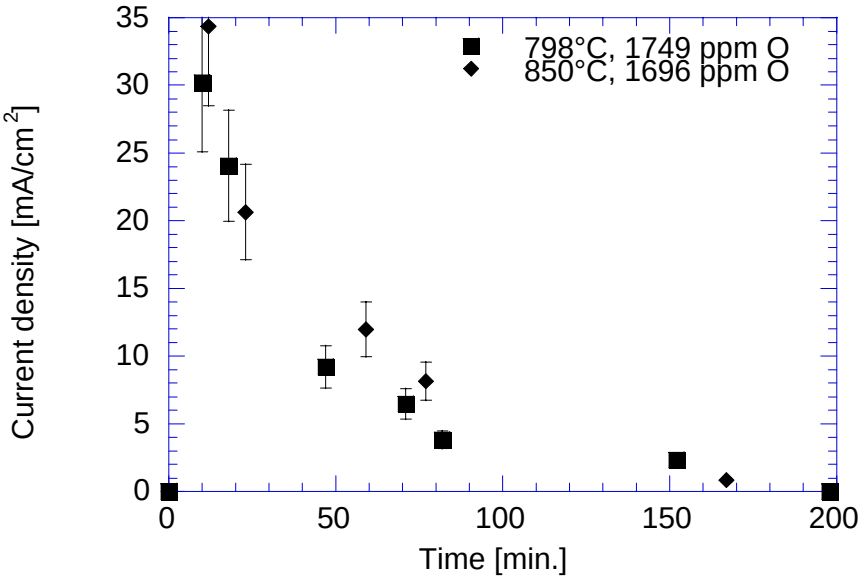

Figure 4.32. The cathodic current density of reaction B in a MgO-saturated 10 mole % $MgCl_2$ melt versus time after addition of MgOHCl(s). Added MgOHCl is measured as ppm O.

In the 30 mole % $MgCl_2$ binary the dissolution and decomposition reaction seems to be somewhat faster at 850°C than at 730°C. In the 20 mole % $MgCl_2$ melt only one temperature was investigated successfully and thus no conclusions can be drawn on the temperature dependency. In the 10 mole % $MgCl_2$ melt the decomposition reaction is measured to be slower at higher temperature. This cannot be correct and must be due to experimental difficulties coming from the large underpotential deposition of sodium.

4.5.2. Analytical measurements

Concentration measurements of oxide and hydroxide in the 30, 20 and 10 mole % $MgCl_2$ binaries have been performed using carbothermal reduction and acid consumption analyses. Samples for analysis were withdrawn from the melt at regular intervals after the addition of MgOHCl(s) to the melt. Only melts initially saturated with MgO have been investigated. In Figs. 4.33, 4.34 and 4.35 the concentration of MgOHCl are plotted versus time after addition of MgOHCl(s) to the 30, 20 and 10 mole % $MgCl_2$ binaries, respectively.

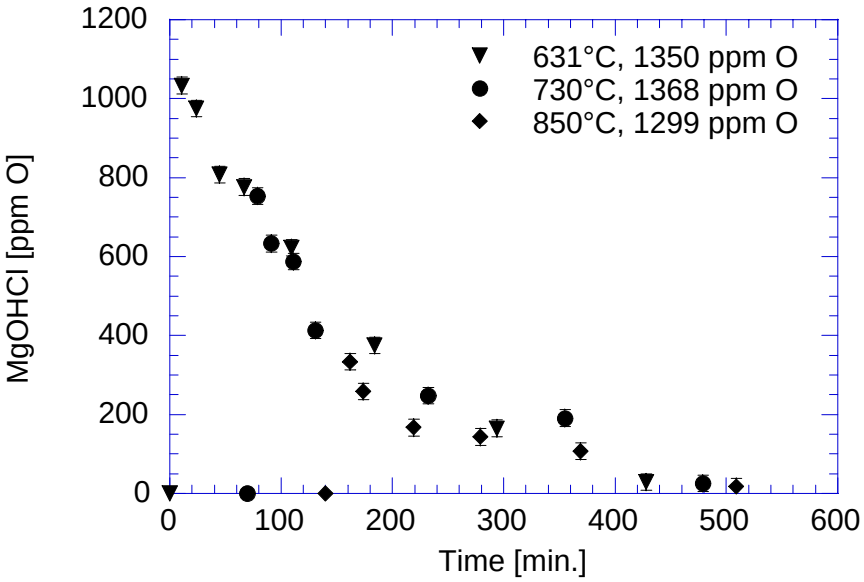

Figure 4.33. The concentration of MgOHCl versus time after addition of MgOHCl to the MgO saturated 30 mole % $MgCl_2$ melt.

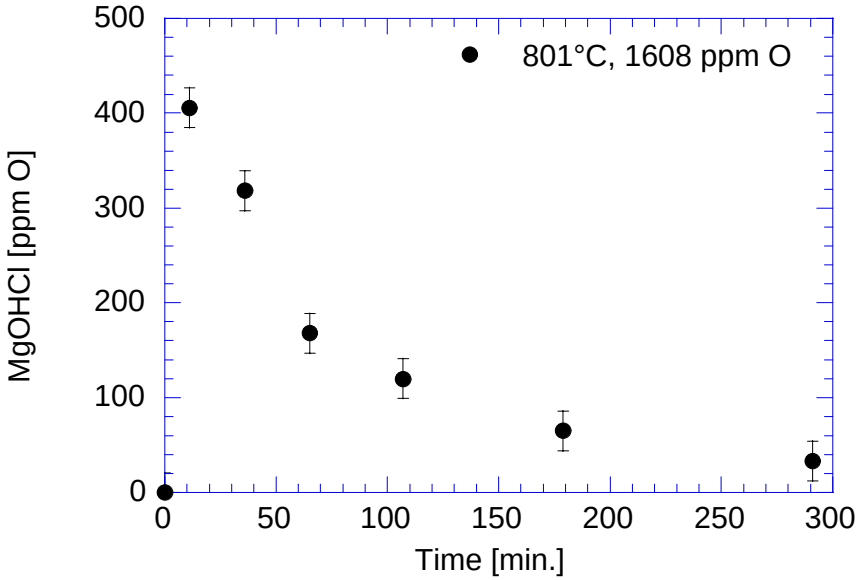

Figure 4.34. The concentration of MgOHCl versus time after addition of MgOHCl to the MgO saturated 20 mole % $MgCl_2$ melt.

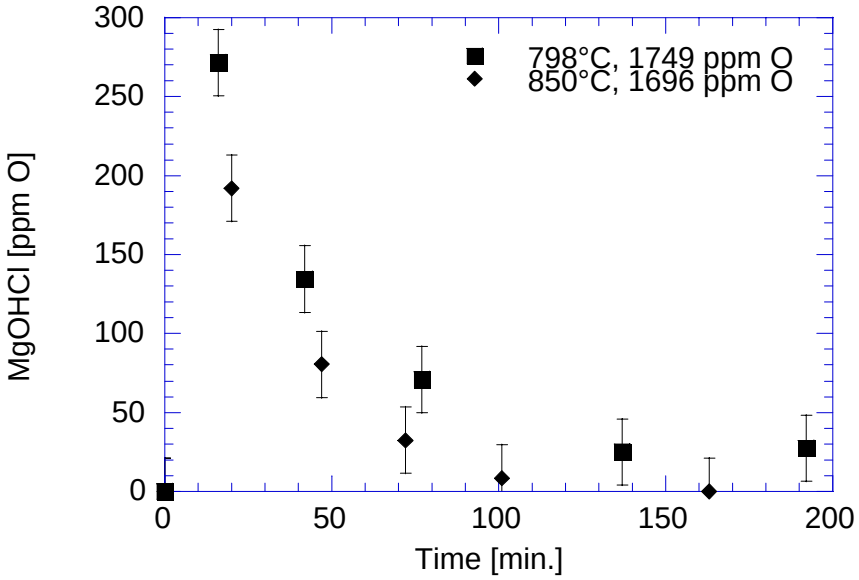

Figure 4.35. The concentration of MgOHCl versus time after addition of MgOHCl to the MgO saturated 10 mole % $MgCl_2$ melt.

There is some scatter in the data, but the decomposition rate increases with increasing the temperature, as expected, and the data in Fig. 4.32 must be due to the difficulty in measuring the currents correctly.

4.5.3. Combination of results from cyclic voltammetry and analytical measurements

In Figs. 4.36, 4.37 and 4.38 the current density is plotted versus the concentration of MgOHCl. For all three compositions, 30, 20 and 10 mole % $MgCl_2$, a linear regression line can be drawn using all data points. The lines go through the origin. This is in agreement with Eq. 2.1. No temperature effect can be observed in the temperature range investigated. For the 10 mole % $MgCl_2$ binary the data are less accurate. This is not surprising considering the difficulties in determining current densities as mentioned above for this melt composition.

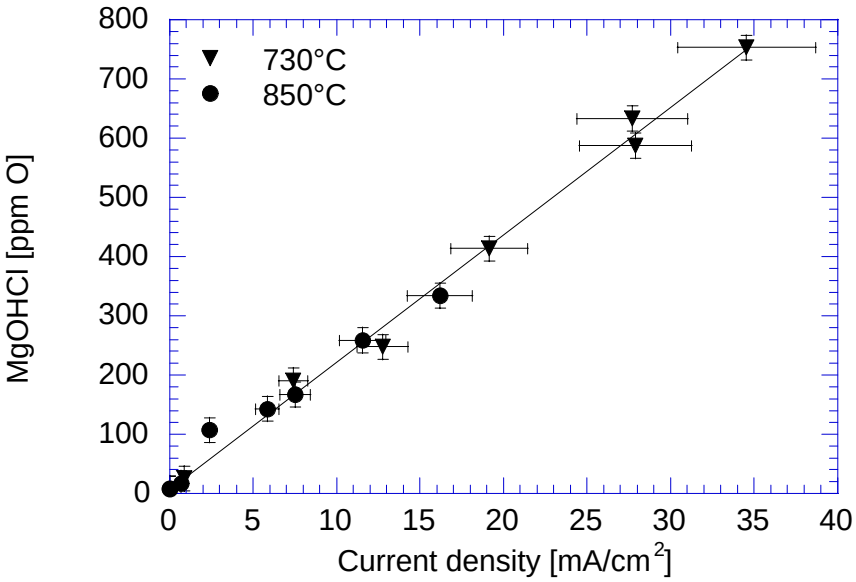

Figure 4.36. MgOHCl concentrations versus current density of reaction B for the 30 mole % $MgCl_2$ melt at 730 and 850°C. The solid line is the linear regression.

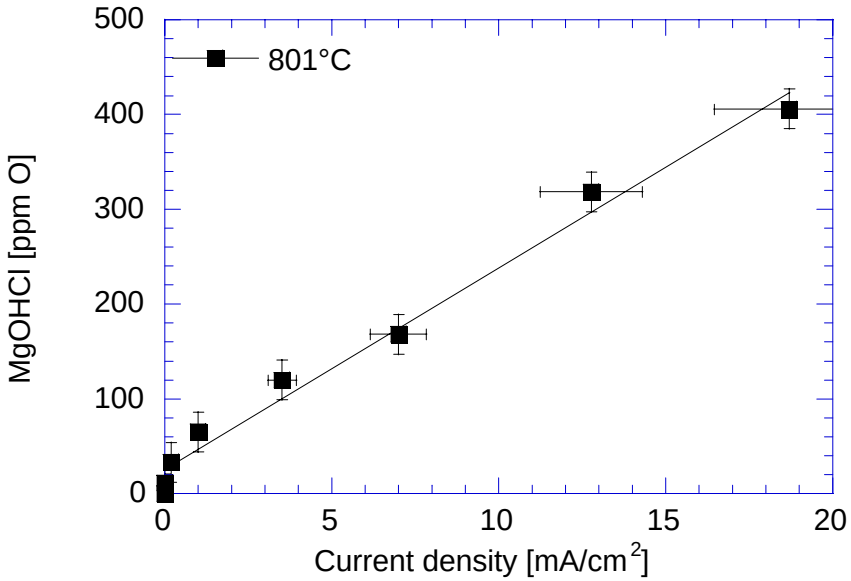

Figure 4.37. MgOHCl concentrations versus current density of reaction B for the 20 mole % $MgCl_2$ melt at 801°C. The solid line is the linear regression.

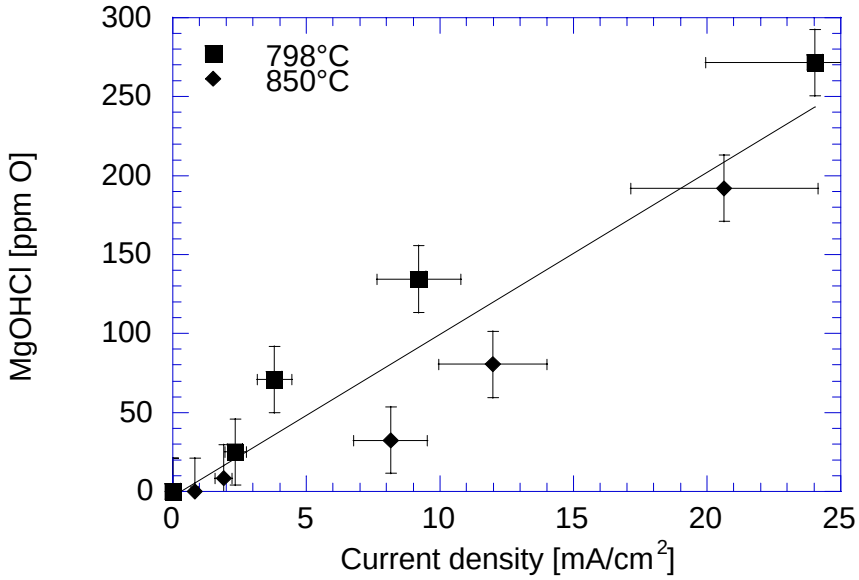

Figure 4.38. MgOHCl concentrations versus current density of reaction B for the 10 mole % $MgCl_2$ melt at 798 and 850°C. The solid line is the linear regression.

4.5.4. Anodic current density and MgO analysis

Some investigations of the current densities and MgO concentrations in the 30, 20 and 10 mole % $MgCl_2$ binary melts have been performed, but due to the small solubility of MgO in these melts the errors in the current densities and the MgO solubilities were too large to obtain meaningful diffusion data. Only the saturation concentrations are therefore reported. In the 30 mole % $MgCl_2$ binary the average saturation concentrations measured using the acid consumption method were 37, 19 and 30 ppm O at 631, 730 and 850°C, respectively. In the 20 mole % $MgCl_2$ binary the average saturation concentration measured using the acid consumption method was 23 ppm O at 801°C. In the 10 mole % $MgCl_2$ binary the average saturation concentrations measured using the acid consumption method were 13 and 14 ppm O at 798 and 850°C, respectively.

4.5.5. Diffusion coefficients

Assuming a diffusion controlled reversible electrochemical reaction as in pure $MgCl_2$, the diffusion coefficient for the reacting species can be calculated

according to Eq. 2.1. The slopes of the linear relationship between c and i_p in Figs. 4.36, 4.37 and 4.38 have been used in the equation. The results are presented in Tab. 4.4. The diffusion coefficient for 10 mole % $MgCl_2$ melts is not calculated. This was because the current increase was not even close to a peak and difficult to determine. The current density measured is therefore not considered to be the real current density and the diffusion coefficient is not calculated.

Table 4.4. The diffusion coefficients of MgOHCl and MgO in 30, 20 and 10 mole % $MgCl_2$ binaries at different temperatures.

Melt composition [mole % $MgCl_2$]	**Temperature** [°C]	$\mathbf{D_{MgOHCl}}$ [$10^{-5}cm^2/sec$]	$\mathbf{D_{MgO}}$ [$10^{-5}cm^2/sec$]
30	730	4.5	
	850	5.5	
20	801	5.6	
10	798		
	850		

4.6. Analysis of possible error sources

4.6.1. Uncertainties in the current density data for MgOHCl reduction

The current density data appears to be in good internal agreement for all compositions, but three main errors must be considered. It was impossible to use an electrode with a fixed area. Attempts to fix the electrode area by encapsulating it in pyrex were unsatisfactory. With the very small amounts of oxide in the melt, dissolution of oxide from the pyrex shield made the use of pyrex impossible. Therefore the electrode area had to be measured before each measurement started, and then recalculated after each sampling. This introduces a systematic error within each set of experimental data and a random error when considering all experimental data as a whole. The area was calculated by measuring the current response at different depths of immersion of the electrode. Using linear regression, a straight line was drawn through the points in a current versus area plot. The slope of this line was used to find the initial area of the electrode. The uncertainty in the electrode area was calculated to be approximately ± 5 %, based on the uncertainty in the regression line.

The second main error is related to the determination of the current peak. The reading of the current from the cyclic voltammogram was standardised. A certain percentage of i_p(C) was subtracted from peak B when determining the correct i_p(B). This method may, however, introduce a systematic error since an error in the estimate of this percentage will introduce a systematic error in i_p(B). Since both peaks increase with concentration of MgOHCl, this error will have a larger impact on the evaluated data at higher concentrations. This could further lead to an incorrect evaluation of the decomposition rate of MgOHCl, di_p/dt. Since the same method of calculation is used for all temperatures, this error is the same for all temperatures, and has therefore no consequence for the observed temperature variation in the decomposition rates. It is difficult to estimate how the error in i_p(C) will influence the error in i_p(B) and the error in the final results. The best estimate of the error in i_p(B) is ± 5 % of the current density. Since this systematic error increases with concentration, this could give a systematic error when calculating the corresponding concentration versus i_p plots. These plots would still be straight lines, but the slopes of the lines could be incorrect. This could further result in an error when calculating the diffusion coefficients, which are based on these slopes.

In melts containing sodium chloride, underpotential deposition of sodium introduces further uncertainties in the reading of the cathodic current, compared with data obtained in pure $MgCl_2$. The more sodium chloride in the melt the higher the background current from underpotential deposition. This background current increases the uncertainty in the i_p(B) data. In addition, in melts containing more than 50 mole % NaCl there are no clear current peaks, and this makes it difficult to determine exactly the potential at which i_p(B) is to be found. For the eutectic melt the peak potential was defined to be at the same potential with respect to Mg deposition as for the 90 and 80 mole % $MgCl_2$ melts. It is known that the reversible deposition potential for magnesium is shifted towards more negative potentials with the addition of NaCl to the melt. An equal shift was observed for reaction B as for Mg deposition in the eutectic melt. For the 30, 20 and 10 mole % $MgCl_2$ melts the peak potential seemed to have shifted somewhat closer to the Mg deposition potential, and 0.27V(Mg) was chosen as the peak potential. This is the potential at which the curvature of the current increase is steepest. An example is given in Fig. 4.15. This introduces a systematic error in the value of the current since this might not be the true peak potential for reaction B. These factors are believed to be the most important errors in i_p(B) for melts containing more than 50 mole % NaCl. The uncertainties are estimated to be ± 5 % of the current density in the eutectic melt, ± 10 % in the binaries

containing 30 and 20 mole % $MgCl_2$ and ± 15 % in the binary containing 10 mole % $MgCl_2$.

For some cyclic sweeps, instabilities occurred in the potential region of reaction B. Such instabilities could be seen as repeated drops and increases in the current. This made it impossible to obtain a well-defined value for the current, but in some cases it was still possible to use an average value. This of course introduces a larger error in the current density, depending on how large the fluctuations were. Based on these fluctuations only the extra error in the current density was estimated to be about ± 1 %.

An important point is also the influence of the instability in the reference electrode potential on the uncertainty in the peak current. The potential shift can either be slow and steady, like 1 mV/s for several seconds, or "jumps" in potential, like 10 mV in less than 1 second. A steady shift in potential will not have other effects than giving a small error in the applied sweep rate. The shape of the cyclic voltammogram would be unaffected by such a steady shift in the reference potential. The sweep rate used was 200 mV/s and thus the error introduced would be less than 1%. If the shift was a sudden one, the effect would be that the cyclic voltammogram would be drawn out or pushed together where the shift occurred, and at the same time the sweep rate would differ from the applied sweep rate. If this happened at a potential where the electrochemical reactions occurred, the result could give an odd shape to the cyclic voltammogram, and the current density measured would be incorrect. Such occurrences should be possible to detect experimentally and were not included in the data analysis. This is therefore not considered an important error source.

In melts containing more than 50 mole % NaCl another problem was observed regarding the instability in the reference potential. With the high background current from the underpotential deposition of sodium, it was difficult to define exactly where the Mg-deposition potential was. This made it difficult to find the exact same potential on voltammograms both before and after MgOHCl additions. This complicated the calculation of i_p(B). A change in potential of 10 mV could change the current with up to 4 % in melts with high concentration of MgOHCl. The Mg-deposition potential could normally be found within ± 5 mV, giving an uncertainty in i_p(B) of ± 2 %.

For some of the experiments performed in pure $MgCl_2$ melts, the peak potential, E_p, shifted somewhat towards a more negative potential with increasing concentration of MgOHCl. Due to the fact that it was difficult to establish an absolute potential and that the background current changed with

potential, an error was introduced in the deducted background current. It is difficult to say if the chosen way of finding the increased background current will give a too high or too low estimate, but it will be a systematic error. This is not believed to be an important error for the pure $MgCl_2$ melts since the background current is not very large in this system.

As described in chapter 3 the experimental set-up was designed to reduce the uncompensated resistance between the electrodes in the melt. Considering the high conductivity of the melt, relatively low concentration and low sweep rates, one would assume the uncompensated resistance to be very small.

Impurities in the melt could have quite different influences on the current readings. Especially impurities being reduced at potentials close to those of reaction B would introduce further uncertainties in the current densities. If these impurities were stable in the melt they could be taken into account by measuring their current densities at the potential of reaction B before addition of MgOHCl(s). Other impurities could have effects on the current density if they reacted with dissolved MgOHCl and MgO. An experiment was performed in pure $MgCl_2$ to test additions of different possible impurities, i.e. iron and Al_2O_3, and none were observed to have much influence on the current densities.

If melts containing NaCl with concentrations equal to or exceeding the eutectic composition, were kept just above the melting point, passivation of the working electrode occurred. This resulted in very low apparent current densities. One possible explanation is that the melt froze at the electrode surface, and an insulating layer of NaCl(s) was formed. This reduced the active surface area of the electrode, and the current was reduced. This could easily occur due to the higher Na^+ concentration close to the cathode during electrolysis. All current density data from experiments where this occurred have therefore been disregarded.

To summarise, the total amount of uncertainty in the current density of reaction B is given in Tab. 4.5.

Table 4.5. Total uncertainty in i_p(B) for different melt compositions.

Composition [mole % $MgCl_2$]	**uncertainty in i_p(B)** [%]
100, 90 and 80	7
41.5	9
30 and 20	12
10	17

4.6.2. Uncertainties in the analytical measurements

As explained in 2.2.3, a small difference between two large numbers will lead to a large relative uncertainty in the difference. This was observed for some samples where the measured concentration of MgOHCl was higher than what was calculated from the amount of MgOHCl added to the melt. In other cases the measurements showed more MgO dissolved than the saturation concentration. These data have been omitted. As an example, lets look at sample no. 3 taken from a pure $MgCl_2$ melt at 728°C (Table B.1, appendix B). The n_O^{tot} measured was 875 ppm O with a standard deviation of 39 ppm O (5%), while the n_O^{bas} was 1129 with a standard deviation of 24 ppm O (2%). The calculated amount of oxygen as MgOHCl and MgO are 449 and 340 ppm O, respectively. Using a Gaussian error estimate, the standard deviations for oxygen as MgOHCl and MgO are then 82 (18%) and 46 ppm O (14%), respectively. The saturation concentrations of MgO in $MgCl_2$ - NaCl melts are well known. Whenever the starting melt was saturated with MgO, the MgOHCl concentration could be calculated by subtracting the MgO saturation concentration from the total oxygen concentration. The MgO concentration is well known in MgO saturated melts[13]. Both the carbothermal reduction and acid consumption analysis can therefore be used to obtain the MgOHCl concentration in MgO saturated melts. This reduces the uncertainty in the calculated concentrations considerably. Let us for the sake of argument assume that the previous example was from a saturated melt. Then, using a Gaussian error estimate, the standard deviation for oxygen as MgOHCl is only 27 ppm O (6%), assuming a standard deviation of 10 ppm O for the oxygen determination of a MgO saturated melt. This is a considerable reduction in the error. This method was therefore always used whenever the melt was saturated with MgO. In the eutectic melt typical values for the standard deviations were 25 and 15 ppm O for the carbothermal reduction and acid consumption analysis, respectively. This gives an uncertainty in the MgOHCl concentration of 21 ppm O. The results in the binaries containing 30, 20 and 10 mole % $MgCl_2$ were 15 and 13 ppm O, giving an uncertainty of 18 ppm O. The results in the binaries containing 90 and 80 mole % $MgCl_2$ were comparable to the results in pure $MgCl_2$.

Pure molten $MgCl_2$ and the $MgCl_2$ rich $MgCl_2$ – NaCl binaries are highly hygroscopic. Even a small absorption of humidity on extracted samples will contribute to the total amount of oxygen measured using the carbothermal reduction analysis, as described in 3.4. Even though extreme care was taken to avoid absorption of water on the samples as explained earlier, it is not possible to totally eliminate this error. Absorbed water does not affect the acid consumption analysis. The effect is therefore to increase the total amount

of oxygen relative to the amount of base equivalents detected, i.e. n_O^{tot} increases while n_O^{bas} is unaffected. One time distilled $MgCl_2$ has analysed oxygen content between 100 and 150 ppm O using the carbothermal reduction analysis. The same values for the acid consumption analysis is between 50 and 100 ppm O. After a second distillation the results from the carbothermal reduction and acid consumption analysis are usually less than 80 and 40 ppm O, respectively. Melts containing NaCl were easier to analyse than pure $MgCl_2$. The results were more uniform and the standard deviations of the analytical data were significantly smaller. In the eutectic melt carbothermal reduction and acid consumption analysis performed before any addition of oxygen showed oxygen contents of 80-110 and 10 – 25 ppm O. For comparison, measurements done on pure NaCl show less than 10 ppm O for both the carbothermal reduction and acid consumption methods. This shows that $MgCl_2$ is very difficult to analyse correctly. Most probably absorption of humidity occurs resulting in increased scatter in the data and a too high n_{MgOHCl} and a too low n_{MgO} analysed. This has been taken account for by subtracting a fixed value from the carbothermal reduction analysis. This value is determined by the difference between the two analytical methods prior to addition of MgOHCl to the melt. An uncertainty in the measured data of minimum ± 30 ppm O must therefore be allowed for in pure $MgCl_2$, while an uncertainty of minimum ± 20 ppm O is estimated for the eutectic melt and the binaries containing 90 and 80 mole % $MgCl_2$. In the binaries containing 30, 20 and 10 mole % $MgCl_2$ an uncertainty of minimum ± 10 ppm O is estimated.

The difference between the two analysis methods found prior to addition of MgOHCl(s) could also be because the oxygen containing specie is not in the form of MgO, but rather something that reacts with only one HCl, like MgOHCl. This would explain the difference since the amount of oxygen found by the acid consumption analysis and reported as MgO, has to be doubled. This would give comparable values for the two analysis methods. Still, after 18 hours at temperatures above 700°C we believe that all oxygen exists as MgO and the problem is due to absorption of humidity on the samples.

Another problem is the possibility that solid MgO particles get into the sample. The oxygen in MgO will count double in the acid consumption analysis method. If a combination of carbothermal reduction and acid consumption analysis is used to calculate the MgOHCl concentration, solid MgO will have no influence on the analysed MgOHCl content, but the MgO concentration analysed will be too high, since there is no way to distinguish between solid and dissolved MgO. If the MgO saturation concentration is

used to obtain the MgOHCl concentration in MgO saturated melts, the calculated MgOHCl concentration will be too high. This can be seen from the equations:

$$n_{MgOHCl} = n_O^{tot} - n_{MgO}^{sat} \tag{2.14}$$

$$n_{MgOHCl} = n_O^{bas} - 2n_{MgO}^{sat} \tag{2.15}$$

n_O^{tot} will be too high when MgO(s) is present. n_O^{bas} however will also be larger, but in this case each mole solid MgO will count double towards the n_{MgOHCl}, and n_{MgOHCl} will therefore always be larger when calculated from n_O^{bas} if solid MgO is present. No systematic difference between calculations of n_{MgOHCl} from n_O^{tot} and n_O^{bas} was observed. Since the melt samples have been filtered through quartz or graphite filters and the sampling tubes were kept well above the bottom of the crucible during sampling, solid MgO particles are not considered a big problem.

Decomposition of MgOHCl during sample extraction, according to the equation:

$$MgOHCl(l) = MgO(l) + HCl(g) \tag{4.7}$$

must also be considered. Due to this decomposition the amount of MgO increases on behalf of the amount of MgOHCl. If the decomposition occurs to a significant extent before the sample is analysed, the concentration of MgOHCl in the sample will be lower than in the melt when the sample was extracted. The sample extraction procedure was performed as fast as possible and the melt sample was quenched quickly to room temperature. This procedure took usually less than 2 minutes. If this time is compared with the data shown in Figs. 4.5, 4.6, 4.18, 4.23, 4.24, 4.33, 4.34 and 4.35, it is possible to see that at high temperature and high concentration of MgOHCl, such decomposition may have some influence on the analysis. This gives an additional uncertainty in the analysed content of about ± 20 ppm O in pure $MgCl_2$ melts, ± 10 ppm O in the binaries containing 90 and 80 mole % $MgCl_2$, and ± 5 ppm O in the eutectic melt and binaries containing 30, 20 and 10 mole % $MgCl_2$. At lower MgOHCl concentrations and lower temperatures such a decomposition will not influence the analysis.

HCl dissolved in the solidified melt samples can also be a problem. Tunold[50] has summarised measurements performed by other authors on the solubility of HCl in different chloride melts. Measurements done in pure $MgCl_2$ at

800°C show a HCl solubility of 2.7 mole/m^3atm. Pure NaCl has a HCl solubility of 0.84 mole/m^3atm at 900°C. The dissolved HCl will react with basic oxide just like the added HCl in the acid consumption analysis. The consumption of HCl measured will then be too low, resulting in a too low value of n_O^{bas}. For unsaturated melts the consequence is that the measured concentration of MgO will be too low and thus the MgOHCl concentration too high. For saturated melts, where the concentration of MgOHCl is found from n_O^{bas} according to Eq. 2.15, the data should give a too low value for n_{MgOHCl}. Since n_O^{tot} is unaffected by dissolved HCl in the melt, n_{MgOHCl} calculated from Eq. 2.14 is also unaffected by HCl in the melt. There should be a clear difference between the calculated MgOHCl concentration in saturated melts depending on whether n_O^{tot} or n_O^{bas} is used for the calculations. No systematic differences between these methods were observed. This indicates very strongly that dissolved HCl is not a major source of error.

To summarise, the total amount of uncertainty in the analytical data for MgOHCl is given in Tab. 4.6.

Table 4.6. Total uncertainty in MgOHCl concentration for different melt compositions.

Composition [mole % $MgCl_2$]	**uncertainty in MgOHCl** [ppm O]	
	high conc.	low conc.
100, MgO-free	90	87
100, MgO-sat.	45	40
90 and 80, MgO-free	85	84
90 and 80, MgO-sat.	35	34
41.5, MgO-sat.	29	29
30, 20 and 10, MgO-sat	21	21

4.6.3. Uncertainties in the anodic current density and MgO analysis

As explained in 4.5.1 it was not possible to make an electrode with a given electrode area. This area had to be measured before each measurement, and recalculated after each sampling. This introduces a systematic error within each set of experimental data for the anodic current density and a random error when considering all experimental data for the anodic current density as a whole. The uncertainty in the electrode area was calculated to be approximately ± 5%.

The oxidation peak was well defined when no MgOHCl was present in the melt. When MgOHCl was present in the melt, the oxidation reaction of MgO

was shifted closer to the chlorine evolution reaction. The peak D appeared more like a shoulder on the chlorine evolution wave, giving a larger uncertainty in the evaluated current density due to the additional background current. This background current was subtracted from the i_p(D), but an error in estimating this background was introduced. This error was estimated to be 5% of i_p(D), based on two different estimates for the current versus potential curves for the chlorine evolution wave.

The stability of the reference electrode potential is important when calculating the cathodic current density. This problem was discussed in 4.6.1 for the cathodic current density. The same is true for the anodic current density. A steady change in the reference potential will give an uncertainty in the applied sweep rate of less than 1%. A sudden change in the reference potential should be possible to observe experimentally and take into account. These uncertainties are therefore not considered important in this work.

In 4.6.2 it was described how sensitive calculations were with respect to the method used to obtain analytical data. An example from pure $MgCl_2$ showed an error of ± 46 ppm O (14%) in the MgO concentration when both MgOHCl and MgO were present in the pure $MgCl_2$ melt. If there is no MgOHCl, all oxygen measured is calculated as MgO. Then both analytical methods can be used to obtain an average value for the MgO concentration. The error in the MgO concentration was now less than ± 20 ppm O while it was ± 46 ppm O if MgOHCl was present. This is less than 3% error in the saturation concentration. Another point is that MgO is stable in the melt. This means that a known amount of MgO can be added to the melt, and several melt samplings can be done to obtain an average value of the concentration. The comparison between added and measured amounts showed good agreement.

Solid MgO particles represent a problem since the analysis methods do not distinguish between solid and dissolved MgO. The melt samples have been filtered through quartz filters to remove solid particles. As discussed in 4.6.2 solid MgO is not believed to be a serious problem in the analytical measurements. The current density, i_p(D), measures only dissolved MgO.

$MgCl_2$ – NaCl melts are very hygroscopic and even a small absorption of humidity on extracted samples will influence the measured oxide in the sample. Without MgOHCl present, the carbothermal reduction analysis showed somewhat more oxygen than the acid consumption analysis, measured as MgO. Absorbed humidity can only be observed by carbothermal reduction, and it seems therefore like it was difficult to avoid absorbed humidity on the melt samples. This has been taken account for by subtracting

a fixed value from the carbothermal reduction data. This value is the difference between the measured amount of O^{2-} between the two methods prior to addition of MgOHCl. An uncertainty in the measured data of minimum ± 30 ppm O must therefore be allowed for in pure $MgCl_2$, while an uncertainty of minimum ± 20 ppm O is estimated for the eutectic melt and the binaries containing 90 and 80 mole % $MgCl_2$. In the binaries containing 30, 20 and 10 mole % $MgCl_2$ an uncertainty of minimum ± 10 ppm O is estimated.

Decomposition of MgOHCl was discussed in 4.6.2. The effect of this decomposition is that the amount of MgO increases on behalf of the amount of MgOHCl. This was a problem only for high concentrations at high temperatures, where the decomposition reaction is quite fast. This gives an additional uncertainty in the analysed content of about ± 25 ppm O. At lower $MgCl_2$ concentrations and lower temperatures such a decomposition will not influence the analysis.

Also dissolved HCl in the solidified melt could be a problem. This dissolved HCl will react with basic oxide just like the added HCl in the acid consumption. The consumption of HCl measured will then be too low, resulting in a too low value of n_O^{bas}. For unsaturated melts the measured concentration of MgO will be too low and thus the MgOHCl concentration too high. This was discussed above and it turned out not to be a serious problem.

To summarise, the total amount of uncertainty in the anodic current density and for MgO concentration is given in Tab. 4.7.

Table 4.7. Total uncertainty in the anodic current density and MgO concentration for different melt compositions.

Composition [mole % $MgCl_2$]	**uncertainty in i_p(D)** [%]		**uncertainty in MgO concentration** [ppm O]	
	MgOHCl present	MgOHCl not present	MgOHCl present	MgOHCl not present
100	7	5	58	36
90 and 80	7	5	51	28
41.5	7	5	36	24
30, 20 and 10	7	5	23	13

4.7. Alternative data treatment of reactions B and C

It has so far been assumed that reaction B corresponds to the electrochemical reduction of MgOHCl in the melt while reaction C corresponds to the electrochemical reduction of a hydrogen containing species other than MgOHCl, like HCl, H_2O or some C-H species. This is based on the conclusions of previous works[44,45]. It is felt that this needs some further discussion, since previous works have not addressed this problem in much detail.

Both reactions B and C appear after MgOHCl is added to the melt. The maximum current densities of both reactions occur within a few minutes after addition and then the current densities of both reactions gradually decline to 0 current, but not necessarily equally fast. This shows that this "hydrogen containing species" is introduced to the melt with the MgOHCl addition. One of the possibilities mentioned is that reaction C corresponds to reduction of HCl. If it is HCl, it has to come from decomposition of MgOHCl according to reaction 1.8:

$$MgOHCl(l) = MgO(s\ or\ l) + HCl(g) \tag{1.8}$$

This means that HCl should not have maximum concentration from start when the MgOHCl concentration in the melt is high and little has decomposed, but rather increase in concentration as more MgOHCl decomposes. The solubility of HCl in the melt is small and it is questionable if the HCl concentration at saturation is large enough to give the peak intensity observed for reaction C. The solubility of HCl in pure $MgCl_2$ is reported to be[50] 2.7 mole/m^3atm at 800°C. The same work did not report any diffusion coefficient for HCl in $MgCl_2$ or NaCl melts, but a value of 2.0 10^{-4} cm^2/sec was reported in a eutectic LiCl - KCl melt. This value is very high, but even such a high value will only give a current density for the reduction of HCl of 2.4 mA/cm^2, which is far below the values observed. During decomposition of MgOHCl the melt will be saturated with HCl. When all MgOHCl has decomposed, HCl will only very slowly leave the melt. The current density from the reduction of HCl should therefore increase in the initial stages after addition of MgOHCl and then reach a constant value. Some MgOHCl will also decompose directly from the solid state and create some HCl in the initial stages after addition. Calculations in pure $MgCl_2$ melt at 800°C show that the solubility limit of HCl is 59.3 ppm (2.7 mole/m^3atm) HCl. Recalculated to MgOHCl this shows that 26 ppm O (vt basis oxygen) of

MgOHCl has to decompose directly from the solid state to saturate the solution. Several of the experiments show that close to all MgOHCl dissolves upon addition. This is not the case for all experiments, but it shows that HCl formed from decomposition of solid MgOHCl cannot account for the high current density observed. Bjørgum et al.[43] made some investigations with HCl(g) bubbled through $MgCl_2$ – NaCl melts. They showed that a current increase occurred in the potential range 1.3 – 1.8V positive of Mg deposition and a larger current increase in the potential range 0.5 – 1.0V(Mg). These potential ranges are about the same as the potential ranges where reactions C and B, respectively, were observed in the present work. The current in the potential range 1.3 – 1.8V(Mg) disappeared within 2 hours after the bubbling of HCl(g) was stopped. Bjørgum et al. claimed that this shows that the reduction of HCl took place in the potential range 1.3 – 1.8 V(Mg). The second current increase (0.5 – 1.0V) lasted for a much longer time and was believed to be reduction of MgOHCl. These experiments were not performed inside a glove box and the $MgCl_2$ used probably also contained some hydroxychloride impurities. MgOHCl might therefore be present in the melt. It is therefore not possible to verify that the current increase in the potential range 1.3 – 1.8V(Mg) was due to the reduction of HCl.

This discussion has shown that there are several inconsistencies when trying to attribute the electrochemical reduction of HCl as the reaction C.

Another possibility is that reaction C is due to reduction of H_2O. H_2O must be due to either absorbed humidity on the added MgOHCl or some other H_2O impurities in the added MgOHCl. The solid MgOHCl used in this work was analysed by Aasheim[51] and was found to consist of 90 - 96% MgOHCl, 1 - 10% MgOHCl*0.3H_2O and 1 - 6% $MgCl_2$. It was claimed that it was very unlikely that MgO was present in the MgOHCl. The hypothesis that a large amount of H_2O was introduced with the added MgOHCl is therefore not reasonable. H_2O is very little soluble in $MgCl_2$ melts as the tendency for hydrolysis of the latter is too strong. It is believed that the current density of reaction C is too large to be due to the reduction of H_2O.

The analysis shows that both MgOHCl and MgOHCl*0.3H_2O could possibly exist in the melt. It is possible that these different species give different electrochemical reactions, but it is difficult to see how the two reactions can give comparable current densities when the difference in amount is as large as the analysis shows. Differences in the diffusion coefficients cannot account for the higher current density, since larger species most likely would have smaller diffusion coefficient and thus reduce the current density. MgOHCl*0.3H_2O is therefore not considered to be the cause of reaction C.

It was also suggested that some C-H species could be reduced in the potential range where reaction C is observed. It is, however, difficult to see how the added MgOHCl can give a substantial amount of C-H species in the melt. C-H compound is therefore not considered the source of reaction C in this work.

The work of Schenin-King and Picard[12] suggest that MgOHCl dissolves in the melt as a dimer, $(MgOHCl)_2$. This gives another way of interpreting the two reactions, B and C. The dimer has two OH-groups. During a cathodic sweep, two different reduction reactions would occur, one at the potential of reaction C and the other at the potential of reaction B. The first corresponds to the electrochemical reaction:

$$Mg_2(OH)_2^{2+} + e^- = Mg_2O_2H^+ + \tfrac{1}{2}H_2(g) \qquad (4.8)$$

The second corresponds to the electrochemical reaction:

$$Mg_2O_2H^+ + e^- = 2MgO + \tfrac{1}{2}H_2(g) \qquad (4.9)$$

The more negative potential needed for the second reduction could be due to higher stability of $Mg_2O_2H^+$, and thus a higher potential is needed to produce hydrogen gas. If MgOHCl does dissolve as a dimer the two peaks in the cyclic voltammograms should be equally high after background currents have been subtracted. They should have maximum value at the same time and they should decline equally fast with time. In Figs. 4.39 through 4.46 the current densities of reactions B and C are plotted versus time after addition of MgOHCl to different melts. It can be seen that although the current densities of the two reactions follow the same trend, they are not identical and the ratio of the currents change with changing composition of the melt. In the melts containing 100, 90 and 80 mole % $MgCl_2$ the current density of reaction B is found to be higher than that of reaction C. In the eutectic melt and in melts containing 30 and 20 mole % $MgCl_2$ the two reactions have close to the same current density. In the 10 mole % $MgCl_2$ melt reaction B has a higher current density than reaction C. This difference in current densities could be due to the relatively large uncertainties in the current densities for reaction B. As mentioned earlier the uncertainties increase with increasing content of sodium chloride. Especially the 10 mole % $MgCl_2$ melt has a high uncertainty for reaction B. An incorrect estimation of the uncertainties could be the reason

for the change in ratio between the two reactions when the melt composition is changed. In the data analysis performed so far it has been assumed that reaction B is the only source for reduction of MgOHCl, so that the concentration of MgOHCl can be found from the current density of reaction B, as described by Eq. 2.1. If MgOHCl exist in the melt as a dimer, $(MgOHCl)_2$, the concentration of the dimer can be found from the current density of reaction B. The concentration of the dimer is half the concentration of MgOHCl. This would mean that the calculations for diffusion coefficients done previously in this work are not correct. Since both reactions are one electron transfer reactions the diffusion coefficients should be 4 times higher than the previous calculations showed. Furthermore this means that the concentration of MgOHCl could be found by using the current density of reaction C. In the experiments done with controlled atmosphere and known additions, it is much easier to get current readings for reaction C and the readings are more accurate. In technical melts, which very well may contain HCl, reduction of HCl will occur at about the same potential and may influence the reading of the current. A data analysis based on the current density of reaction C will be more uncertain than the analysis based on the current density of reaction B, mainly due to the possible interference of HCl, and has therefore not been performed.

The MgOHCl dimer gives perhaps a better explanation for the source of the two reactions, B and C. It has, however, not been chosen in the interpretation of the data. This is due to the findings of Vindstad[8] and also due to the fact that Schenin-King and Picard[12] did not produce any evidence for their claim that MgOHCl dissolves as a dimer. In addition the lack of consistency in the ratio between the current densities of reaction B and C in the current investigation makes this explanation questionable.

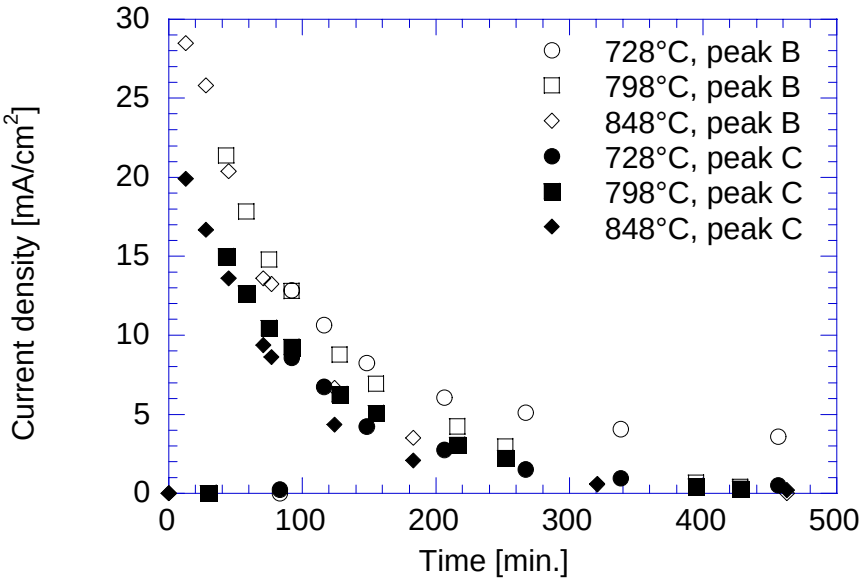

Figure 4.39. The current densities of reactions B and C versus time in $MgCl_2$ melts initially free of MgO.

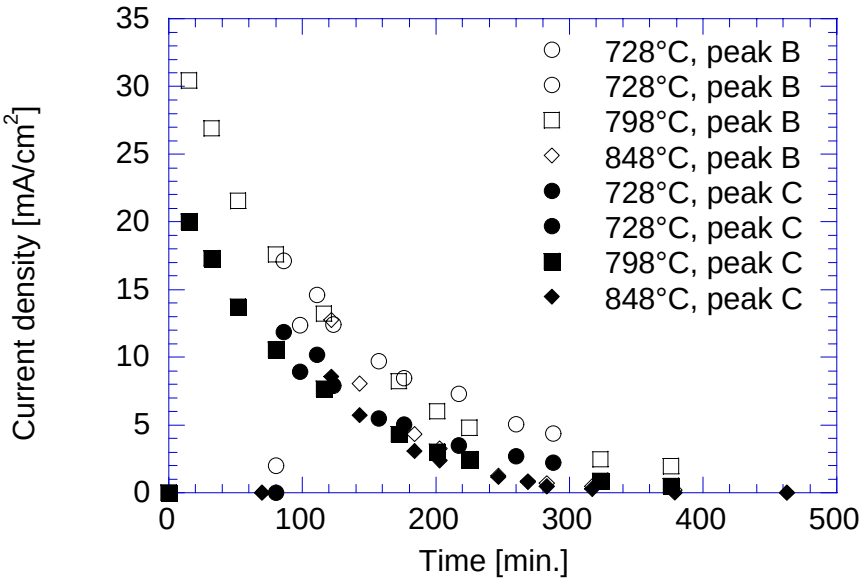

Figure 4.40. The current densities of reactions B and C versus time in $MgCl_2$ melts initially saturated with MgO.

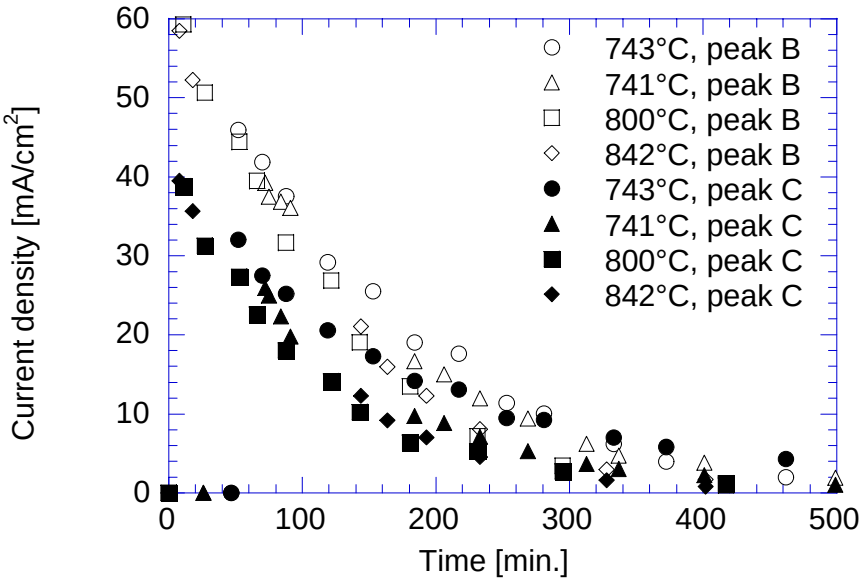

Figure 4.41. The current densities of reactions B and C versus time in $MgCl_2$ – NaCl melts containing 90 mole % $MgCl_2$. Circles are melts initially free of MgO, otherwise the melts are initially saturated with MgO.

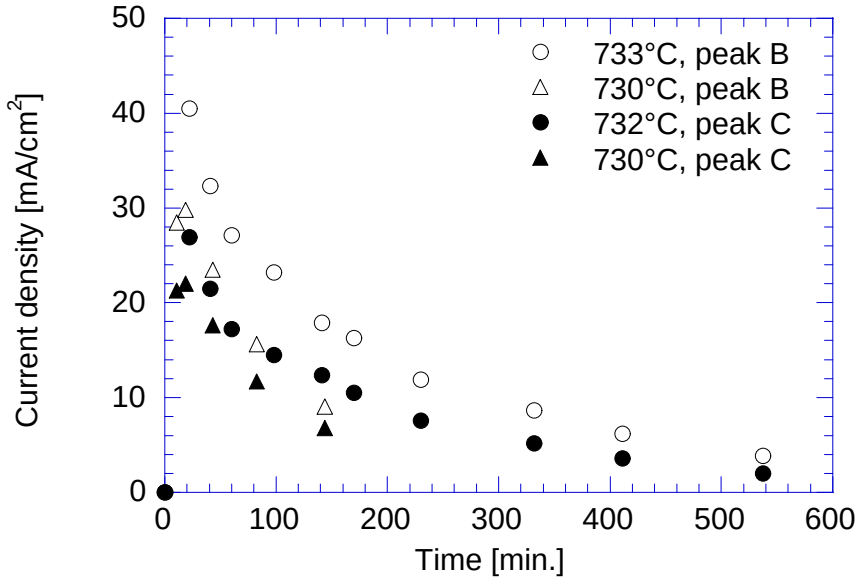

Figure 4.42. The current densities of reactions B and C versus time in $MgCl_2$ – NaCl melts containing 80 mole % $MgCl_2$. The melts are initially free of MgO.

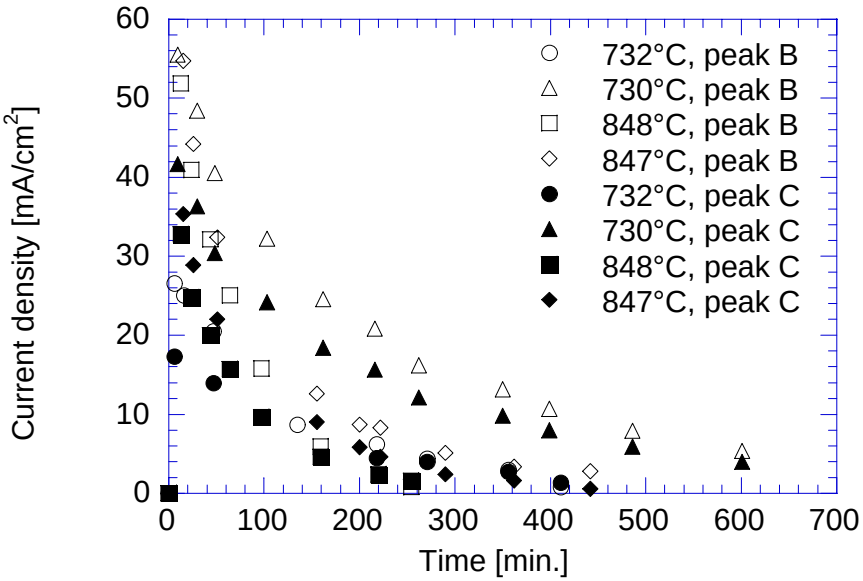

Figure 4.43. The current densities of reactions B and C versus time in $MgCl_2$ – NaCl melts containing 80 mole % $MgCl_2$. The melts are initially saturated with MgO.

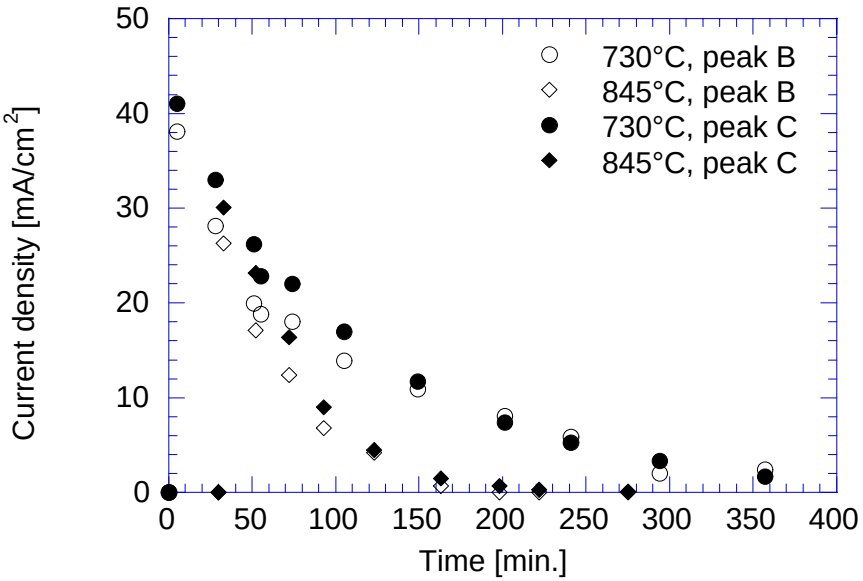

Figure 4.44. The current densities of reactions B and C versus time in eutectic melts initially saturated with MgO.

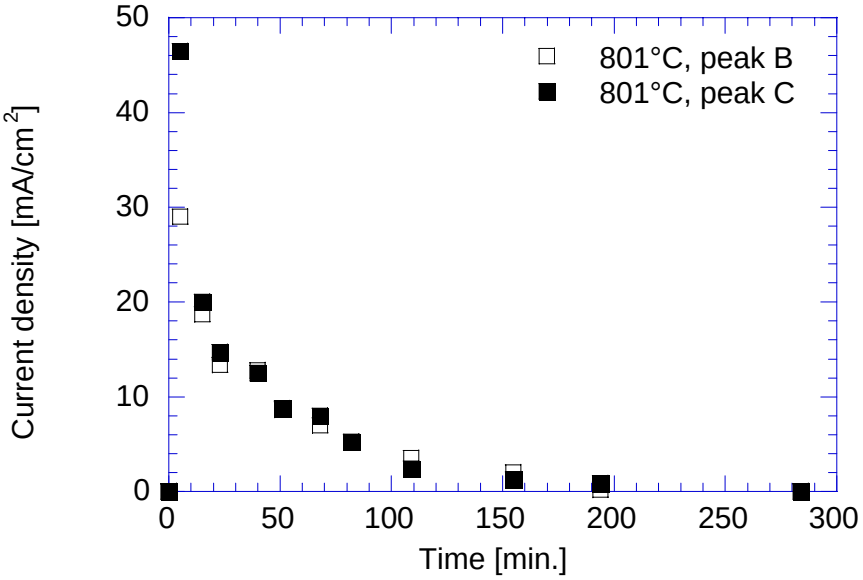

Figure 4.45. The current densities of reactions B and C versus time in $MgCl_2$ – NaCl melts containing 20 mole % $MgCl_2$. The melts are initially saturated with MgO.

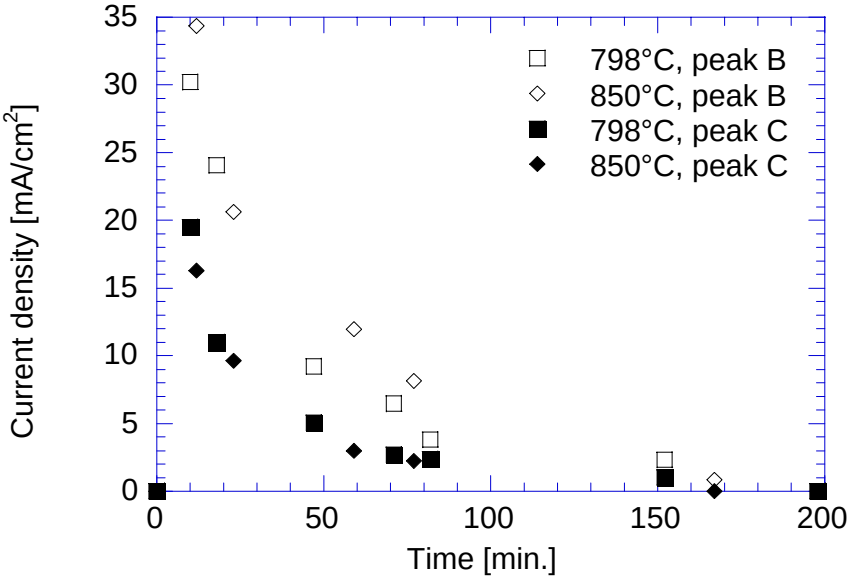

Figure 4.46. The current densities of reactions B and C versus time in $MgCl_2$ – NaCl melts containing 10 mole % $MgCl_2$. The melts are initially saturated with MgO.

Another possibility was presented by Ito et al[45]. They investigated a LiCl - KCl melt and claimed that hydrogen, either as gas or adsorbed hydrogen, could be electrochemically reduced to produce hydride ions, H^-. The H^- ions were electrochemically oxidised to hydrogen gas during the reverse anodic sweep. By comparing the cyclic voltammograms obtained by Ito et al. and the ones obtained in this work, it may be possible that this can be the source of reaction C. In Figs 4.47, 4.48 and 4.49 some cyclic voltammograms in binaries containing 90 mole % $MgCl_2$ are shown. In general the reverse sweep in this system is difficult to interpret. Figs 4.48 and 4.49 also show cyclic voltammograms obtained by reversing the potential just after the potential of reaction C. The anodic peak on the reverse sweep is small compared to the cathodic peak (reaction C) on the forward sweep (Fig. 4.49). This shows some similarities to the work of Ito et al[45] as Ito et al. also observed that the reverse anodic peak was much smaller than the forward cathodic peak for the reduction of hydrogen gas in LiCl – KCl melts.

Another interesting idea is that if reaction C is the electrochemical reduction of MgOHCl with production of $H_2(g)$, then reaction B could be the electrochemical reduction of the newly produced hydrogen gas, as described by Ito et al. This mechanism would imply that at low sweep rates reaction B should give a smaller current density than at high sweep rates, since hydrogen gas will leave the melt. This was not observed in this work and therefore this mechanism is not considered likely.

If reaction C in this work is reduction of hydrogen gas, the hydrogen gas must be introduced to the melt with the addition of MgOHCl, since the current density is large just after addition of the salt and being reduced as time passes. It is also observed that the disappearance of H_2 from the melt has to occur with approximately the same rate as the decomposition of MgOHCl. It is difficult to give a good explanation for this and reaction C cannot positively be identified as the reduction of hydrogen gas.

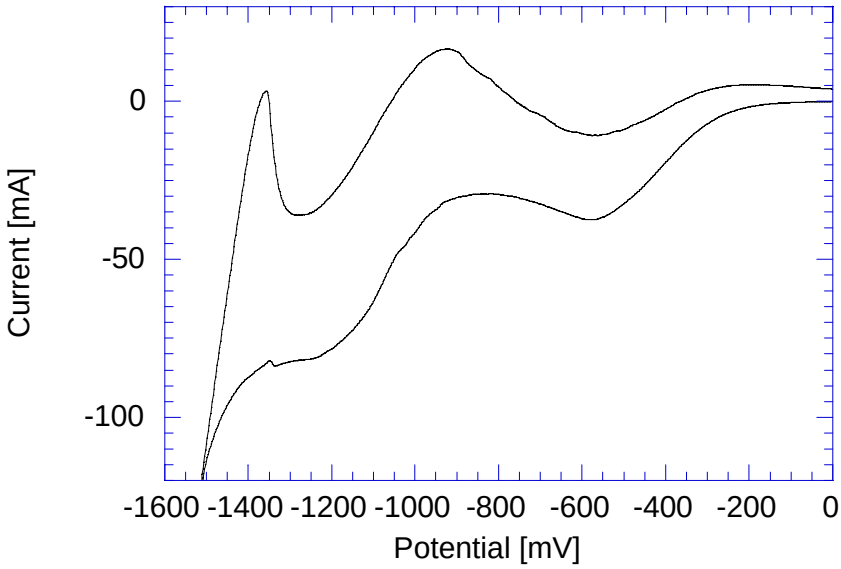

Figure 4.47. Current versus potential obtained in the binary containing 90 mole % $MgCl_2$ 15 minutes after addition of MgOHCl.

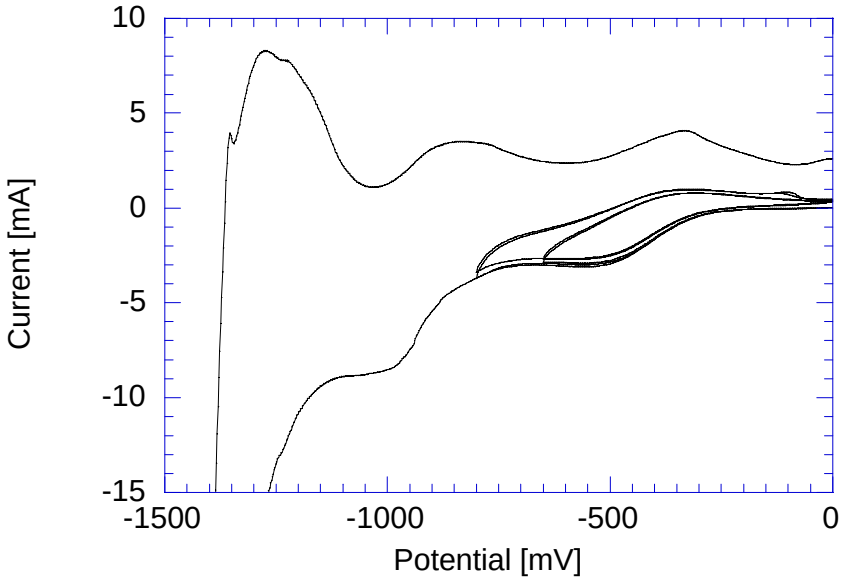

Figure 4.48. Current versus potential obtained in the binary containing 90 mole % $MgCl_2$ approximately 4.5 hours after addition of MgOHCl. Cyclic voltammetry is performed both in the whole cathodic range, and also only around the potential of reaction C.

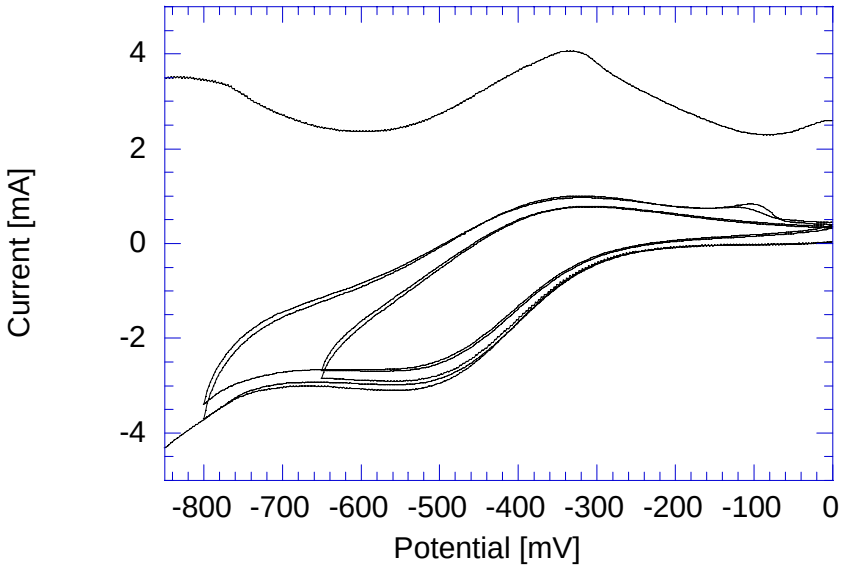

Figure 4.49. Close up of Fig. 4.48. The cyclic voltammogram obtained around the potential of reaction C.

The conclusion must be that we don't really know the exact electrochemical reactions observed at the two peak potentials B and C. We have not been able to identify the "MgOHCl species" in the melt, although the most likely from the observations done in this work is the dimer, $(MgOHCl)_2$. We therefore have to rely on previous investigations when we assume or guess the electrochemical reactions. In this work reaction B has been assumed to represent the reduction of a "MgOHCl species" dissolved in the melt. All the MgOHCl dissolved has further been assumed to be contained in this species.

4.8. Summary of results

To give a brief summary of the results for the MgOHCl concentrations versus cathodic current density of reaction B, the slopes of the linear regression lines for all measured compositions of $MgCl_2$ / NaCl are given in Fig. 4.50. It can be seen that the slope decreases when going from 100 to 80 mole % $MgCl_2$. Only a very small difference can be observed between 80 and 20 mole % $MgCl_2$, but the slope decreases again when going from 20 to 10 mole % $MgCl_2$.

The slopes shown in Fig. 4.50 were used to calculate the diffusion coefficients for the MgOHCl species at the different compositions and

temperatures. The diffusion coefficients for the MgO species were calculated for the compositions where MgO - data were available. The diffusion coefficients are given in Tab. 4.8.

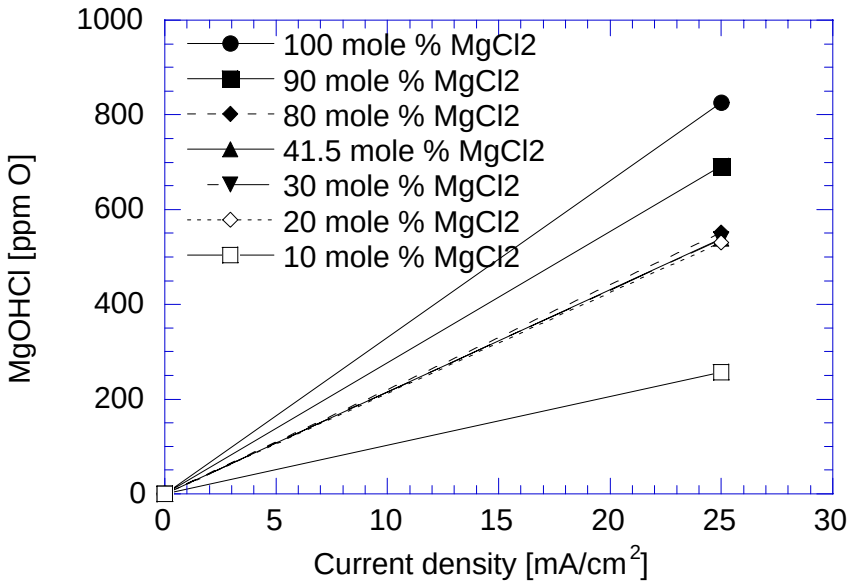

Figure 4.50. The concentration of MgOHCl versus the current density obtained from the electrochemical reduction of MgOHCl.

Table 4.8. Diffusion coefficients of MgOHCl and MgO in $MgCl_2$ / NaCl binaries at different temperatures.

Melt composition [mole % $MgCl_2$]	**Temperature** [°C]	$\mathbf{D_{MgOHCl}}$ [$10^{-5}cm^2/sec$]	$\mathbf{D_{MgO}}$ [$10^{-5}cm^2/sec$]
100	728	1.9	0.8
	798	2.1	0.9
	848	2.3	0.9
90	741	2.7	0.9
	800	3.0	1.0
	842	3.2	1.1
80	730	4.2	1.4
	847	5.0	1.6
41.5	730	4.7	6
	845	5.6	7
30	730	4.5	
	850	5.5	
20	801	5.6	
10	798		
	850		

5. Conclusion

5.1. Conclusion

The decomposition and dissolution of MgOHCl have been investigated in melts containing $MgCl_2$ and NaCl. The relationship between concentration and current density of the electrochemical reduction of MgOHCl was investigated. The range of melt compositions investigated extends from pure liquid $MgCl_2$ to 10 mole % $MgCl_2$ – 90 mole % NaCl.

It was observed that in the whole composition range the rate of decomposition of dissolved MgOHCl was higher at higher temperature. This temperature dependency was expected. The amount of temporarily dissolved MgOHCl was observed to be higher in melts rich in $MgCl_2$ than in NaCl rich melts. In the 10 and 20 mole % $MgCl_2$ binaries less than 500 ppm O, coming from added MgOHCl was dissolved although more than 1500 ppm O was added. In 80 and 90 mole % $MgCl_2$ binaries and in pure $MgCl_2$ more than 1000 ppm O was dissolved. The amount of temporarily dissolved MgOHCl was also dependent on temperature. In melts containing 58.5 mole % NaCl or more, less MgOHCl was dissolved at higher temperatures. This is due to the higher decomposition rate at higher temperatures. It is also possible that more MgOHCl is decomposed directly from the solid state at high temperatures. For melts containing 80, 90 and 100 mole % $MgCl_2$ the results are ambiguous and no conclusion can be drawn on the effect of temperature on the amount of dissolved MgOHCl.

The uncertainty in the current density for the electrochemical reduction of MgOHCl is mainly determined by the underpotential deposition of sodium and the current contribution from the preceding electrochemical reduction of a hydrogen containing species like HCl, H_2O or some C-H species. The underpotential deposition of sodium increases with increasing content of NaCl. In melts containing 58.5 mole % NaCl or more, the current density from underpotential deposition of sodium is quite substantial. At these NaCl concentrations the current peak from the electrochemical reduction of MgOHCl is no longer a real current peak. It looks more like a shoulder on the existing current wave.

For the analytical data the reverse is true. The data become more reliable when the content of NaCl increases. Pure $MgCl_2$ is very hygroscopic and small amounts of absorbed humidity have a large influence on the measured O / OH contents. It is also difficult to obtain consistent data.

The combination of chemical analysis and voltametric measurements showed that there exists a quantitative relationship between the MgOHCl content of the melt and the cathodic current density for MgOHCl reduction. The slope of this linear relationship changed with changing composition of the melt, with a higher ratio of concentration versus current density at higher $MgCl_2$ contents. The difference between the binaries containing 20 through 80 mole % $MgCl_2$ is very small. No effect of temperature was observed in these plots.

The diffusion coefficients of the dissolved MgOHCl species was calculated based on these linear relationships. It was found that the diffusion coefficient of the MgOHCl species increases with increasing content of NaCl in the melt. The diffusion coefficients are given in Tab. 4.8. Pure molten $MgCl_2$ is a partly ionic, and a partly network-like melt. In network like melts we would expect lower diffusion coefficients. When NaCl is added to the melt this network-like structure is broken down and the melt becomes more ionic and diffusion of ions should be facilitated. This is in agreement with our observations.

The concentration of MgO and the current density of the electrochemical oxidation of MgO have also been measured for $MgCl_2$ rich melts. A linear relationship was also found between current density for the oxidation peak of MgO and the concentration of MgO in the melt. It was observed that the MgO concentration increased after addition of MgOHCl until the solubility limit was reached and the solubility limit increased with increasing temperature. In the eutectic melt and the 30, 20 and 10 mole % $MgCl_2$ melts the solubility of MgO is so small that only the solubility limit was measured.

Dissolution of the added MgOHCl(s) and decomposition of dissolved MgOHCl occurred simultaneously. This was verified by measuring that both the MgOHCl and MgO concentrations increased the first hour after addition of MgOHCl(s).

Passivation of the working electrode was observed at temperatures close to the melting point in melts containing 58.5 mole % NaCl or more. This could be due to an increase in the melting point as Mg is removed from the melt close to the working electrode with a resulting salt precipitation on the electrode.

5.2. Industrial aspect

This work has shown that *in situ* measurements of the content of MgOHCl in pure molten $MgCl_2$ using cyclic voltammetry is possible. The liquid feed for the process of Norsk Hydro consists mainly of $MgCl_2$. The results of this work can therefore be used to measure the O / OH contents in this liquid feed. A probe has been developed and is undergoing tests in a joint research project between Norsk Hydro and SINTEF. The probe is equipped with a glassy carbon rod sealed with pyrex to obtain a fixed area. A carbon rod serves as a counter electrode and a magnesium nickel solid alloy is used as reference electrode. This is fixed within a boron nitride holder and laboratory trials have proven successful[52]. It would also be beneficial if this technique could be used to determine O / OH contents in the bulk electrolyte itself. A problem will certainly be the underpotential deposition of sodium. Investigations in technical melts are already in progress and preliminary results show that voltammetry can be used as a semi-quantitative analytical method to determine O / OH in these melts[52].

References

1. Thonstad, J., “Some Recent Trends in Molten Salt Electrolysis of Titanium, Magnesium and Aluminium”, *High temp. Mat. Proc.*, **9** (2-4), 135-146 (1990).

2. Kannan, G.N. and Desikan, P.S., “Current Trends Towards Energy Reduction in Electrolytic Magnesium Production”, *Bull. Electrochem.*, **6** (9), 776-779 (1990).

3. Rosenkilde, C., Norsk Hydro Magnesium division. Correspondence, 2000/2001.

4. Strelets, K.L., “Electrolytic Production of Magnesium”. Keterpress Enterprises, a: p 226-227, b: p 238-239, c: p 77 (1977).

5. Kipouros, G.J. and Sadoway, D.R., “The Chemistry and Electrochemistry of Magnesium Production”, *Adv. Molten Salt Chem.*, **6**, Mamantov, G., Mamantov, C.B. and Bruanstein, J. Eds., 127-209 (1987).

6. Lockwood, L.F., Ansel, G. and Haddad, P.O., “Kirk-Othmer Encyclopedia of Chemical Technology”, 3rd. ed. Vol. 14, 570 (1981).

7. Wallevik, O., Amundsen, K., Faucher, A. and Mellerud, T., “Magnesium electrolysis – A Monopolar Viewpoint”, Magnesium Technology 2000, *The Minerals, Metals & Materials Society*, Kaplan, H.I., Hryn, J.N. and Clow, B.B. Eds., 13-16 (2000).

8. Vindstad, J.E., "Hydrolysis of And Oxide Solubilities in Melts Related to Electrolytic Magnesium Production", Ph.D. thesis, Department of Inorganic Chemistry, The Norwegian University of Science and Technology, Trondheim, Norway, (1996).

9. Aarebrot, E:, Andresen, R.E., Østvold, T. and Øye, H.A., “A Model for the Back Reaction in the Magnesium Eletrolysis”, *Light Metals*, Vol. 1, Higbie, K.B., Eds., 491-512 (1977).

10. Aarebrot, E:, Andresen, R.E., Østvold, T. and Øye, H.A., "The Recombination Reaction in Magnesium Electrolysis", *Metall*, **32**, 41-44 (1978).

11. Østvold, T. and Øye, H.A., "Recombination of Magnesium and Chlorine in the Technical Electrolysis", *Light Metals*, McMinn, C.J., Eds., 937-947 (1980).

12. Schenin-King, J. and Picard, G.S., "Oxoacidity Effect on Metallic Oxide Dissolution Reactions in Fused Chlorides", *Molten Salt Forum*, **1-2,** 13-22 (1993/94).

13. Boghosian, S., Godø, A., Mediaas, H., Ravlo, W. and Østvold, T., "Oxide Complexes in Alkali-Alkaline-Earth Chloride Melts", *Acta Chem. Scand.*, **45,** 145-157 (1991).

14. Combes, R., de Andade, F., de Barros, A. and Ferreira, H., "Dissociation and Solubility Variation vs pO^{2-} of some Alkaline-Earth Oxides in Molten NaCl-KCl (at 1000K)", *Electrochim. Acta.*, **25,** 371-374 (1980).

15. Mediaas, H., Vindstad, J.E. and Østvold, T., "Solubility of MgO in Mixed Chloride-Fluoride Melts Containing $MgCl_2$", *Acta Chem. Scand.*, **51**, 504-514 (1997).

16. Brooker, M.H., and Huang, C.-H., "Raman Spectroscopic Studies of Structural Properties of Solid and Molten States of Magnesium Chloride-Alkali Metal Chloride System", *Can. J. Chem.*, **58**, 168-179 (1980).

17. Vindstad, J.E., Mediaas, H. and Østvold, T., "Hydrolysis of $MgCl_2$-Containing Melts", *Acta Chem. Scand.*, **51**, 1192-1200 (1997).

18. Vilnyansky, Ya.E. and Savinkova, E.I., "Solid Solutions of Magnesium Hydroxychloride in Magnesium Chloride", *J. Appl. Chem. USSR*, **26**, 735-739 (1953).

19. Vilnyansky, Ya.E. and Savinkova, E.I., "Thermal Dissociation of Magnesium Hydroxychloride", *J. Appl. Chem. USSR*, **28**, 827-832 (1955).

20. Vilnyansky, Ya.E. and Bakina, N.P., "Solubility of Water and Magnesium oxide in Fused Carnalite", *J. Appl. Chem. USSR*, **29**, 615-619 (1956).

21. Savinkova, E.I., Lelekovaand, R.P. and Brayalovskaya, V.L., "Crystallization of Magnesium Oxide in a Hydrolyzed $MgCl_2$-KCl-NaCl Melt", *J. Appl. Chem. USSR* **50** (10), 2065-2067 (1977).

22. Muzhzhavlev, K.D. and Ivanov, A.B., "Influence of Atmospheric Moisture and Additions of Lithium Chloride on Hydrolysis of Magnesium Chloride in Various Electrolytes", *J. Appl. Chem. USSR.*, **45** (6), 1211-1215 (1972).

23. Ivanov, A.B. and Zuev, N.M., "Equilibria of Magnesium Chloride Hydrolysis in an Electrolyte", *J. Appl. Chem. USSR.*, **41** (8), 1693-1698 (1968).

24. Savinkova, E.I. and Lelekova, R.P., "Equilibrium of Magnesium Chloride Hydrolysis in Chloride Melts", *J. Appl. Chem. USSR.*, **51** (7), 1453-1456 (1978).

25. Klemm, W. and Weiss, P., "Das System Natriumchlorid-Magnesiumchlorid", *Z. anorg. allgem. Chem.*, **245**, 279-284 (1940).

26. Grjotheim, K., Holm, J.L., and Røtnes, M., "The Phase Diagrams of the Systems NaCl-MgCl2 and KCl-$MgCl_2$", *Acta Chem. Scand.*, **26** (9), 3802-3803 (1972).

27. Kleppa, O.J. and McCarty, F.G., "Thermochemistry of Charge-Unsymmetrical Binary Fused Halide Systems. II. Mixtures of Magnesium Chloride with Alkali Chlorides and with Silver Chloride", *J. Phys. Chem.*, **70** (4), 1249-1255 (1966).

28. Østvold, T., "EMF Measurements of the Change in Chemical Potential of One Component on Mixing in fused Binary Alkali-Alkaline Earth Halide Systems", *High Temp. Sci.*, **4** (1), 51-81 (1972).

29. Kosnyrev, G.T., Savinkova, E.I. and Vilnyansky, Y.E., "Thermodynamic Properties of Magnesium Chloride in Molten Chlorides", *Izv. Vyssh. Ucheb. Zaved., Tsvet. Met*., no. 5, 57-64 (1966).

30. Karakaya, I. and Thompson, W.T., "Thermodynamic Properties of $MgCl_2$-NaCl Melts from EMF Measurements", *J. Electrochem. Soc*. **133** (1), 702-706 (1986).

31. Flood, H. and Urnes, S., "Die Berechnung der Aktivitäten in Magnesiumchlorid-Alkalichlorid-Schmeltzen aus Strukturmodellen", *Z. Elektrochem*., **59** (9), 834-839 (1955).

32. Maroni, V.A., "Vibrational Frequencies and Force Constants for Tetrahedral MgX_4^{2-} (X = Cl, Br and I) in MgX_2-KX Melts", *J. Chem. Phys.*, **76** (1), 4789-4792 (1971).

33. Maroni, V.A., Hathaway, E.J. and Cairns, E.J., "Structural Studies of Magnesium Halide–Potassium Halide Melts by Raman Spectroscopy", *J. Phys. Chem.*, **76** (1), 155-159 (1971).

34. Capwell, R.J., "Raman Spectra of Crystalline and Molten $MgCl_2$", *Chem. Phys. Lett*., **12** (3), 443-446 (1972).

35. Brooker, M.H., and Huang, C.-H., "Raman Spectrum of Molten $MgCl_2$", *Chem. Phys. Lett.*, **43** (1), 180-182 (1976).

36. Haarberg, G. M., Johansen, S.R., Melaas J. and Tunold, R., "Nucleation of Droplets and Metal Fog During Deposition of Liquid Mg from Molten Chlorides", *Proceedings of the Seventh International Symposium on Molten Salts, The Electrochem. Soc.*, **90-17**, Hussey, C.L., Flengas, S.N., Wilkes, J.S., Ito, Y., Eds., 449-456 (1990).

37. Børresen, B., Haarberg, G.M., Tunold, R., Kisza, A. and Kazmierczak, J., "Electrodeposition of Magnesium from Halide Melts", *Proceedings of the Tenth International Symposium on Molten Salts, The Electrochem. Soc.*, **96-7**, 157-170 (1996).

38. Kisza, A., Kazmierczak, J., Børresen, B., Haarberg, G.M. and Tunold, R., "Kinetics and Mechanism of the Magnesium Electrode Reaction in Molten Magnesium Chloride", *J. of Appl. Electrochem.*, **25,** 940-946 (1995).

39. Eie, M., Haarberg, G.M., Osen, K.S. and Tunold, R., "Elektrokjemiske undersøkelser i systemet NaCl-KCl-NaOH", Tech. Rep., Lab. of Ind. Electrochem., NTH, Trondheim, Norway., (1989), in Norwegian.

40. Haarberg, G.M., Aalberg, N., Osen, K.S. and Tunold, R., "Anodic Oxidation of Dissolved Oxides in Chloride Melts", *Proceedings of the Eighth International Symposium on Molten Salts, The Electrochem. Soc.*, **93-9**, Saboungi, M-L., Kojima, H., Eds., 376-381 (1993).

41. Haarberg, G.M., Aalberg, N., Osen, K.S. and Tunold, R., "Electrochemical Behaviour of Dissolved CaO in Molten $CaCl_2$", *Molten Salt Forum*, **1-2**, 5-10 (1993/94).

42. Mohamedi, M., Børresen, B., Haarberg, G.M. and Tunold, R., "Anodic Behaviour of Carbon Electrode in CaO-$CaCl_2$ Melts at 1123K", *J. of Electrochem. Soc.*, **146** (4), 1472-1477 (1999).

43. Bjørgum, A., Eriksen, U. and Tunold, R., "Voltametrisk Karakterisering av Hydrogen- og Oksygen-holdige Komponenter i Magnesiumkloridsmelter", Tech. Rep., Lab. of Ind. Electrochem., NTH, Trondheim, Norway., (1986), in Norwegian.

44. Haarberg, G.M. and Tunold, R., "Elektrokjemiske Metoder for Undersøkelse av Forurensninger i Mg-elektrolytt", Tech. Rep., Lab. of Ind. Electrochem., NTH, Trondheim, Norway., (1989), in Norwegian.

45. Ito, H. and Hasegawa, Y., "Electrode Behavior of Hydrogen Reduction in LiCl-KCl Melt", *J. of Electrochem. Soc.*, **147** (1), 289-295 (2000).

46. Zeng, K., Klassen, T., Oelerich, W. and Bormann, R., "Critical Assessment and Thermodynamic Modeling of the Mg-H System", *Inter. J. of Hydrogen Energy*, **24**, 989-1004 (1999).

47. Greef, R., Peat, R., Peter, L.M., Pletcher, D. and Robinson, J., "Instrumental Methods in Electrochemistry", ed. T.J. Kemp, Ellis Horwood Limited, Cornwall, England (1990).

48. Bard, A.J. and Faulkner, L.R., "Electrochemical methods", John Wiley & sons, Singapore (1980).

49. Rudolph, M. and Feldberg, S.W., "Digisim 3.0" simulation program, Bioanalytical Systems Inc., 2701 Kent Ave, West Lafayette, IN 47906 USA.

50. Tunold, R., private comunications, unpublished results.

51. Aasheim, A., "Tillaging av MgOHCl for voltametriforsøk", Internal report, Norsk Hydro, in Norwegian.

52. Haarberg, G.M., Tunold, R. and Osen, K.S, "Voltammetric characterization of dissolved oxygen and hydrogen containing species in chloride melts", Jondalen symposium (2000), in print.

Appendices

Appendix A

Current density data for reaction B and C in 100 mole % $MgCl_2$ (voltammetry at 200mV/s).

Table A.1. Current density at 728°C in 100 mole % $MgCl_2$ melt, unsaturated with MgO at start.

Time [min]	Current density reaction B [mA/cm^2]	Current density reaction C [mA/cm^2]
0	0.00	0.25
9	12.83	8.60
33	10.67	6.73
65	8.28	4.25
123	6.08	2.77
184	5.11	1.51
255	4.08	0.97
373	3.58	0.50

Table A.2. Current density at 728°C in 100 mole % $MgCl_2$ melt, saturated with MgO at start.

Time [min]	Current density reaction B [mA/cm^2]	Current density reaction C [mA/cm^2]
0	2.00	0.00
18	12.37	8.93
43	12.43	7.91
77	9.72	5.48
137	7.31	3.50
Addition 2		
11	17.15	11.90
36	14.60	10.20
101	8.49	5.02
185	5.07	2.70
213	4.37	2.25

Table A.3. Current density at 798°C in 100 mole % $MgCl_2$ melt, unsaturated with MgO at start.

Time [min]	Current density reaction B [mA/cm^2]	Current density reaction C [mA/cm^2]
0	0.00	0.14
13	21.40	15.00
28	17.83	12.64
45	14.81	10.45
62	12.80	9.27
98	8.79	6.26
125	6.96	5.06
186	4.22	3.07
222	2.96	2.25
365	0.68	0.45
398	0.39	0.27

Table A.4. Current density at 798°C in 100 mole % $MgCl_2$ melt, saturated with MgO at start.

Time [min]	Current density reaction B [mA/cm^2]	Current density reaction C [mA/cm^2]
0	0.00	0.00
15	30.44	20.00
32	26.89	17.33
52	21.58	13.75
80	17.59	10.58
116	13.24	7.67
172	8.23	4.34
201	5.99	3.03
225	4.82	2.48
323	2.46	0.88
376	1.94	0.54

Table A.5. Current density at 848°C in 100 mole % $MgCl_2$ melt, unsaturated with MgO at start.

Time [min]	Current density reaction B [mA/cm^2]	Current density reaction C [mA/cm^2]
0	0.00	0.00
13	28.48	19.90
28	25.82	16.70
45	20.41	13.60
71	13.61	9.38
77	13.26	8.61
124	6.68	4.33
183	3.50	2.08
321	0.57	0.60
463	0.00	0.20
590	0.88	0.10

Table A.6. Current density at 848°C in 100 mole % $MgCl_2$ melt, saturated with MgO at start.

Time [min]	Current density reaction B [mA/cm^2]	Current density reaction C [mA/cm^2]
0	0.00	0.00
52	12.77	8.57
73	8.04	5.75
114	4.32	3.10
133	3.28	2.39
177	1.28	1.15
199	0.80	0.86
213	0.70	0.45
247	0.48	0.27
309	0.19	0.00
393	0.00	0.00
482	0.00	0.00

Current density data for reaction B and C in 90 mole % $MgCl_2$ / 10 mole % NaCl (voltammetry at 200mV/s).

Table A.7. Current density at 743°C in 90 mole % $MgCl_2$ / 10 mole % NaCl melt, unsaturated with MgO at start.

Time [min]	Current density reaction B [mA/cm^2]	Current density reaction C [mA/cm^2]
0	0.00	0.00
5	45.96	32.10
23	41.93	27.50
41	37.56	25.20
72	29.23	20.60
106	25.52	17.30
137	19.11	14.20
170	17.61	13.10
206	11.40	9.53
234	10.10	9.28
286	6.23	7.02
325	3.97	5.87
415	1.99	4.30

Table A.8. Current density at 800°C in 90 mole % $MgCl_2$ / 10 mole % NaCl melt, saturated with MgO at start.

Time [min]	Current density reaction B [mA/cm^2]	Current density reaction C [mA/cm^2]
0	0.00	0.00
11	59.34	38.80
27	50.72	31.30
53	44.47	27.40
66	39.53	22.60
88	31.70	18.00
122	26.86	14.10
143	19.11	10.20
181	13.52	6.40
231	7.22	5.30
295	3.49	2.70
417	0.96	1.20
501	0.07	0.50

Table A.9. Current density at 842°C in 90 mole % $MgCl_2$ / 10 mole % NaCl melt, saturated with MgO at start.

Time [min]	Current density reaction B [mA/cm^2]	Current density reaction C [mA/cm^2]
0	0.00	0.00
8	58.53	39.50
18	52.24	35.70
144	21.07	12.31
164	15.95	9.15
193	12.30	7.00
233	8.03	4.54
328	2.96	1.62
402	1.69	0.85

Table A.10. Current density at 741°C in 90 mole % $MgCl_2$ / 10 mole % NaCl melt, saturated with MgO at start.

Time [min]	Current density reaction B [mA/cm^2]	Current density reaction C [mA/cm^2]
0	0.00	0.40
46	39.24	25.91
49	37.50	24.97
58	36.83	22.32
65	36.05	19.81
158	16.66	9.72
180	15.01	8.91
207	11.98	7.07
243	9.39	5.26
287	6.23	3.71
311	4.68	3.01
375	3.82	2.23
473	1.92	1.04

Current density data for reaction B and C in 80 mole % $MgCl_2$ / 20 mole % NaCl (voltammetry at 200mV/s).

Table A.11. Current density at 733°C in 80 mole % $MgCl_2$ / 20 mole % NaCl melt, unsaturated with MgO at start.

Time [min]	Current density reaction B [mA/cm^2]	Current density reaction C [mA/cm^2]
0	0.00	0.00
22	40.50	26.90
41	32.33	21.50
60	27.16	17.20
98	23.18	14.50
141	17.92	12.40
170	16.28	10.50
230	11.88	7.60
332	8.66	5.20
411	6.18	3.60
537	3.90	2.00

Table A.12. Current density at 848°C in 80 mole % $MgCl_2$ / 20 mole % NaCl melt, saturated with MgO at start.

Time [min]	Current density reaction B [mA/cm^2]	Current density reaction C [mA/cm^2]
0	0.00	0.40
13	51.84	32.80
24	40.94	24.80
44	32.20	20.00
64	25.04	15.70
97	15.84	9.70
159	5.93	4.60
220	2.37	2.30
254	0.78	1.60

Table A.13. Current density at 732°C in 80 mole % $MgCl_2$ / 20 mole % NaCl melt, saturated with MgO at start.

Time [min]	Current density reaction B [mA/cm^2]	Current density reaction C [mA/cm^2]
0	0.00	0.30
6	26.62	17.30
16	25.10	
47	20.50	14.00
135	8.73	6.60
218	6.20	4.00
271	4.39	2.70
356	2.97	1.40
411	0.84	0.70

Table A.14. Current density at 730°C in 80 mole % $MgCl_2$ / 20 mole % NaCl melt, unsaturated with MgO at start.

Time [min]	Current density reaction B [mA/cm^2]	Current density reaction C [mA/cm^2]
0	0.00	0.50
11	28.49	21.30
19	29.79	22.00
43	23.48	17.60
83	15.66	11.70
144	9.07	6.80

Table A.15. Current density at 847°C in 80 mole % $MgCl_2$ / 20 mole % NaCl melt, saturated with MgO at start.

Time [min]	Current density reaction B [mA/cm^2]	Current density reaction C [mA/cm^2]
0	0.00	0.00
15	54.77	35.40
26	44.20	28.90
51	32.40	22.00
155	12.65	9.00
200	8.69	5.80
222	8.33	4.60
290	5.12	2.40
362	3.38	1.60
442	2.83	0.60

Table A.16. Current density at 730°C in 80 mole % $MgCl_2$ / 20 mole % NaCl melt, saturated with MgO at start.

Time [min]	Current density reaction B [mA/cm^2]	Current density reaction C [mA/cm^2]
0	0.00	0.00
9	55.56	41.67
30	48.44	36.33
48	40.56	30.42
103	32.23	24.17
162	24.56	18.42
216	20.87	15.65
262	16.18	12.13
350	13.13	9.85
399	10.70	8.02
486	7.90	5.92
601	5.36	4.02

Current density data for reaction B and C in 41.5 mole % $MgCl_2$ / 58.5 mole % NaCl (voltammetry at 200mV/s).

Table A.17. Current density at 730°C in 41.5 mole % $MgCl_2$ / 58.5 mole % NaCl melt, saturated with MgO at start.

Time [min]	Current density reaction B [mA/cm^2]	Current density reaction C [mA/cm^2]
0	0.00	0.26
5	38.12	41.00
28	28.12	33.00
51	19.98	26.20
55	18.84	24.30
74	18.01	22.80
105	13.92	17.00
149	10.91	11.70
201	8.04	7.40
241	5.89	5.30
294	1.99	3.30
357	2.41	1.70

Table A.18. Current density at 845°C in 41.5 mole % $MgCl_2$ / 58.5 mole % NaCl melt, saturated with MgO at start.

Time [min]	Current density reaction B [mA/cm^2]	Current density reaction C [mA/cm^2]
0	0.00	0.16
3	26.31	30.04
22	17.12	23.14
42	12.38	16.34
63	6.78	8.99
93	4.23	4.45
133	0.68	1.44
168	0	0.68
192	0	0.29
245	0	0.10

Current density data for reaction B and C in 30 mole % $MgCl_2$ / 70 mole % NaCl (voltammetry at 200mV/s).

Table A.19. Current density at 850°C in 30 mole % $MgCl_2$ / 70 mole % NaCl melt, saturated with MgO at start.

Time [min]	Current density reaction B [mA/cm^2]	Current density reaction C [mA/cm^2]
0	0.00	0.30
10	16.40	18.00
24	16.19	14.70
36	11.56	11.03
62	7.54	7.95
83	5.84	5.45
121	3.26	3.11
146	2.38	2.35
154	2.40	2.00
225	0.70	0.00
326	0.30	0.00

Table A.20. Current density at 730°C in 30 mole % $MgCl_2$ / 70 mole % NaCl melt, saturated with MgO at start.

Time [min]	Current density reaction B [mA/cm^2]	Current density reaction C [mA/cm^2]
0	0.00	0.80
7	41.14	42.80
12	34.56	32.10
25	27.71	24.20
43	27.89	27.80
64	19.14	19.70
105	12.75	13.00
167	7.40	8.00
222	4.09	4.68
295	0.86	2.54

Current density data for reaction B and C in 20 mole % $MgCl_2$ / 80 mole % NaCl (voltammetry at 200mV/s).

Table A.21. Current density at 801°C in 20 mole % $MgCl_2$ / 80 mole % NaCl melt, saturated with MgO at start.

Time [min]	Current density reaction B [mA/cm^2]	Current density reaction C [mA/cm^2]
0	0.00	0.00
5	28.98	46.50
15	18.70	20.00
23	13.39	14.70
40	12.78	12.50
51	8.64	8.80
68	7.00	8.00
82	5.21	5.30
109	3.52	2.40
155	2.01	1.30
194	0.19	0.90
284	0.00	0.00

Current density data for reaction B and C in 10 mole % $MgCl_2$ / 90 mole % NaCl (voltammetry at 200mV/s).

Table A.22. Current density at 798°C in 10 mole % $MgCl_2$ / 90 mole % NaCl melt, saturated with MgO at start.

Time [min]	Current density reaction B [mA/cm^2]	Current density reaction C [mA/cm^2]
0	0.00	0.00
10	30.23	19.50
18	24.05	11.00
47	9.21	5.10
71	6.49	2.70
82	3.81	2.37
152	2.35	1.03
198	0.00	0.00

Table A.23. Current density at 850°C in 10 mole % $MgCl_2$ / 90 mole % NaCl melt, saturated with MgO at start.

Time [min]	Current density reaction B [mA/cm^2]	Current density reaction C [mA/cm^2]
0	0.00	0.00
12	34.33	16.30
23	20.65	9.67
59	11.98	3.00
77	8.15	2.25
167	0.83	0.00

Appendix B

Analysed content of MgOHCl and MgO by carbothermal reduction analysis and iodometric titration in 100 mole % $MgCl_2$.

Table B.1. Measured contents at 728°C in 100 mole % $MgCl_2$ melt, unsaturated with MgO at start.

Total oxygen measured by carbothermal reduction	Basic oxygen measured by iodometric titration	MgOHCl measured as ppm O (Combo of methods)	MgO measured as ppm O (Combo of methods)	MgOHCl [ppm O] (Total O – c_{sat})	MgOHCl [ppm O] (Basic O – c_{sat})
145	118	0	59		
793	961	453	254		
875	1129	449	340		
923	1310	364	473		
899	1320	306	507		
1099	1303				253

Table B.2. Measured contents at 728°C in 100 mole % $MgCl_2$ melt, saturated with MgO at start.

Total oxygen measured by carbothermal reduction	Basic oxygen measured by iodometric titration	MgOHCl measured as ppm O (Combo of methods)	MgO measured as ppm O (Combo of methods)	MgOHCl [ppm O] (Total O – c_{sat})	MgOHCl [ppm O] (Basic O – c_{sat})
882	1390	202	594	0	0
1509	1501	1345	78	808	271
1257	1660	682	489	556	430
Addition 2					
1306	1830	610	610	605	600
1336	1733	767	483	635	503
1208	1648	596	526	507	418
973	1469	305	582	272	239

Table B.3. Measured contents at 798°C in 100 mole % $MgCl_2$ melt, unsaturated with MgO at start.

Total oxygen measured by carbothermal reduction	Basic oxygen measured by iodometric titration	MgOHCl measured as ppm O (Combo of methods)	MgO measured as ppm O (Combo of methods)	MgOHCl [ppm O] (Total O – c_{sat})	MgOHCl [ppm O] (Basic O – c_{sat})
142	283	1	141		
982	1500	464	518	78	
936	1588	284	652	32	

Table B.4. Measured contents at 798°C in 100 mole % $MgCl_2$ melt, saturated with MgO at start.

Total oxygen measured by carbothermal reduction	Basic oxygen measured by iodometric titration	MgOHCl measured as ppm O (Combo of methods)	MgO measured as ppm O (Combo of methods)	MgOHCl [ppm O] (Total O – c_{sat})	MgOHCl [ppm O] (Basic O – c_{sat})
866	1758	-26	892	0	0
1792	2013	1571	221	888	
1640	2352	928	712	736	
1652	2313	991	661	748	
1335	2007	663	672	431	
1156	2082	230	926	252	274

Table B.5. Measured contents at 848°C in 100 mole % $MgCl_2$ melt, unsaturated with MgO at start.

Total oxygen measured by carbothermal reduction	Basic oxygen measured by iodometric titration	MgOHCl measured as ppm O (Combo of methods)	MgO measured as ppm O (Combo of methods)	MgOHCl [ppm O] (Total O – c_{sat})	MgOHCl [ppm O] (Basic O – c_{sat})
364	750	-22	386		
1510	1810	1210	300		
1361	1871	851	510		

Table B.6. Measured contents at 848°C in 100 mole % $MgCl_2$ melt, saturated with MgO at start.

Total oxygen measured by carbothermal reduction	Basic oxygen measured by iodometric titration	MgOHCl measured as ppm O (Combo of methods)	MgO measured as ppm O (Combo of methods)	MgOHCl [ppm O] (Total O – c_{sat})	MgOHCl [ppm O] (Basic O – c_{sat})
1008				0	
1906				888	
1633				615	

Analysed content of MgOHCl and MgO by carbothermal reduction analysis and iodometric titration in 90 mole % $MgCl_2$ / 10 mole % NaCl.

Table B.7. Measured contents at 743°C in 90 mole % $MgCl_2$ / 10 mole % NaCl melt, unsaturated with MgO at start.

Total oxygen measured by carbothermal reduction	Basic oxygen measured by iodometric titration	MgOHCl measured as ppm O (Combo of methods)	MgO measured as ppm O (Combo of methods)	MgOHCl [ppm O] (Total O – c_{sat})	MgOHCl [ppm O] (Basic O – c_{sat})
237	200	74	63		
1637	1817	1257	280		
1519	1776	1062	357		
1384	1759	809	475		
1318	1710	726	492		
1234	1674	594	540		
1036	1539	333	603		

Table B.8. Measured contents at 800°C in 90 mole % $MgCl_2$ / 10 mole % NaCl melt, saturated with MgO at start.

Total oxygen measured by carbothermal reduction	Basic oxygen measured by iodometric titration	MgOHCl measured as ppm O (Combo of methods)	MgO measured as ppm O (Combo of methods)	MgOHCl [ppm O] (Total O – c_{sat})	MgOHCl [ppm O] (Basic O – c_{sat})
848	745	951	-103	0	0
2069	2729	1409	660	1697	
1746				1374	
1684	2452	916	768	1312	
1227	2340	114	1113	855	
969	2085	-147	1116	597	
668	1844	-508	1176	296	

Table B.9. Measured contents at 842°C in 90 mole % $MgCl_2$ / 10 mole % NaCl melt, saturated with MgO at start.

Total oxygen measured by carbothermal reduction	Basic oxygen measured by iodometric titration	MgOHCl measured as ppm O (Combo of methods)	MgO measured as ppm O (Combo of methods)	MgOHCl [ppm O] (Total O – c_{sat})	MgOHCl [ppm O] (Basic O – c_{sat})
1094	2082	-124	1103	0	
2689				1533	
1498	2360	407	977	342	

Table B.10. Measured contents at 741°C in 90 mole % $MgCl_2$ / 10 mole % NaCl melt, saturated with MgO at start.

Total oxygen measured by carbothermal reduction	Basic oxygen measured by iodometric titration	MgOHCl measured as ppm O (Combo of methods)	MgO measured as ppm O (Combo of methods)	MgOHCl [ppm O] (Total O – c_{sat})	MgOHCl [ppm O] (Basic O – c_{sat})
825	1372	0	686	0	0
1876	2421	1053	684	1051	1049
1288	2308	-10	1159	463	936
1174	1999	71	964	349	627
1127	1812	164	824	302	440
967	1552	104	724	142	180

Analysed content of MgOHCl and MgO by carbothermal reduction analysis and iodometric titration in 80 mole % $MgCl_2$ / 20 mole % NaCl.

Table B.11. Measured contents at 732°C in 80 mole % $MgCl_2$ / 20 mole % NaCl melt, saturated with MgO at start.

Total oxygen measured by carbothermal reduction	Basic oxygen measured by iodometric titration	MgOHCl measured as ppm O (Combo of methods)	MgO measured as ppm O (Combo of methods)	MgOHCl [ppm O] (Total O – c_{sat})	MgOHCl [ppm O] (Basic O – c_{sat})
1206	1099	1255	-78	627	0
2031	1744	2260	-258	1452	644
1441	1243	1581	-169	862	143

Table B.12. Measured contents at 730°C in 80 mole % $MgCl_2$ / 20 mole % NaCl melt, saturated with MgO at start.

Total oxygen measured by carbothermal reduction	Basic oxygen measured by iodometric titration	MgOHCl measured as ppm O (Combo of methods)	MgO measured as ppm O (Combo of methods)	MgOHCl [ppm O] (Total O – c_{sat})	MgOHCl [ppm O] (Basic O – c_{sat})
1304	1339	0	669.5	0	0
1721	1677	496	590.5	536.5	577
1619	1577	392	592.5	434.5	477
1557	1487	358	564.5	372.5	387
1457	1312	333	489.5	272.5	212

Table B.13. Measured contents at 730°C in 80 mole % $MgCl_2$ / 20 mole % NaCl melt, unsaturated with MgO at start.

Total oxygen measured by carbothermal reduction	Basic oxygen measured by iodometric titration	MgOHCl measured as ppm O (Combo of methods)	MgO measured as ppm O (Combo of methods)	MgOHCl [ppm O] (Total O – c_{sat})	MgOHCl [ppm O] (Basic O – c_{sat})
119	89	0	44.5	0	0
1939	1901	1828	36.5	1314.5	801
1416	1366	1317	24.5	791.5	
1150	1308	843	232.5	525.5	
1069	1208	781	213.5	444.5	
847	871	674	98.5	222.5	

Analysed content of MgOHCl and MgO by carbothermal reduction analysis and iodometric titration in 41.5 mole % $MgCl_2$ / 58.5 mole % NaCl.

Table B.14. Measured contents at 730°C in 41.5 mole % $MgCl_2$ / 58.5 mole % NaCl melt, saturated with MgO at start.

Total oxygen measured by carbothermal reduction	Basic oxygen measured by iodometric titration	MgOHCl measured as ppm O (Combo of methods)	MgO measured as ppm O (Combo of methods)	MgOHCl [ppm O] (Total O – c_{sat})	MgOHCl [ppm O] (Basic O – c_{sat})
199	184	0	92	0	0
873	756	776	-10	694	612
669	710	414	148	490	566
582	468	482	-7	403	324
503	388	404	-8	324	244
416	277	341	-32	237	133
298				119	
285	272	84	94	106	128
227	226	14	106	48	82

Table B.15. Measured contents at 845°C in 41.5 mole % $MgCl_2$ / 58.5 mole % NaCl melt, saturated with MgO at start.

Total oxygen measured by carbothermal reduction	Basic oxygen measured by iodometric titration	MgOHCl measured as ppm O (Combo of methods)	MgO measured as ppm O (Combo of methods)	MgOHCl [ppm O] (Total O – c_{sat})	MgOHCl [ppm O] (Basic O – c_{sat})
311	273	135	69	0	0
479	388	356	16	300	244
290	268	98	85	111	124
256	188	110	39	77	44
272	179	151	14	93	35
182	90	60	15	3	

Table B.16. Measured contents at 475°C in 41.5 mole % $MgCl_2$ / 58.5 mole % NaCl melt, saturated with MgO at start.

Total oxygen measured by carbothermal reduction	Basic oxygen measured by iodometric titration	MgOHCl measured as ppm O (Combo of methods)	MgO measured as ppm O (Combo of methods)	MgOHCl [ppm O] (Total O – c_{sat})	MgOHCl [ppm O] (Basic O – c_{sat})
106	68	0	34	0	0
825	778	728	25	719	710
950	922	834	44	844	854
974	930	874	28	868	862
911	938	740	99	805	870
871	838	760	39	765	770
784	779	645	67	678	711
415	414	272	71	309	346
329	298	216	41	223	230

Analysed content of MgOHCl and MgO by carbothermal reduction analysis and iodometric titration in 30 mole % $MgCl_2$ / 70 mole % NaCl.

Table B.17. Measured contents at 850°C in 30 mole % $MgCl_2$ / 70 mole % NaCl melt, saturated with MgO at start.

Total oxygen measured by carbothermal reduction	Basic oxygen measured by iodometric titration	MgOHCl measured as ppm O (Combo of methods)	MgO measured as ppm O (Combo of methods)	MgOHCl [ppm O] (Total O – c_{sat})	MgOHCl [ppm O] (Basic O – c_{sat})
43	69	0	34.5	0	0
412	394	413	-9.5		334
192	319	48	135.5		259
154	227	64	81.5		167
215	203	210	-3.5		143
196	167	208	-20.5		107
81	52	93	-20.5	42.5	-8

Table B.18. Measured contents at 730°C in 30 mole % $MgCl_2$ / 70 mole % NaCl melt, saturated with MgO at start.

Total oxygen measured by carbothermal reduction	Basic oxygen measured by iodometric titration	MgOHCl measured as ppm O (Combo of methods)	MgO measured as ppm O (Combo of methods)	MgOHCl [ppm O] (Total O – c_{sat})	MgOHCl [ppm O] (Basic O – c_{sat})
55	20	0	10	0	0
921	687	1065	-189	857	649
765	603	837	-117	701	565
693	584	712	-64	629	546
494	435	463	-14	430	397
331	266	306	-20	267	228
271	212	240	-14	207	174
90	63	27	18	26	25

Table B.19. Measured contents at 631°C in 30 mole % $MgCl_2$ / 70 mole % NaCl melt, saturated with MgO at start.

Total oxygen measured by carbothermal reduction	Basic oxygen measured by iodometric titration	MgOHCl measured as ppm O (Combo of methods)	MgO measured as ppm O (Combo of methods)	MgOHCl [ppm O] (Total O – c_{sat})	MgOHCl [ppm O] (Basic O – c_{sat})
103	53	23	15	0	0
1250	993	1377	-192	1148	919
1169	958	1250	-146	1067	884
968	824	982	-79	866	750
956	773	1009	-118	854	699
787	634	810	-88	685	560
488	439	407	16	386	365
254	252	126	63	152	178
130	105	25	40	28	31

Analysed content of MgOHCl and MgO by carbothermal reduction analysis and iodometric titration in 20 mole % $MgCl_2$ / 80 mole % NaCl.

Table B.20. Measured contents at 801°C in 20 mole % $MgCl_2$ / 80 mole % NaCl melt, saturated with MgO at start.

Total oxygen measured by carbothermal reduction	Basic oxygen measured by iodometric titration	MgOHCl measured as ppm O (Combo of methods)	MgO measured as ppm O (Combo of methods)	MgOHCl [ppm O] (Total O – c_{sat})	MgOHCl [ppm O] (Basic O – c_{sat})
50	34	0	17	0	0
490	406	508	-51	440	372
394	327	395	-34	344	293
236	184	222	-19	186	150
179	145	147	-1	129	111
111	103	53	25	61	69
94	56	66	-5	44	22

Analysed content of MgOHCl and MgO by carbothermal reduction analysis and iodometric titration in 10 mole % $MgCl_2$ / 90 mole % NaCl.

Table B.21. Measured contents at 798°C in 10 mole % $MgCl_2$ / 90 mole % NaCl melt, saturated with MgO at start.

Total oxygen measured by carbothermal reduction	Basic oxygen measured by iodometric titration	MgOHCl measured as ppm O (Combo of methods)	MgO measured as ppm O (Combo of methods)	MgOHCl [ppm O] (Total O – c_{sat})	MgOHCl [ppm O] (Basic O – c_{sat})
42	12	0	6	0	0
284	313	183	65	242	301
169	154	112	21	127	142
101	95	35	30	59	83
48	56	-32	44	6	44
55	54	-16	35	13	42

Table B.22. Measured contents at 850°C in 10 mole % $MgCl_2$ / 90 mole % NaCl melt, saturated with MgO at start.

Total oxygen measured by carbothermal reduction	Basic oxygen measured by iodometric titration	MgOHCl measured as ppm O (Combo of methods)	MgO measured as ppm O (Combo of methods)	MgOHCl [ppm O] (Total O – c_{sat})	MgOHCl [ppm O] (Basic O – c_{sat})
38	14	0	-24	0	0
225	211	177	-14	187	197
108	105	49	-3	70	91
70	47	31	-23	32	33
47	22	10	-25	9	8
36	15	-5	-21	-2	1